c.1

A SYSTEMATIC STUDY OF MUON CAPTURE

by Takenori Suzuki

M.Sc., University of Tokyo, 1970
M.Sc., University of British Columbia, 1976

A THESIS SUBMITTED IN PARTIAL FULFILLMENT OF

THE REQUIRMENTS FOR THE DEGREE OF

DOCTOR OF PHILOSOPHY

IN

THE FACULTY OF GRADUATE STUDIES

(DEPARTMENT OF PHYSICS)

WE ACCEPT THIS THESIS AS CONFORMING

TO THE REQUIRED STANDARDS

THE UNIVERSITY OF BRITISH COLUMBIA
October, 1980

In presenting this thesis in partial fulfilment of the requirements for an advanced degree at the University of British Columbia, I agree that the Library shall make it freely available for reference and study. I further agree that permission for extensive copying of this thesis for scholarly purposes may be granted by the Head of my Department or by his representatives. It is understood that copying or publication of this thesis for financial gain shall not be allowed without my written permission.

Department of PHYSICS

The University of British Columbia
2075 Wesbrook Place
Vancouver, Canada
V6T 1W5

Date October 14, 1980

Abstract

Negative muon lifetimes have been measured in 48 elements including four pairs of separated isotope targets (^{6}Li,^{7}Li,^{10}B,^{11}B,^{12}C,^{13}C,^{16}O,^{18}O). The experimental set-up and electronics logic were checked against the positive muon lifetime, which was measured to be 2197.0±0.7 ns, in good agreement with the accepted value of 2197.120±0.077 ns. Muons were produced by the backward decay of pions which were provided by the M20 beam channel at TRIUMF.

The negative muon lifetimes were measured for all light elements except H and He. An improved accuracy has been achieved in Be, N, O, F, Na, Cl, and K, and new measurements were performed for ^{13}C, ^{18}C, Dy and Er. Strong isotope effects were observed in Li, B, and O, but there was no isotope effect in C. Our results in ^{6}Li and ^{7}Li were in good agreement with the predicted values by Lodder and Jonker. Our measurements confirm that the even-odd effect in heavy nuclei is not strong and the increase of the odd-Z capture rates is smaller than that expected from the quenching of the Cabibbo angle in large magnetic fields.

The negative muon beam was also stopped in 23 metallic oxides in order to measure the atomic capture ratios. The number of muons captured by each element was deduced by lifetime analysis. Our result reproduced the periodic dependence and agreed well with earlier X-ray measurements. The results however are of higher accuracy and are liable to very different systematic errors, which gives added confidence to the overall situation.

TABLE OF CONTENTS

List of Figures

List of Tables

ACKNOWLEDGEMENTS

I am most grateful to Professor David F.Measday not only for his help in completing this thesis, but also for his guidance in understanding physical phenomena. I would like to thank members of the supervising committee, Professors D.S.Beder, F.W.Dalby, and B.L.White for their advice and effort in reading this work.

I would like to thank Dr.J.H.Brewer and Dr.D.M.Garner for many enlightening discussions and in particular for their help with the MSR data taking system which was essential for the success of this experiment. It is my pleasure to acknowledge the invaluable assistance of Dr.Jan-Per Roalsvig throughout the last two-week experiment. Thanks are also due to the other members of the MSR gruop, Dr.D.C.Walker, Dr.D.G.Fleming, R.Kiefl, G.Marshall, R.J.Mikula, B.Ng, and D.Spencer for their many years assistance thrcugh the MSR meeting.

I also wish to thank Dr.M.Hasinoff, Dr.J.M.Poutissou, and Dr.M.Salcmcn for their kind advice during this work. Without a loan of targets frcm five groups, UBC chemistry (Dr.D.C.Walker, Dr.D.G.Fleming), UVIC TRIUMF (Dr.R.M.Pearce), DR.J.B.Warren, Dr.R.R.Jchnscn, and TOKYO MSR group (Dr.T.Yamazaki), this experiment wculd have not been completed. I would like to express many thanks to all of the above for their cooperation.

Finally I thank my wife Ycshiko for her many years of encouragement.

CHAPTER I

Introduction

I.A Discovery of the Muon and its Behavior in Matter

The muon was discovered by Anderson and Neddermeyer (AND38) in cosmic rays. When it was found, it was thought tc be the meson responsible for nuclear forces as predicted by Yukawa in 1935 (YUK35). However, it was difficult tc explain the fact that it had penetrated the earth's atmosphere without absorption. This was because the Yukawa mesons responsible for the strong interaction should have been absorbed quickly via nuclear reactions with atoms in the atmosphere. Through the work cf Conversi et al. (CON47), who measured the ratio of nuclear absorption of negative muons in light elements, it became clear that the muons did not interact strongly with the nucleus. The discovery of pions by Lattes et al. (LAT47) resolved the contradiction. They cbserved that the muons from cosmic rays were the decay products of the pions. It is now understood that pions are the Yukawa mesons and muons -which are similar to electrons in many ways- are now classified as leptons and are not mesons in the modern use of the term. Thus muons are particles of mass 105.6 MeV/c^2 (206.8 times the mass of the electron) and they experience the weak and

the electrcmagnetic interactions but not the strong interaction.

The behavior of negative muons in matter may be conveniently divided into the following four stages (WU69). The slowing dcwn mechanism and its duration have been discussed in detail by Fermi and Teller (FER47).

1, High energy to a few keV:

Mucns with several tens of MeV lose their energy mainly by collisions with atomic electrons. At the end of this stage, when the muon's energy is a few keV, its velocity is almost equal to the valence electron velccity. The slowing down time in the condensed material is between 10^{-9} and 10^{-10} sec.

2, A few keV to rest:

The mucns exchange energy with electrons and come to rest in about 10^{-13} sec. The details of this process depend on whether the material is a metal, insulator, gas, etc.

3, Atomic capture and electromagnetic cascade:

The muons are eventualy trapped into highly excited states of a particular atom and cascade down to the lowest state of the muonic atom. Auger processes (i.e. emission of atomic electrons) are dominant in the transition between the higher levels and radiative processes between the lower levels. The cascade time is about 10^{-13} sec.

4, Disappearance:

Most of the muons reach the 1S orbit of the muonic atom and they either decay or are captured by the nucleus from this orbit via the weak interaction. In light elements, it takes approximately 2.2 microseconds, the lifetime of positive muons, for the muons to disappear. In heavy elements it takes about 80 nanoseconds (ns).

In this thesis, the physics of the third and the fourth stages will be discussed.

The atomic capture rate of negative muons in chemical compounds was investigated by Fermi and Teller (FER47) and the so called "Z-law" was proposed. According to the Z-law, the probability for capture by an atom in a chemical compound would be proportional to its atomic number. However, the Z-law was not supported by subsequent experiments (SEN58, ECK62, BAI63), which observed a periodicity of the atomic capture rate in the metallic oxides (ZIN66), and thus it was realized that the capture process is strongly affected by the chemical structure. Even though there has been considerable progress in clarifying the capture process (DAN79, SCH78), the detailed explanation of the observed chemical effect still remains incomplete (SCH77).

There have been several attempts to calculate the kinetic energy of muons when captured by the atom. Although early calculations (HAF74) suggested that the capture occurs while the muons kinetic energy is still hundreds of eV, it is now believed that the energy is less than 15 eV in the

case of the hydrogen atom (LE079). The lower kinetic energy makes it easier to understand the effect of the molecular structure on the capture process.

I.B Free Muon Decay

A muon is the decay product of a pion. The decay scheme is

$$\pi^+ \longrightarrow \mu^+ + \nu_\mu \ , \qquad \pi^- \longrightarrow \mu^- + \bar{\nu}_\mu \tag{1.1}$$

Because this decay does not conserve parity, the muon is produced in a particular helicity state, namely its spin and magnetic moment are aligned (or anti-aligned) with the momentum vector. Although this effect is essential for MSR work, it turns out to be an inconvenience for the experiments described in this thesis. The muon decays into an electron and two neutrinos.

$$\mu^+ \longrightarrow e^+ + \nu_e + \bar{\nu}_\mu \ , \qquad \mu^- \longrightarrow e^- + \bar{\nu}_e + \nu_\mu \tag{1.2}$$

This three-particle decay hypothesis was confirmed by the observation on the energy spectrum of the decay electrons and their energy (TI049-1). The simple additive law of lepton conservation has only recently been confirmed by experiments at LAMPF (Willis et al.(WIL80-1)) (for instance in the μ^+ decay the quantum number for anti-muons has to be conserved, necessitating a $\bar{\nu}_\mu$ in the decay products and forbidding a ν_μ). Tiomno and Wheeler (TI049-2) proposed a Universal Fermi interaction , in which the coupling

constants of beta decay, muon decay and nuclear muon capture are of the same order of magnitude. The weak interaction scheme can then be expressed by the following picture (Puppi triangle)

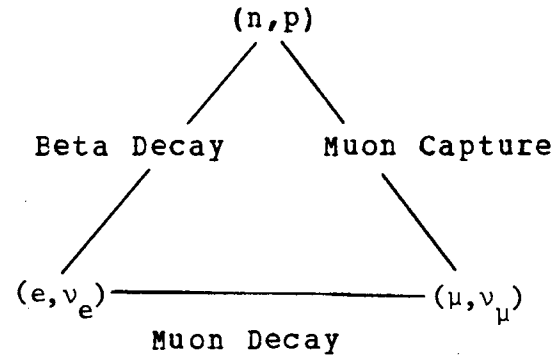

The Hamiltonian of the decay process (1.2) is described by the following four-fermion interaction (SAC75)

$$H = \frac{G}{\sqrt{2}} \sum_i \{\bar{\Psi}_\nu \Gamma_i \Psi_\mu\}\{\bar{\Psi}_e \Gamma_i (g_i + g_i^\dagger)\Psi_\nu\} + H.C. \qquad (1.3)$$

where i runs over the scalar, vector, tensor, axial vector, and pseudo-scalar interactions, and G is a coupling constant of the weak interaction (see in detail section IV.A). The Hamiltcnian (1.3) leads to the energy spectrum term M(X) (Michel spectrum) and the asymmetry term B(X) for the decay of a polarized muon. Hence, The general formula of the decay electron spectrum of the polarized positive muon is expressed as

$$dN(X,P,q) \propto \{M(X) + B(X)\cos(q)\}X^2 dX \qquad (1.4)$$

where P is the mucn polarization, q the angle between the

decay electron momentum and the spin direction of the muon.

In figure I-1, the experimental energy spectrum data points measured at TRIUMF are shown along with the theoretical curve. This figure and the following experimental results measured at TRIUMF were presented at the CAP conference in 1979 (SUZ79). The theoretical energy spectrum for the positive muons has been shown by Michel (MIC57, SAC75) to be

$$M(X) = 2(X)^2 \cdot \{6(1-X) + 4\rho((4/3)X-1)\} \qquad (1.5)$$

where X is the electron momentum in units of the peak momentum (52.8 MeV/c) and ρ is the so-called Michel parameter. ρ is predicted to be 0.75 by the two-component neutrino and V-A theories (KIN57, SAC75). The experimental values found by Bardon (BAR65) and Fryberger (FRY68) are 0.750±0.003 and 0.762±0.008, respectively. The TRIUMF result is 0.749±0.003. Thus the experiments are in good agreement with the theoretical prediction.

In the case of polarized positive muons, the asymmetry term (SAC75) is given by

$$B(X) = 2(X)^2 \cdot \{2(1-X) + 4\delta((4/3)X-1)\} \qquad (1.6)$$

where δ is the asymmetry parameter. Again δ is predicted to be 0.75, the same as ρ. At TRIUMF, the polarized positive muon with a 84% beam polarization was stopped in a

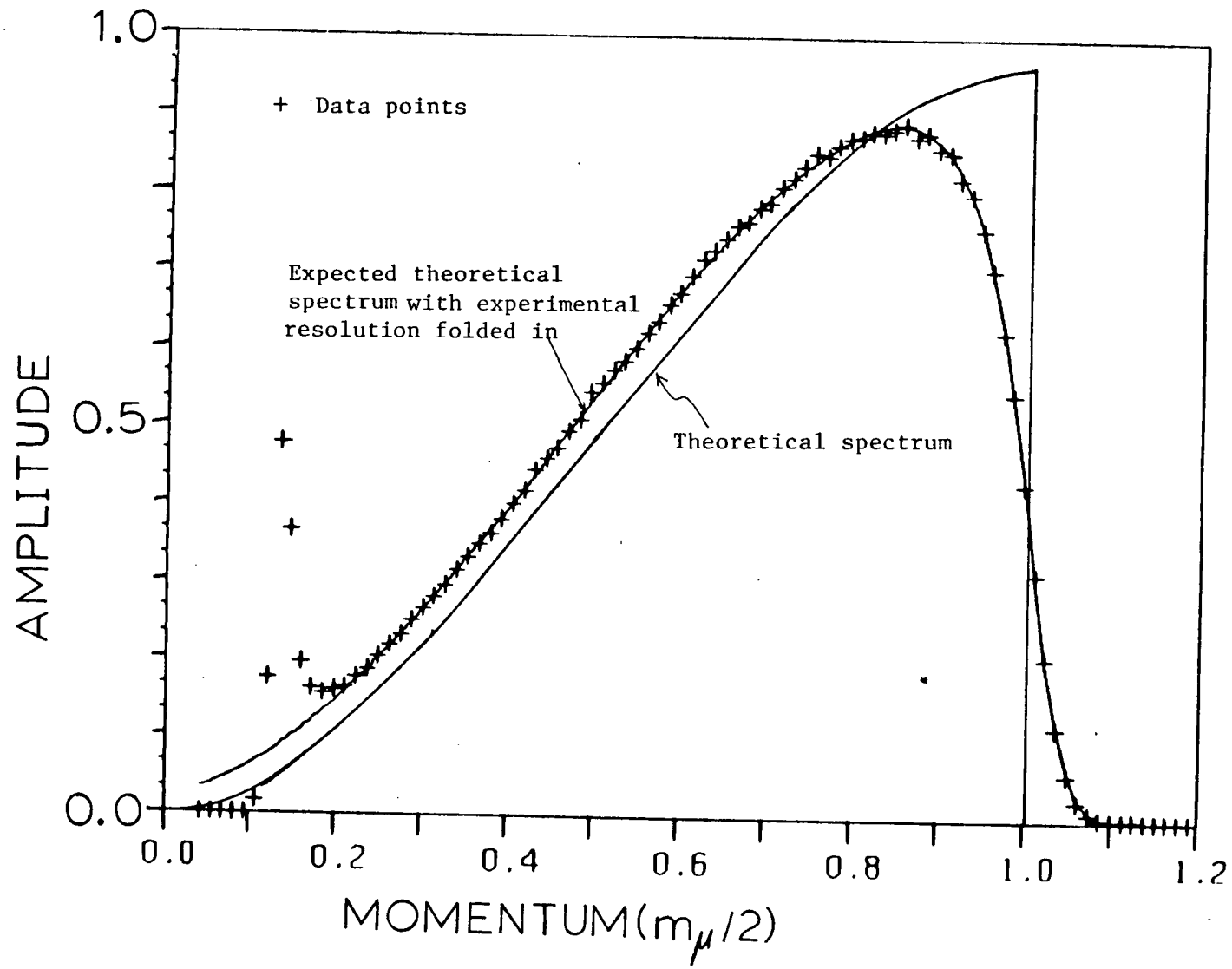

Figure I-1, Energy spectrum of positrons from positive muon decay. The x axis shows the positron momentum in units of (muon mass)/2.

carbon target and the energy dependent asymmetry was measured. This is shown in figure I-2 along with the asymmetry spectra of negative muons in a carbon and a titanium target. From the data analysis of the positive muon asymmetry, δ is equal to 0.753±0.005. This agrees well with Fryberger's finding of 0.752±0.008 and also with the predicted value.

In the usual counter experiment, the electron energy is not measured. The angular distribution of electrons is of the form

$$dN(P,q) \propto \{1+APcos(q)\}\,dq \qquad (1.7)$$

where A is the asymmetry and P the muon polarization. This is an equation for the muon precession under the influence of a magnetic field. The integration of equation (1.6) for the electron momentum (X) between 0 and 1 gives

$$A = 1/3 \qquad (1.8)$$

when P=1 (namely 100% beam polarization).

I.C Bound Muon Decay

The bound muon decay has a few different characteristics from a free muon decay. First, a negative muon in the K orbit of the muonic atom has a lower decay probability than a free muon due to the reduced phase space.

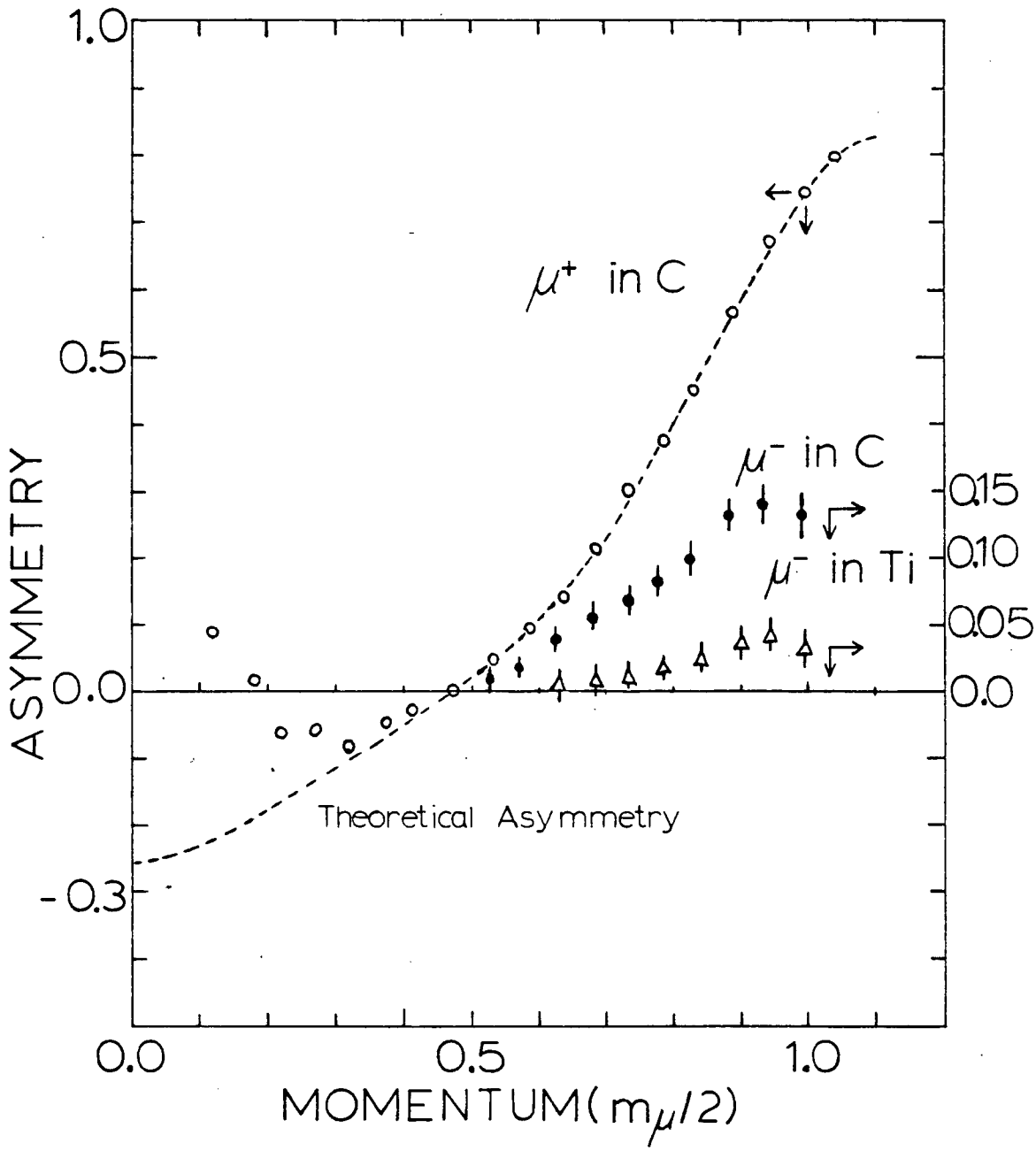

Figure I-2, Energy dependent asymmetry for positive and negative muon decay in carbon. Also the asymmetry of negative muons in titanium is shown.

The decay rate of the free positive muon is

$$Rd(+) \propto (\text{muon mass})^5$$

The energy of the bound muon is equal to the energy of the free muon (105.6 MeV) minus the binding energy of the K orbit of the muonic atom which reaches a value of about 12 MeV in uranium. That is

$$Rd(-) \propto (\text{muon mass-binding energy})^5$$

This corresponds to the reduction of the phase space accessible to the decay products. Secondly, due to the motion of the bound muon in the K orbit, the decay electron has a Doppler effect and the maximum energy is greater than the cut-off energy (=52.8 MeV) of decay electrons from free muons. Hence, the energy spectrum of the bound muon decay stretches to the high-energy side. Thirdly, the decay probability and the decay electron energy spectrum are affected by the nuclear coulomb field. The peak of the spectrum is shifted into the lower energy side as the atomic number of the target nucleus increase.

In figure I-3, there are four decay electron spectra from carbon, titanium, copper, and lead. Before the TRIUMF measurement (SUZ79), there had been two experiments by Culligan et al. (CUL61) for an iron target and Beilin (BEI68) for a copper target. The TRIUMF experiment was the

first attempt to demonstrate the variation of the energy spectrum for the various nuclei. The second and third effects above are clearly demonstrated in the figure. The energy spectra obtained at TRIUMF have shown good agreement with Huff's theory (HUF61). His theoretical curves are shown in figure I-4. As discussed in section I.B, the theoretical curve must take into account the detector resolution and energy loss in the electron counters in order to compare the theory with the experiment. We have already reported that the theory is in good agreement with the bound muon decay spectra (SUZ79).

In the experiment of the atomic capture ratio in a chemical compound, it must be noted that the energy spectra of decay electrons are different for different nuclei. In the heavy elements, like lead, the ratio of low energy electrons to high energy electrons is greater than the ratio in the lighter element. Thus, the loss of low energy decay electrons from the heavy element constituent in the chemical compound target is larger than that from the light element constituent.

A negative muon loses polarization quickly during the cascade in the muonic atom. The TRIUMF experiment (SUZ79) is the first attempt at measuring the energy dependence of the asymmetry of negative muons. In figure I-2, two asymmetry spectra for carbon and titanium targets are shown. The calculation of the energy dependent asymmetry has been done for an iron target by Gilinsky and

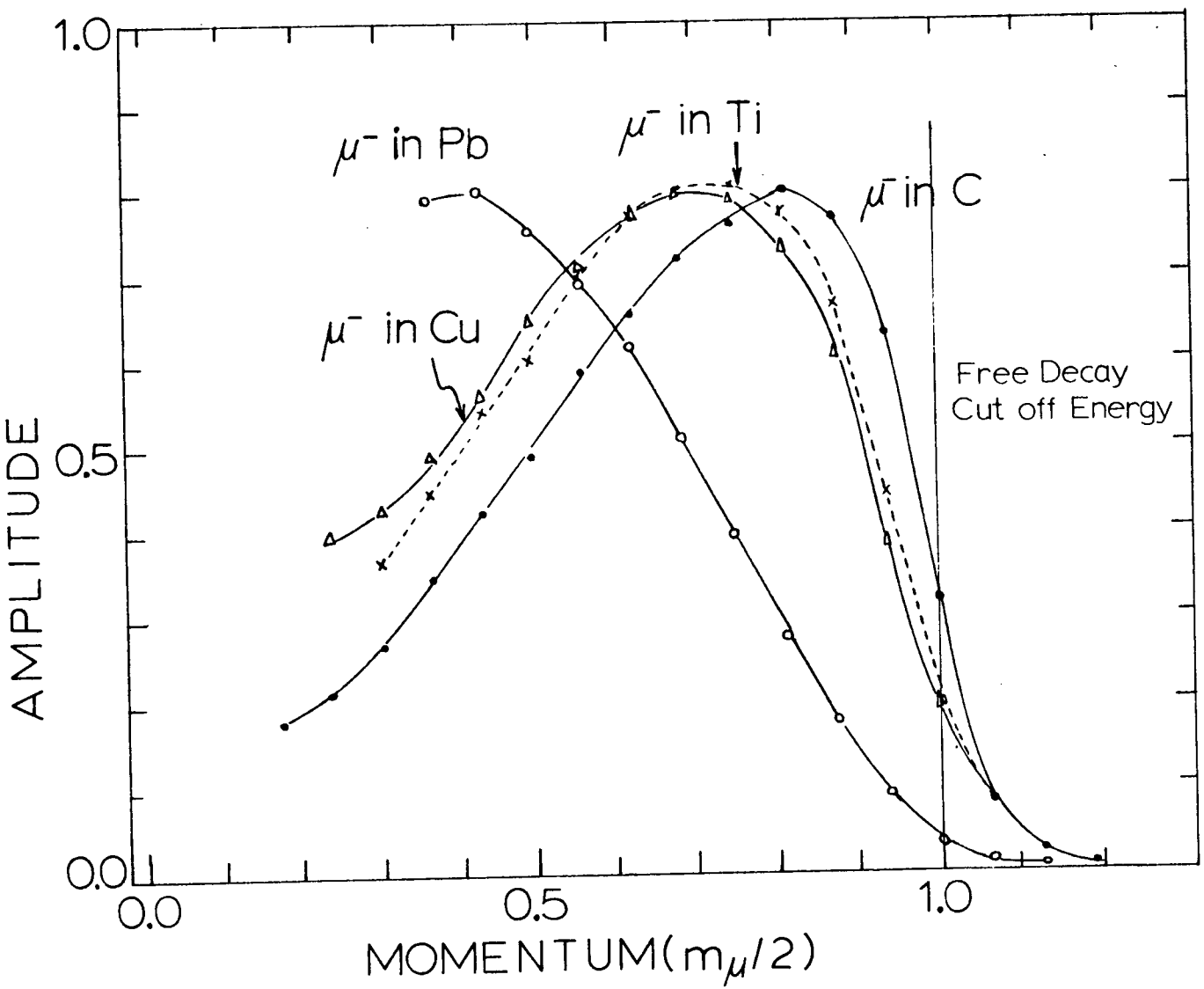

Figure I-3, Experimental energy spectra of decay electrons from negative muons in carbon, titanium, copper, and lead.

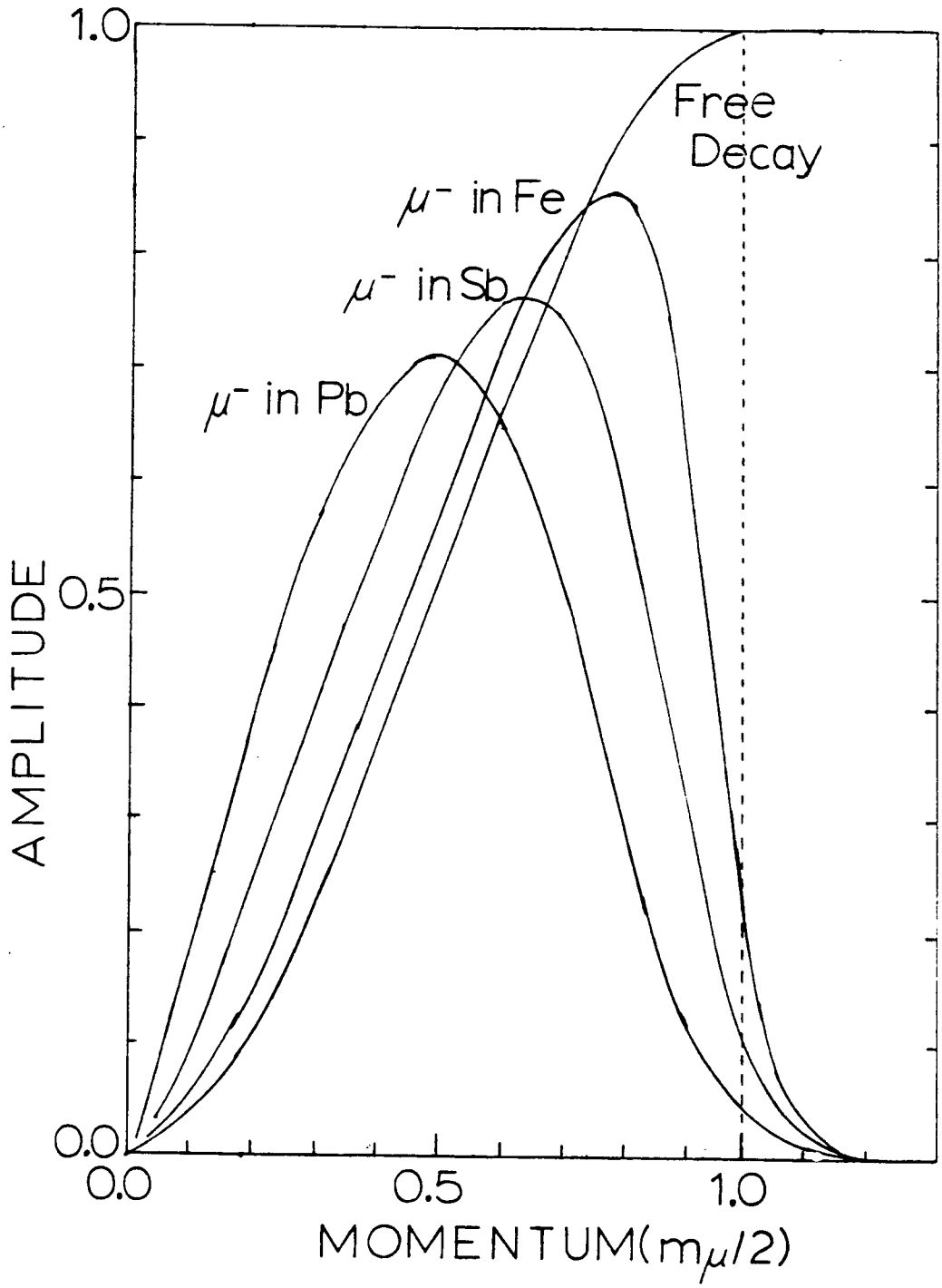

Figure I-4, Theoretical spectra of decay electrons from negative muons in lead, antimony and iron (HUF61)

Mathews (GIL60). Their calculation predicts that the asymmetry at the high energy end drops down to zero.

The residual polarization of negative muons for spinless nuclei has been theoretically analyzed by Scmushkevich (SHM59) and Mann and Rose (MAN61). The behavior of negative muons in matter has been discussed in section I.A. During the slowing down process from high energy to rest, the muons lose most of their kinetic energy by collisions with electrons but the depolarization in this stage is negligible. When the muons are trapped into excited bound states of the muonic atom, they lose most of their polarization, retaining only about 1/3 of the initial value. Then the muons undergo many transitions via Auger processes in higher orbits and radiative processes in lower orbits, and finally reach the ground state of the muonic atom. During the cascade in the muonic orbits, the muons lose 50% of the remaining polarization. Thus, in the case of carbon, the final polarization is estimated to be about 15%. This estimate of the residual polarization is in good agreement with experiments as shown below. If the nucleus has a spin, there is a spin-spin interaction between the muons and the host nucleus. Due to this interaction, the additional depolarization occurs during the cascade. Furthermore, at the ground state, the hyperfine coupling between the muon and nuclear spins produces a strong depolarization. Consequently, the residual polarization of negative muons in the nucleus with a spin is expected to be

much smaller than that in the spinless nucleus. In the case of ^{19}F (I=1/2), the residual polarization is reported to be 4±4% (AST61).

The residual polarizations of negative muons in carbon and titanium are 20±3% and 7±3%, respectively, from the TRIUMF experiment (SUZ79). These polarizations have been investigated by Dzhuraev et al. (DZH72), who measured the total asymmetry (A) expressed by equation (1.7). Their findings were 19.4±1.1% and 15.5±1.8% for carbon and titanium, respectively. In the case of carbon, both experiments agree well. However, in the case of titanium, the TRIUMF result is smaller by a factor of 2. The reason for this is not certain. In the case of titanium, the asymmetry spectrum shows large errors especially at low energy. This measurement will be repeated at TRIUMF with a better quality muon beam in order to reduce the accidental coincidences which are related to the R.F. period in the time spectrum.

I.D Muon Capture in Nuclei

Conversi et al. (CON47) measured the lifetime of positive and negative muons in carbon and iron. They found that the lifetime of negative muons in carbon was almost the same as that of positive muons (2.2 microseconds). On the other hand, decay electrons from the negative muons in iron

were not detected after one microsecond delay. This proved that the negative mucns were captured by the iron nucleus within a microsecond. Since then, the muon capture has been studied experimentally and theoretically and the capture rate has been determined for most nuclei.

The basic process of muon capture in a nucleus is the reacticn:

$$\mu^- + p \longrightarrow n + \nu_\mu \qquad (1.9)$$

which in the case cf bound protons in a nucleus becomes:

$$(A,Z) + \mu^- \longrightarrow (A,Z-1) + \nu_\mu \qquad (1,10)$$

This reaction leads to nuclear exited states (mainly giant resonance states at about 20 MeV excitation) which then de-excite with the emission of one or more neutrons (KAP58). The first theoretical approach to calculate the total capture rate in the nucleus was made by Wheeler (WHE49). He expressed the capture rate by

$$Rc(Z,A) = \text{constant} \cdot \sum_{\substack{\text{all} \\ \text{protons}}} |\Psi(\text{at each proton})|^2 \qquad (1.11)$$

where Ψ is the muon wave function. Now, $|\Psi|^2$ is proportional to Z^3, so that

$$Rc(Z,A) \propto (Zeff)^4 \qquad (1.12)$$

In this equation Z is replaced by Zeff, because the muonic K orbit is inside the nucleus for heavier nuclei and therefore the part of the wave function which is inside the nucleus is

modified because it sees a reduced charge. The $(Zeff)^4$ law is approximately valid for light elements, but it overestimates the rate for heavy elements.

Primakoff (PRI59) derived a simple formula which has a neutron excess term originating from the Pauli principle. He employed a closure approximation in order to calculate the transition matrix elements for all accessible excited states of the daughter nucleus. This formula has been improved by Goulard and Primakoff (GOU74) to overcome the systematic deviation from the Primakoff formula for the heavy elements. These theories will be discussed in more detail in Chapter V.

The first experiment to study systematically the total muon capture rate was made by Sens et al. (SEN57, -59) who determined the apparent lifetime of negative muons which stop in matter. The inverse of the lifetime is the total disappearance rate, Rt, which is composed of two components, the decay rate, Rd, and the capture rate, Rc, ie

$$Rt = Rc + Q(Z) \cdot Rd \qquad (1.13)$$

where Q(Z) is the Huff factor discussed earlier which takes account of the factor that the negative muon is bound in the atom and so the decay rate is reduced (by up to 20% for heavy nuclei). Rd is taken to be the same as that for the positive muon utilizing the CPT theorem which implies that the total lifetimes of particles and anti-particles are

identical. The measurements of Sens et al.(SEN59) in 29 elements from carbon (Z=6) to uranium (Z=92) showed the linear relation between the reduced capture rates and neutron excess term, as predicted by the Primakoff formula. After their experiment, a large number of measurements in different nuclei have been performed with improved instruments and averaged values of the past findings have been summarized by Eckhause et al.(ECK66). Most of the past measurements will be listed in Table IV-2 of this thesis. In the intervening years, the accepted value for the lifetime of the positive muon has changed outside the original error bars (from 2203 ± 2 ns in 1963 to 2197.13 ± 0.08 ns today). As the capture rate is the difference of two numbers, a small change in the positive muon decay rate can have a marked effect in the calculated decay rate, especially for light nuclei. We therefore believe that all early measurements should be approached with some caution.

There have been several theoretical developments since the Primakoff theory. The direct calculation of the transion matrix with the microscopic picture is the shell model calculation (LUY63, GOU71, DUP75). Total muon capture rates by this model are usually higher than the experiments by a factor of 2 or 3. The model can be used to understand the general trend of transitions instead of comparing the result with a experiment.

Foldy and Walecka (FOL64) developed a resonance model, which calculates the giant dipole resonance (GDR)

excitation induced in muon capture. They used an experimental cross section of the photo-nuclear reactions to manipulate the dipole part of the muon capture cross section. They applied this model to the doubly magic nuclei, ^{4}He, ^{16}O and ^{40}Ca, in which the allowed transitions are suppressed. In the case of ^{4}He, the theory was in good agreement with the experiment. The calculated capture rates for ^{16}O and ^{40}Ca were higher than the experiments by 10% and 25%, respectively. Applying the model to ^{12}C and including the allowed contribution (WAL75) to the capture rate, the calculation agreed well with experiment. Lodder and Jonker (LOD67) investigated the total muon capture rate for ^{6}Li and ^{7}Li with the Foldy-Walecka semi-empirical method. Their result for ^{6}Li was smaller than the experimental value of Eckhause et al. (ECK63) whereas for ^{7}Li their value was comparable to the experimental value. Recently the capture rates in ^{6}Li and ^{7}Li were remeasured by Bardin et al. (BAR78) and their experiment agreed well with the results of Lodder and Jonker. It will be shown later that our measurements in these nuclei also support their calculation.

Christillin et al. (CHR73) have attempted to give the total capture rate in terms of a mean nuclear excitation energy and obtained the follwing simple relation

$$Rc(E') \propto \frac{p^4}{(E')^4}(Zeff)^4\left(1+\frac{1}{c^2p^2}\right)$$

where P is the neutrino momentum, E' the mean excitation energy and C a constant. Their calculation indicated that E' agreed with the GDR energy in the light nuclei. On the other hand, E' increased to 45 MeV in the heavy elements, while the GDR energy in photo excitation is only 13 MeV (CAN74). In the GDR process occurring in muon capture, the higher isospin levels (Tz=T+1) are excited and the GDR energy is expected to be larger than that of the photo-excitaticn (CHR75). According to calculations by Nalcioglu et al. (NAL74), the average excitation energy for the muon capture in ^{64}Ni is 28 MeV whereas for photo-excitaticn it is only 17 MeV. It is clear from their calculations that the T+1 excitation is suppressed in the photo-excitation. There have been no experiments to investigate the T+1 level excitation in muon capture because neutrino spectroscopy is unfortunately impossible and the neutron energy spectrum from the decay of the nucleus gives ambigucus informaticn.

Bernabeu (BER73) has proposed a model which avoids the uncertainty of the neutrino energy in the total capture rates. Khoyama and Fujii (KOH76, -79) adopted this model and calculated the total capture rates using the statistical method. They performed numerical calculations for 35 elements frcm Z=11 to Z=92 and their predicted capture rates reproduced the experimental data within 15%.

Before completing this section we should discuss an important ccmplication which confuses the comparison of

experiment with theory. For a nucleus with a spin, the muon in the 1S orbit has its own spin coupled to the nuclear spin resulting in two possible states termed the hyperfine (hf) states. For example, when a negative muon is captured by a proton, the capture probability depends on the mutual orientation of the spins of the two particles. It has been predicted theoretically that the capture rate (Rc^+) from the F=1 triplet state is equal to 1/sec for V-xA interaction with x=1.2 and, from the F=0 singlet state, Rc^-=635 /sec (MUK77). The singlet state capture rate was measured by the CERN-Bologna group (ALB69) who obtained Rc^-=651±57 /sec. They employed ultrapure gaseous hydrogen (8 atm, 293 K) as a target. In a system of pure hydrogen, the muon-proton muonic atoms are initially formed in a statistical mixture of triplet and singlet states. Through the scattering process between the muonic atom and hydrogen, there is the rapid conversion of the muonic atoms from the triplet state to the singlet state. For hydrogen gas at 300 K, the calculated conversion time is 1.2 microseconds at 0.5 atm of pressure and 82 ns at 8 atm (MAT71). For capture in a liquid the muon is bound in a $p\mu p$ molecule and the capture rate Rc(orthomolecule) is given by

$$Rc(OM) = 3/4 \cdot Rc^- + 1/4 \cdot Rc^+$$

Experimentally Rc(OM)= 460±20 /sec (BAR80) which shows that $Rc^+ < 100$ /sec.

If a complex nucleus has a non-zero nuclear spin (I), the capture probability of a negative muon in the

nucleus also depends on the total angular momenta $F^+=I+1/2$ and $F^-=I-1/2$. Bernstein et al.(BER58) calculated this effect for a model consisting of a spinless core and an external proton without allowing a conversion from the higher hf state to the lower hf state. But there is, in fact, a fast conversion (TEL59) through the ejection of Auger electrons which is more than 400 times faster than the M1 transition rate. These conversion rates were calculated by Winston (WIN63) who showed that for heavy elements (Z>10) the rate is so fast that the muons are normally captured from the lowest energy state. The rate for various nuclei will be listed in Table IV-6 along with the capture rates from two hf states. There have been several measurements to determine the conversion rates (WIN63, FAV70). Because of the fast conversion, the experimental determination is limited only for light nuclei. Since the effect of the hf conversion is very small (<0.01) in the decay electron spectrum, it is much harder to determine the rate by detecting decay electrons than by detecting neutrons or gamma rays (see section III.G). Only for chlorine and fluorine are the rates comparable to capture rates and therefore readily observable. So far, the conversion rate has been determined only for ^{19}F by a muon capture experiment. The standard method is the muon spin resonance method (MSR), which measures the precession damping and determines the relaxation rate. Favart et al. (FAV70) employed this method to obtain the conversion rates for ^{6}Li,

^{7}Li, ^{9}Be, ^{10}B and ^{11}B. These results are listed in Table IV-6.

The present work is a detailed description of an experiment to determine the mean muon lifetimes in complex nuclei and muon atomic capture ratios in metallic oxides. The experimental set-ups and method are described in Chapter II. The data analysis is discussed in Chapter III. In Chapter IV, the lifetime results and nuclear capture rates are reported in detail. Chapter V deals with the theoretical aspects of the atomic and nuclear muon capture rate, and a comparison of the experimental results with the theories is made. In Chapter VI, the summary of this experiment is presented.

CHAPTER II

Experimental Method and Set-up

In this chapter we shall describe the experimental method used in this work. In the first section we shall discuss the general procedure and detailed features of the equipment will be given in the following sections.

In this series of lifetime measurements we employed muons which were provided by the stopped muon channel (M20) at TRIUMF. The beam line and the counter set-up of this experiment are shown in figures II-1 and II-2, respectively. A stopped muon signal which was defined by a (1,2,3,$\underline{4}$,$\underline{5}$) coincidence produced a start signal for a clock. Decay electrons from the muons were detected by four electron telescopes: left(5,6), right(5,7), top(5,8) and bottom(5,9), and the electron signal was sent to the clock as a stop signal. The time difference between the start and the stop signals was stored in a histogram by a PDP-11/40 computer which is extensively used for MSR experiments at TRIUMF. There were 2000 channels in the histogram and the lifetime of muons in a target was obtained by a chi-squared minimization of the histogram. This data analysis will be discussed in Chapter III.

When the data taking was started, the detection system was calibrated by measuring the positive muon lifetime which is known precisely (BRI78). When the correct positive muon lifetime was obtained after several runs, the

positive muon beam was switched to the negative muon beam by changing the polarity of magnets of the M20 beam line. Then, at the beginning of negative muon lifetime measurements, the lifetime measurement in carbon was made. This lifetime was used as a calibration of the system and, at least, once a day, the negative muon lifetime in carbon was measured in order to check the detection system. During the two week experiment (first week from 3/10 to 7/10, second week from 21/10 to 28/10 1979), the system, which reproduced the correct positive muon lifetime, was established and the negative muon lifetimes in more than 80 different targets were measured.

II.A Muon BeamLine

The series of measurements of muon lifetimes was performed on the stopped muon channel (M20) at TRIUMF. Throughout these experiments, the proton current was 20 micro-amperes at 500 MeV. The proton beam struck a pion production target, T2, which consisted of a water cooled beryllium strip, 10 cm long in the beam direction, and 5 mm by 15 mm in cross section. Since beryllium targets have shown a relatively high production rate for negative pions and have a low electron contamination in the pion beam, such a target was specially selected for this lifetime

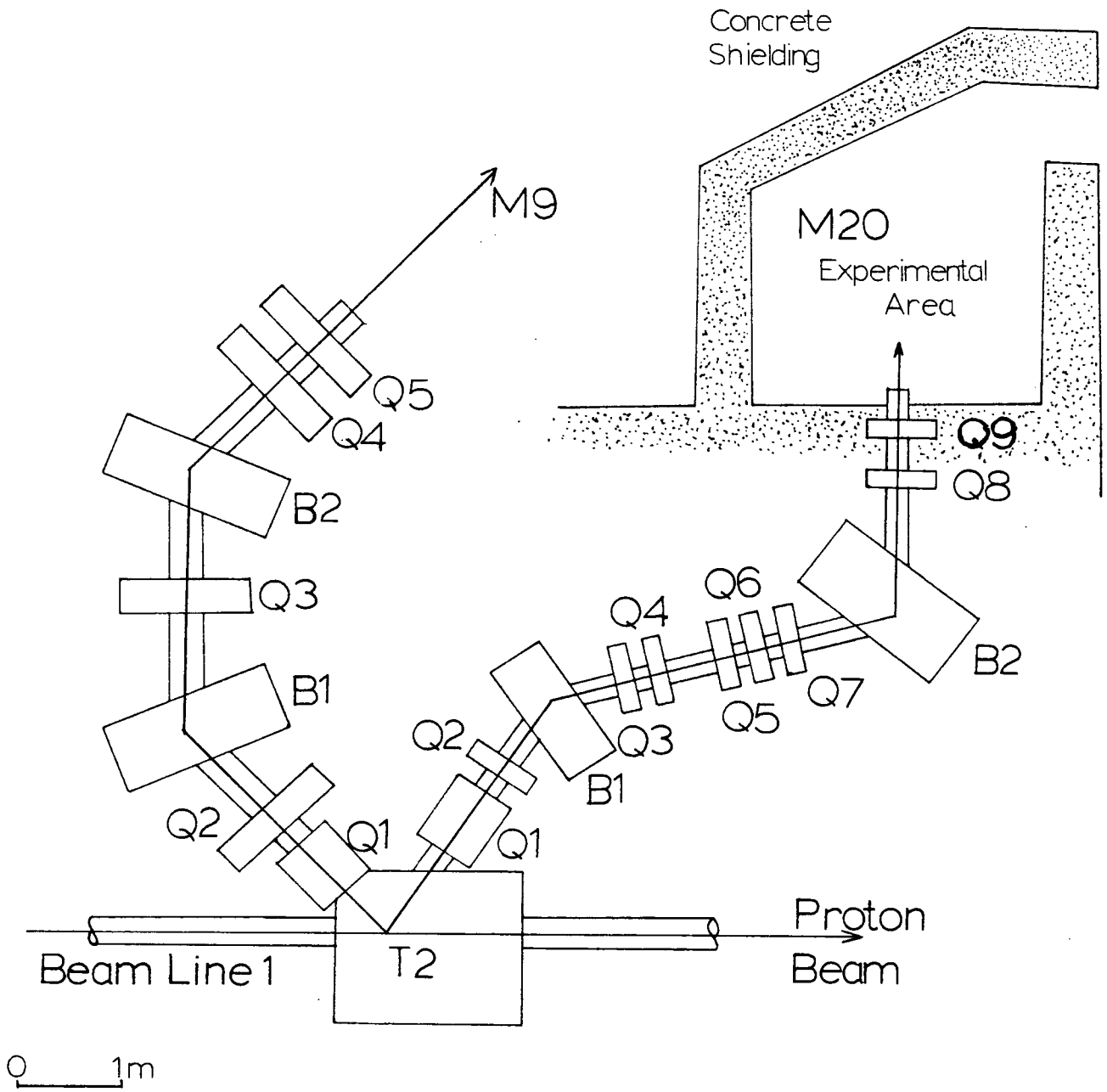

Figure II-1, The M20 beam line.

experiment.

The M20 secondary beam line focused the beam with a series of quadrupole magnets (Q1-Q9) and the momentum was set with two bending magnets (B1,B2). There were three different modes for a positive muon beam: cloud, conventional and surface modes. On the other hand, only two modes, cloud and conventional modes, were available for a negative muon beam. The three modes are defined as follows. The cloud muons are produced by a decay from the cloud of pions between the T2 target and the first bending magnet B1. For conventional muons a fraction of the pions with a particular momentum set by B1 are allowed to undergo the in-flight decay between B1 and B2, and the muons are selected by the B2 magnet. The muons which decay into the same (opposite) direction as(to) the pion beam direction are called forward (backward) muons which have larger (smaller) momentum than the pion beam. Surface muons are produced from the decay of pions at rest on the surface of the T2 target. As negative pions are absorbed on nuclei when they come to rest, they do not decay into muons and so this mode is possible for positive muons only. The energy of surface muons is very low (4 MeV, 29 MeV/c) and so they stop in very thin targets.

In this experiment, backward muons were employed. These muons were selected by setting the second bending magnet for the backward muon momentum. Since a momentum of 170 MeV/c for the first bending magnet was fixed, the

expected backward muon momentum was 87 MeV/c. This mode was chosen for the following reasons. First, it had very low electron contamination in the negative muon beam (8%) compared with other modes (>80%). Secondly, the background associated with pions was reduced. When the negative pions are stopped in a degrader, the pions are absorbed in the nucleus producing neutrons, protons, and gammas which contribute significantly to the background. Thirdly, muons with low momentum were stopped easily in the targets using degraders which were thin, an important advantage.

The time of flight spectrum (TOF) of the negative muon beam is shown in figure II-3. Since this TOF spectrum was taken with the pulse height rejection of counter S2, the electron contamination (<2%) was much lower than that of the beam. Although in the backward muon beam there were mostly muons and electrons, a CH2 degrader 2.5 cm in thickness was placed in the beam to reduce the energy of the muons and to remove the very few pions in the beam. With a 2.5 cm diameter lead collimator, the incoming negative muon beam rate defined by a (1,2,3) coincidence was nearly 1000/sec for a 20 micro-ampere proton current on the T2 target.

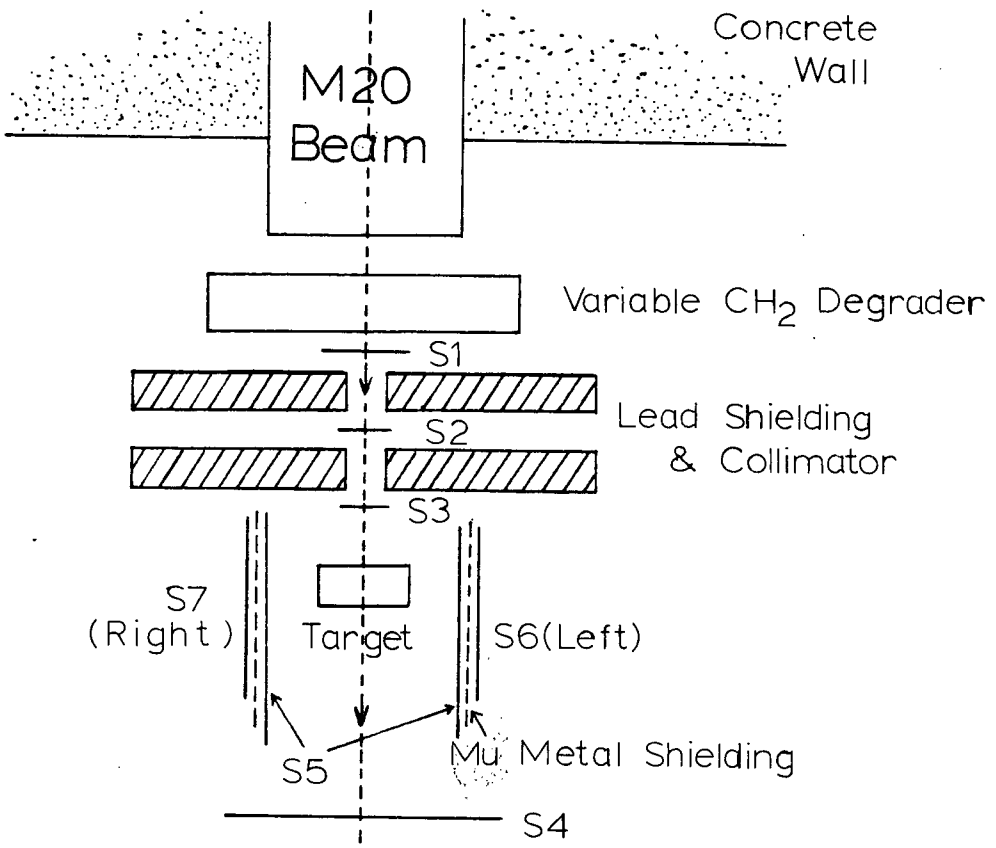

Decay Electron Counters

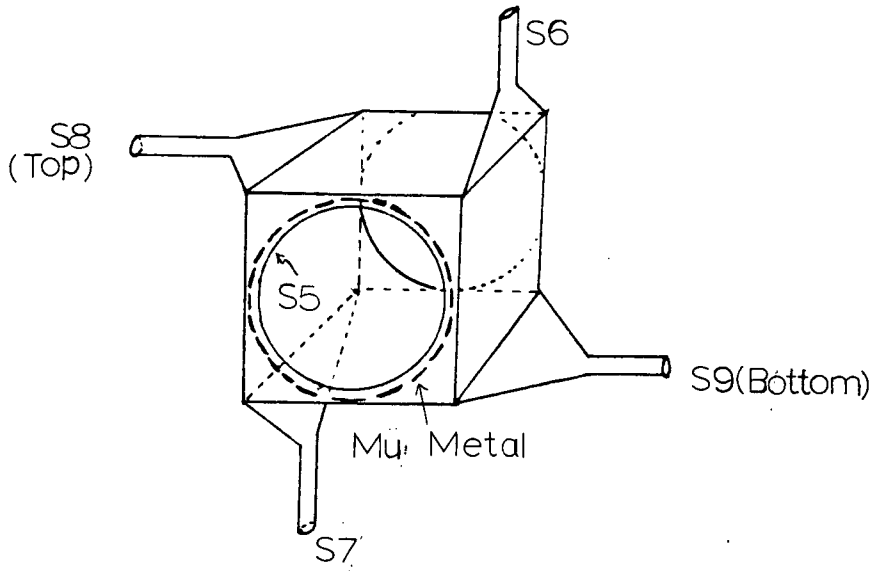

Figure II-2, Experimental set-up and decay electron counters.

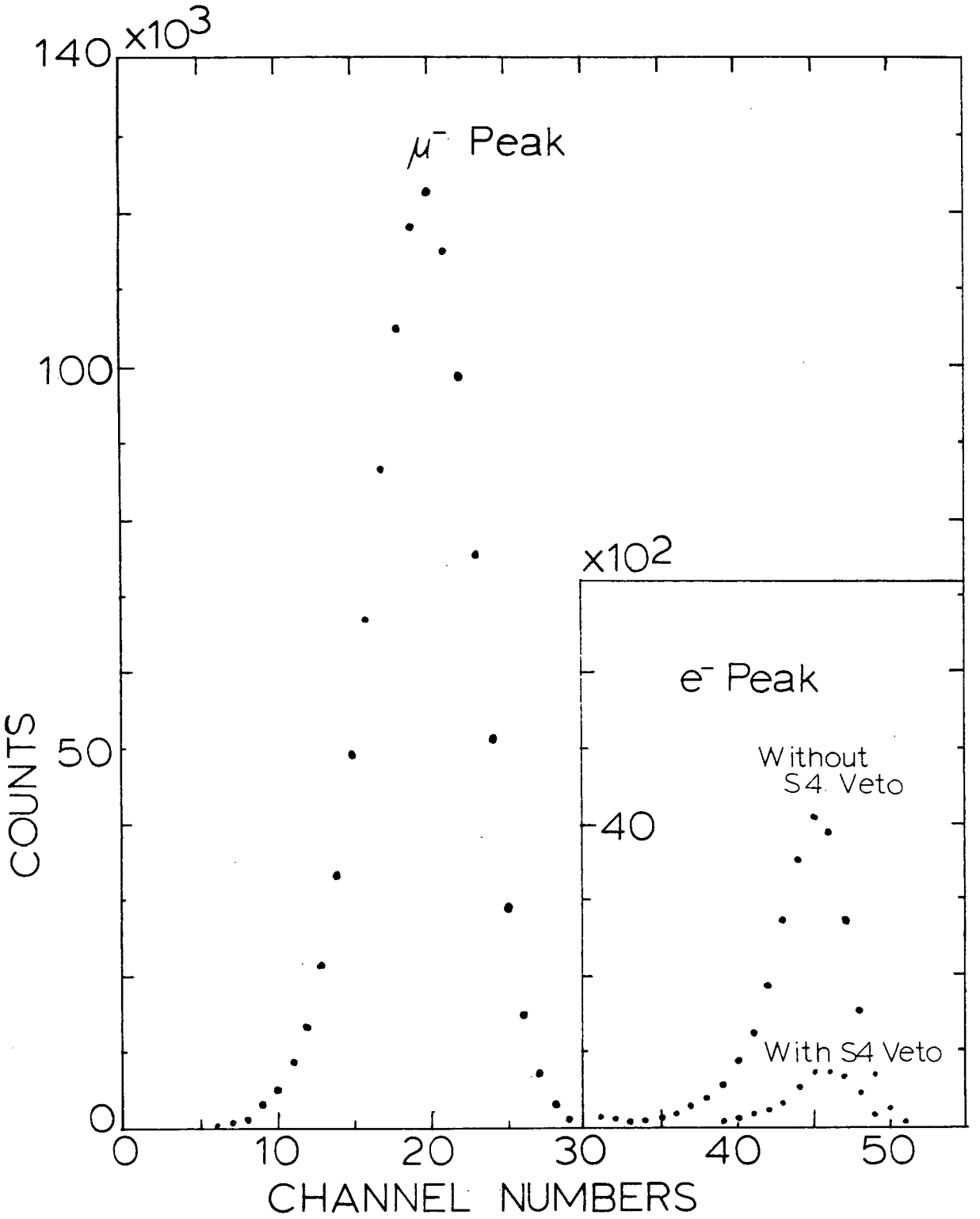

Figure II-3, Time of flight spectrum of incident beam and stopped muon signals.

II.B Scintillation Counters and Geometry

In this experiment, nine counters were used whose dimensions and efficiencies are given in Table II-1. These counters were made of a plastic scintillator (NE110 made by Nuclear Enterprises Ltd.) and viewed by RCA 8575 phototubes. Since all information was supplied from plastic counters, much care was taken in their design and use. In particular:

S1: Counter S1 was big enough to cover the beam collimator.

S2: Counter S2 was made thicker in order to distinguish electrons, muons, slow muons and double muons by pulse height analysis. Slow and double muons showed higher pulse height than ordinary muons. Electrons had little energy loss in the plastic scintillator and the pulse heights were lower than the muon's pulse heights. The typical pulse height for ordinary muons ranged from 250 to 600 mV and the pulse height for electrons from 30 to 150 mV. A pulse height larger than 600 mV was considered as a double muon or a slow muon which stopped in S2 and the event was rejected. Counter S2 was placed in front of the variable lead collimator in order to avoid it being visible to electron telescopes so that this counter did not contribute as a carbon background source.

S3: Counter S3 was the defining counter of muons and was

visible to the electron telescopes. When negative mucns stopped inside counter S3, these were counted as good muon events and this caused carbon background events in the histogram. In order to minimize the background, the counter S3 was made of 0.07 cm thickness plastic scintillator and covered with only 0.001 cm thickness aluminum foil.

S4: Counter S4 was big enough to cover any particles which came through the target and was used as a veto counter.

S5: Counter S5 had a cylindrical shape with 0.3 cm thickness wall, 20 cm long and 20 cm in diameter. It was used in all four electron telescope coincidences. Also it was a veto counter used to reject the scattered particles from the beam which set off towards the electron telescopes. The idea of using a cylindrical counter S5 was to minimize any imbalance between the electron telescopes and to save counters.

S6-S9: Counters S6, S7, S8 and S9 were made of identical shape (see Table II-1) in order to avcid any imbalance in the electron telescopes. Also, they were viewed by new phototubes to get the same counter efficiencies. The configuration of these counters is shown in figure II-2. This set-up had 60 % solid angle for a point source at the center of the cylindrical counter S5.

During the two week experiment, there was a

Table II-1 Counter Geometry and Efficiency

Symbol (Name)	Size (cm)	Efficiency[1]
S1	10x10x0.6	99.9 %
S2(thick counter)	6.4(dia)x1.2	99.9
S3(defining counter)	5.0(dia)x0.07	99.6
S4(veto counter)	30x45x1.2	99.9
S5(cylindrical counter)	20(dia)x0.3	99.8
S6(left E counter)	20x20x0.6	99.9
S7(right E counter)	20x20x0.6	99.9
S8(top E counter)	20x20x0.6	99.9
S9(Bottcm E Ccunter)	20X20X0.6	99.9

1) The counter efficiency test was made by using a Ru electron source.

possibility of counter or electronics failures including drifting of the high voltage, so counting rates of important coincidences and rejecticns were monitored on visual scalers and printed out as a record at the end of every run.

II.C Mu Metal Shielding of Field and Collimator

For the case of the lifetime measurement of a positive muon with a high polarization, the muon precessed in the target because of the magnetic field (about 1 Gauss), which was created by the earth as well as the leakage of magnetic flux from the beam line magnets near the target. In order to reduce the magnetic field, two thin Mu metal cylinders were used inside and outside of the counter S5. With these cylinders, the magnetic field at the target position was down tc 0.05G. Even with this small magnetic field, the precession of muons affected the muon lifetime and the correct lifetime was achieved only by averaging the four electron telescopes. This will be discussed in section III-B.

The M20 beam line formed a broad beam spot 10 cm in diameter. In order to collimate the beam, a lead collimator 14 cm in length and 3.8 cm in diameter was used between counters S1 and S2, and another lead collimater (L=7 cm d=2.5 cm) was placed between counters S2 and S3.

II.D Targets

In this experiment, there were 3 liquid, 27 metal, and 9 powder targets composed of a single element together with targets of 29 chemical compounds. Also, there were 2 targets mixed in Agar. All target information is listed in Table II-2. Half of the targets were borrowed from five groups: UBC Chemistry, Dr Johson's group, Dr Warren's group, UVIC group and the Tokyo MSR group. The diameter of a standard target container was 9.5 cm and the thickness varied with the density of target material. Since the lead collimator which defined the beam was 2.5 cm in diameter, the standard size of the targets was large enough to cover the beam spot. Windows at both ends of the plastic (metal) container were made of thin mylar (stainless) sheets 0.003 cm in thickness. The material of the container was chosen carefully so that a negative muon lifetime in the material was quite different from that in the target. When it was expensive or difficult to get a target in a simple substance form, chemical compounds which had a combination of small Z and large Z were chosen. For a decay electron spectrum of negative muons in such a chemical compound, short (large Z) and long (small Z) lifetime components were easily separated by a chi-squared minimization.

Since the ^{18}O target was made in Agar form, a ^{16}O target in the same form was used in order to compare the

Table II-2(1) List of Targets and Their Form

Z	Element (Isotope Ratio)	Form	Container Material	Size(cm)[1]	Owner[2]
3	Li-6 (95.6%)	Powder	SS	7.2Dx9.5	TINA
	Li-7 (98.2%)	Powder	SS	7.2Dx9.5	TINA
4	Be	Plate	Ni plated	13x13x0.7	UVIC
5	B-10 (96.2%)	Powder	Brass	6Dx1.3	TINA
	B-11 (97.2%)	Powder	Brass	6Dx1.3	TINA
6	C-12 (Natural)	Plate		10x10x2	TINA
	C-13 (99.9%)	Powder	Brass	2.5Dx5	Johnson
7	N	Liquid	SS	7.5Dx15	TINA
8	O-16 (H2O)	Water	Brass	9.5Dx5	TINA
	O-16 (H2O)	Agar		5x5x1	Johnson
	O-18 (98.5%H2O)	Agar		5x5x1	Johnson
9	F--LiF	Powder	Brass	9.5Dx5	TINA
	--C2F4	Plate		13x13x1.3	TINA
	--CaF2	Powder	Plastic	9.5Dx5	TINA
	--PbF	Powder	Plastic	9.5Dx4	TINA
11	Na	Rod	Plastic	9.5Dx7.6	TINA
12	Mg	Rod		3.8Dx7.6	TINA
13	Al	Plate		10x10x2	TINA
14	Si	Granular	Plastic	9.5Dx2.5	CHEM
15	P	Powder	Plastic	9.5Dx3.8	TINA
16	S	Powder	Plastic	9.5Dx3.8	TINA
17	Cl--CCl4	Liquid	Plastic	8x8x5	CHEM
19	K	Stick	Plastic	9.5Dx7.6	TINA
20	Ca	Granular	Plastic	9.5Dx5.0	TINA
22	Ti	Plate		10x8x0.5	TINA
23	V	Disk		5x4x0.5	UVIC
24	Cr	Granular	Plastic	6.0Dx1.5	CHEM
25	Mn--MnO2	Powder	Plastic	9.5Dx2.5	TINA
26	Fe	Plate		7x7x0.5	TOKYO
27	Co	Stick		0.5Dx5.0	TOKYO
28	Ni	Plate		5Dx1.0	TOKYO
29	Cu	Plate		10x10x0.5	TOKYO
30	Zn	Powder		6.5Dx7.5	CHEM
32	Ge--GeO2	Powder	Plastic	6.0Dx1.4	Warren
35	Br--NH4Br	Powder	Plastic	9.5Dx5	TINA
40	Zr	Plate		6x6x0.7	TOKYO
41	Nb	Plate		10x8x0.5	TINA
42	Mo	Plate		8x10x0.2	TOKYO
47	Ag	Plate		5x5x0.5	TOKYO
48	Cd	Plate		5x5x0.5	TOKYO
49	In	Plate		5x5x0.5	TOKYO
50	Sn	Plate		13x8x0.5	TINA

Table II-2(2) List of Targets and Their Form

Z	Element (Isotope Ratio)	Form	Container Material	Size(cm)[1]	Owner[2]
53	I	Powder	Plastic	9.5Dx2.5	TINA
56	Ba--BaO	Powder	Plastic	9.5Dx2.5	CHEM
60	Nd--NdO	Powder	Plastic	9.5Dx2.5	CHEM
64	Gd	Stick		0.5Dx5	TOKYO
66	Dy	Stick		0.5Dx5	TOKYO
68	Er	Stick		0.5Dx5	TOKYO
74	W	Powder	Plastic	6Dx1.4	CHEM
80	Hg--HgO	Powder	Plastic	9.5Dx2.5	TOKYO
82	Pb	plate		10x8x0.2	TINA
83	Bi	plate		10x8x0.5	TINA
* Other oxide targets for muon atomic capture experiment					
6	CO2(Dry Ice)	Solid		10x10x20	CHEM
11	Na2O2	Powder	Plastic	9.5Dx2.5	CHEM
12	MgO	Powder	Plastic	9.5Dx10	Warren
13	Al2O3	Powder	Plastic	9.5Dx2.5	CHEM
14	SiO2	Powder	Plastic	9.5Dx2.5	Warren
15	P2O5	Powder	Plastic	9.5Dx2.5	CHEM
20	Ca(OH)2	Powder	Plastic	9.5Dx2.5	Warren
22	TiO2	Powder	Plastic	9.5Dx2.5	Warren
24	Cr2O3	Powder	Plastic	9.5Dx2.5	TINA
	CrO3	Powder	Plastic	9.5Dx2.5	CHEM
29	CuO	Powder	Plastic	9.5Dx2.5	CHEM
30	ZnO	Powder	Plastic	9.5Dx2.5	CHEM
32	GeO	Powder	Plastic	6.0Dx1.3	Warren
48	CdO	Powder	Plastic	9.5Dx2.5	CHEM
50	SnO2	Powder	Plastic	9.5Dx2.5	CHEM
82	PbO2	Powder	Plastic	9.5Dx2.5	CHEM
	Pb3O4	Powder	Plastic	9.5Dx2.5	TOKYO

1) D=diameter
2) Owner, group and group leader:
   TINA--UBC Physics Dept., (D. F. Measday)
   CHEM--UBC Chemistry MSR Group, (D. Walker and D. Fleming)
   UVIC--U. of Victoria and TRIUMF, (M. Pearce)
   TOKYO-U. of Tokyo MSR Group, (T. Yamazaki)
   Johnson R.R.--UBC Pion Scattering Group Leader
   Warren J.B.--UBC Muon X-ray Group Leader

lifetimes in ^{16}O and ^{18}O targets of similar composition. A liquid nitrogen target container was specially designed to fit the cylindrical counter S5. It was made of stainless steel to reduce the heat conduction loss of liquid nitrogen. It had a vacuum space between the inner and the outer container. The two containers had thin windows made of 0.01 cm thickness stainless steel in order to reduce muons stopped in the windows. The ends of the two containers were made of 0.3 cm thickness stainless steel. This container was able to keep liquid nitrogen for a three hour experiment.

All targets were placed on the target holder at the center of counter S5. Since the target holder was one of the background sources, a plastic holder was used for the plastic container and a metal holder for the metal container. Hence the holder and the target container were counted as the same background source.

In long lifetime measurements for the light elements, it was important to know the carbon background in the histogram. In order to estimate the background, dummy targets which consisted of brass or copper with the same shape and thickness were used for boron and ^{13}C targets. In the case of beryllium and lithium targets, copper plates with the same thickness and size were used for the background runs. The empty liquid nitrogen target was used for the background runs of the nitrogen and oxygen targets.

In the case of the atomic capture experiments,

metallic oxide targets were enclosed in plastic containers with the standard size mentioned above. The carbon background of these targets was estimated from lifetime measurements of heavy elements (for instance Zn powder, S powder, etc) in the plastic container.

II.E Electronics and Timing Consideration

In our lifetime experiment, the MSR data taking system was employed. The system was explained in detail by Garner (GAR79). The simplified data taking system is shown in figure II-4. The main functicns of the system are described as follows

1. muon lcgic - identify muons stopped in a target and send start signals to a clock,
2. electron logic - determine a good electron associated with the stopped muon and send a stop signal to the clock,
3. rejection lcgic - find any event which satisfies the rejection logic,
4. clock - determine a time interval between the start and the stop signals,
5. CAMAC - store all information needed for processing data and send a LAM signal to activate a Microprogrammed Branch Driver (MBD),
6. MBD - control data taking system, read all information stored in CAMAC and send the information to PDP-11/40,
7. PDP-11/40 - process data stored in the MBD, record data on a disk file and renew

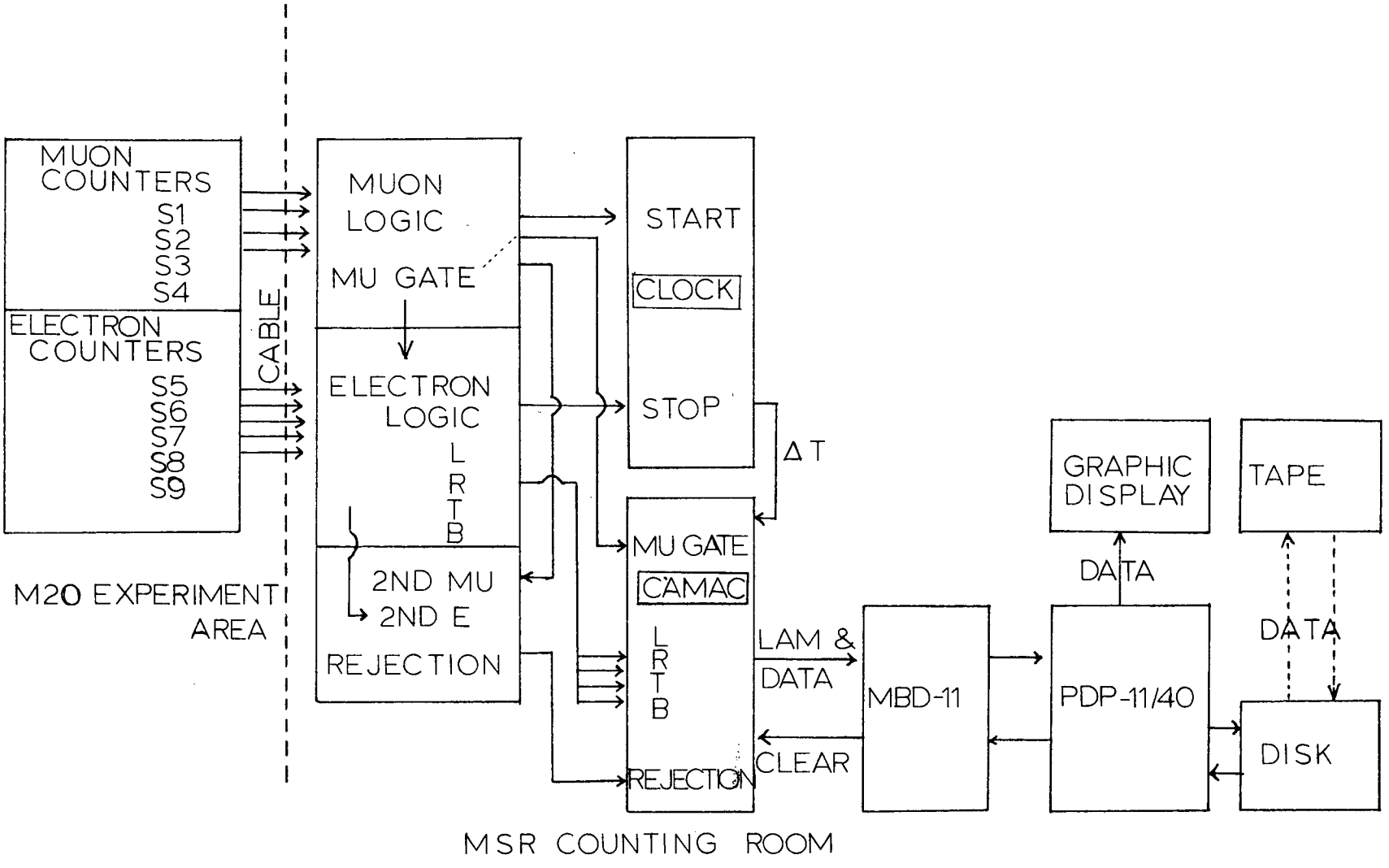

Figure II-4, Simplified MSR data taking system.

histograms on the graphic terminal,

8. magnetic tape - at the end of experiment, transfer data from the disk to tape to keep it permanently and tc analyze it offline.

Figure II-5 shows a schematics of the electronics for the muon, the electron and the rejection logics. Equipment names and meanings of symbols are listed in Table II-3. In figure II-6, timings and definitions of events are explained. Incident particles were determined by a (1,2,3) coincidence and stopped muons in the target by a (1,2,3,$\underline{4}$,$\underline{5}$) (=M) coincidence, where $\underline{4}$($\underline{5}$) means an anti-coincidence of counter S4(S5). The stopped muon signal opened a muon gate(G1) of a pile-up gate generator (PUG) which was dealing with 2nd-muons and pre-muons within 32(16) microseconds for a long(short) lifetime measurement. If there were no pre-muons ($\underline{G1}$), no pulse height rejections ($\underline{G2}$), no MBD busy signals ($\underline{MBD}$) and no protection gates ($\underline{G6}$), a good muon signal (M,$\underline{G1}$,$\underline{P2}$,$\underline{MBD}$,$\underline{G6}$) was sent to a gate generator to produce another muon gate (G4). Two muon gates, G1 and G4, were the same if there was a good muon event. The G1 gate was always created whenever muons stopped in a target and, if there was a 2nd-muon, the gate was stretched by the same length as the original muon gate length (32 or 16 microseconds). In this way, the G1 gate kept track of the stopped muons, while the computer was processing data, and made sure there were no pre-muons before accepting the next good muons. Since the G2 gate was created only by a good

Table II-3 Meanings of Symbols in Logic Diagram

Symbol	Name	Model
—∿∿∿—	Delay	
D	Leading Edge Discriminator	LRS-621BL
DL(DH)	Lower(Higher) Disc. level	LRS-621BL
C	Constant Fraction Discriminator	ORTEC-EGG 934
COI	Coincidence Logic	LRS-465
F	Logic Fan-In and Fan-Out	LRS-429
LF	Linear Fan-In and Fan-Out	LRS-428F
PUG	Pile Up Gate Generator	EGG-GP100/NL
GG	Gate Generator	LRS-222
S1-S9	Counter Name in Table II-1	
→○	Anticoincidence of Logic N	
○→	Inverted Output	
PH	Pulse Height Rejection	
RAW	Raw Electron without Coincidence of Muon Gate	
INC	Incident Mucn (1,2,3)	
ST	With Anti-Coincidence (1,2,3,4,5)	
G	Ordinary Gate from PUG or GG	
P	Pile Up Gate from PUG	
A1-A4	Telescope Identification Input	

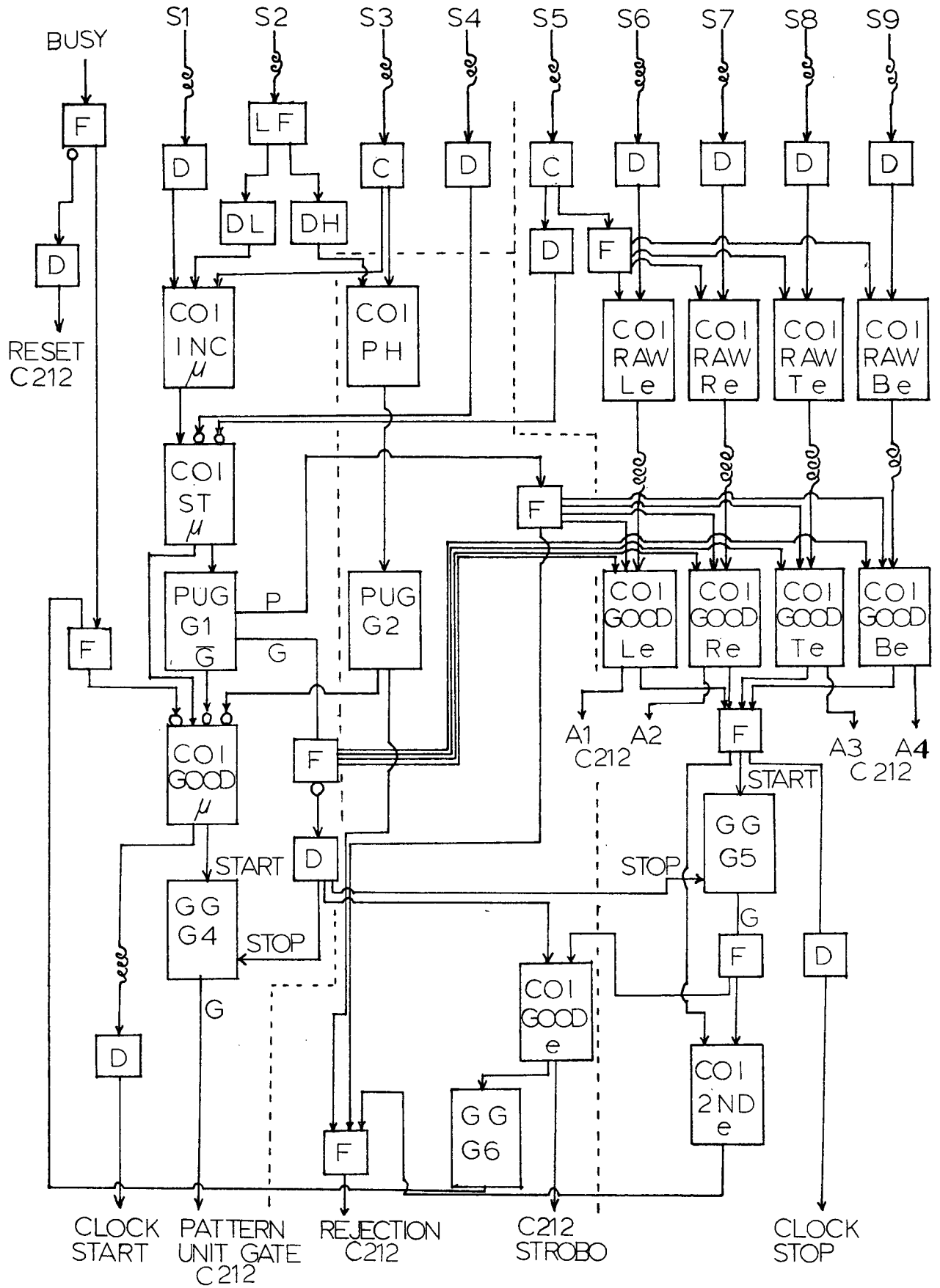

Figure II-5, Electronic logic.

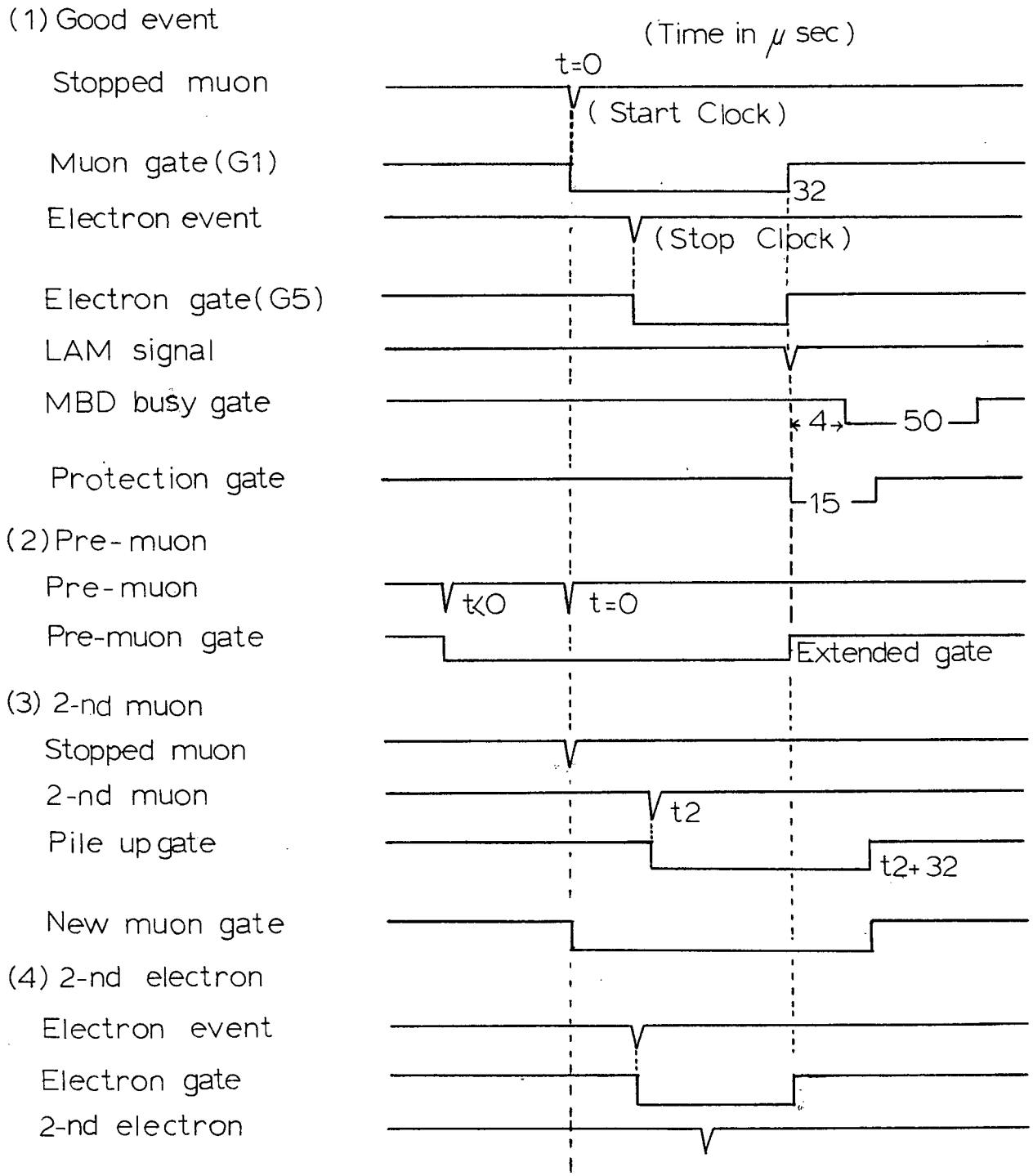

Figure II-6, Timings and difinitions of events.

muon and applied to a pattern unit gate on the CAMAC crate, the pattern unit was protected during the prccessing of data by the computer.

When there was a good muon signal, it was sent to a clock as a start signal. The timing of the start signal was determined by counter S3 whose counter output was fed into a constant fraction discriminator. This discriminator showed a smaller time jitter and better timing compared to a leading-edge type discriminator.

In the electron logic, the output cf counter S5 was fed into another constant fraction discriminator. This counter determined the timings of the four electron telescopes. When there was a good electron event within the muon gate, an electron gate (G5) was opened. Then, the good event signal was sent to a clock as a stop signal and a telescope identification bit in the pattern unit was set. Furthermore, at the end of the muon gate, a IAM signal was generated by a C212 unit mounted in the CAMAC crate and activated the MBD. On the other hand, if there was no good electron event within the muon gate, a clear pulse was generated to reset the pattern unit at the end of the gate.

Since it took about 4 microseconds for the MBD to produce the busy signal, the protection gate (G6) was created at the end cf muon gate to inhibit the clock and the muon logic. After the MBD was activated, the MBD busy signal was supplied from the CAMAC crate to inhibit the muon logic.

Two pile-up rejections and one pulse height rejection were employed. The definition of the pile-up rejection is given in figure II-6. The pile-up events of stopped muons and good electrons are named as 2nd-muons and 2nd-electrons, respectively. The 2nd-muons were determined by the pile-up of a (1,2,3,$\underline{4}$,$\underline{5}$) coincidence instead of the pile-up of a (1,2,3) coincidence. This pile-up logic was examined by comparing the positive muon lifetimes between the two different pile-up rejections. The test runs showed that, if there were too many rejections by the definition of pile up as (1,2,3), the positive muon life changed by 3 nano seconds at a muon rate of 1500/sec. The pile-up rejection was quite a serious problem in the lifetime measurements and will be discussed in Chapter III.

The pulse height rejection was made by the coincidence of counters S2 and S3 with S2 at a high discriminator level. In the output signal of counter S2 with 1.7 kV high voltage, the bright band of electrons (muons) was located from 30(250) mV to 150(600) mV. As mentioned in section II.B, all particles higher than 600 mV were considered as slow muons or double muons and were rejected. If this occurred, the gate G2 was generated to inhibit data taking for 16 or 32 microseconds. By this rejection, slow muons were mostly rejected, because the probability having two muons within 20 ns was extremely small for 1000 /sec muon stopping rate, which was the

standard stopping rate in this experiment.

If there were rejection events, rejection bits were set in the pattern unit and all information stored in the unit was ignored by soft-ware.

In the lifetime measurement, a clock was important to determine a time interval. Before the summer of 1979, only a TDC-100 clock was available and test runs of the system calibration were made by this clock. A new clock with a 1 GHz scaler was assembled by the TRIUMF electronics shop in the summer of 1979. At the beginning of the two week experiment in October, 1979, the two clocks were tested by measuring the positive muon lifetime. From the test, the new clock showed better agreement with the positive muon lifetime. Thus, in the series of lifetime measurements, the new clock was used. The linearity of the new clock was assured by the test with a time calibrator (ORTEC-650).

For convenience, the ultimate logic which was employed in this experiment is summarized in the following page.

Summary of Event Definitions

INCIDENT MUON (come into target region)--(1,2,3)

STOPPED MUON (stop in target)--(1,2,3,4,5)

START (GOOD MUON) (no premuon rejection)--(1,2,3,4,5,G1)

STOP (GOOD ELECTRON)--(5,6) or (5,7) or (5,8) or (5,9)

Event rejected if

PRE MUON--(1,2,3,4,5) within 16(32) microsec before START

2nd MUON--(1,2,3,4,5) within 16(32) microsec after START

TWO COINCIDENT (or SLOW) MUONS

--(2',3) with S2 pulse height > 600 mV

2nd ELECTRON--two STOPs within 16(32) microsec after START

Gate created by

STOPPED MUON (Pile up gate)--G1 (MUON gate 16 or 32 microsec)

TWO COINCIDENT (or SLOW) MUON (Pile up gate)--G2

GOOD MUON (normal gate)--G4 (gate for pattern unit)

GOOD ELECTRON (normal gate)--G5 (ELECTRON gate)

End of G1 + G5--G6 (protection of muon logic)

Note:

32(16) microsecond gate was used for measurments of lifetimes longer(shorter) than 300 ns.

2 means the discriminator level is 35 mV (DL in figure II-5).

2' means the discriminator level is 600 mV (DH in figure II-5).

II.F Running Procedure and Run Record

There was a two-week break between two experiments each of one week duration. At the beginning of the first week , the experiment was done in the following steps:

1. The M20 beam line was set for positive muons.
2. Discriminator levels and high voltages of counters were adjusted and electronics logics were checked.
3. The positive muon lifetime measurement was made with the TDC-100 and the new clock built at TRIUMF. After comparing the results, the new clock was employed for the series of experiments. Since the electronic logic for the new clock was different from the old logic created for the TDC-100 clock, the development of the new logic (LAM signal, protection gate, rejection scheme, etc) took three days (1/3 of our beam time).
4. In order to calibrate the system, the positive muon lifetime was measured with different conditions of rejection schemes and beam rates. The magnetic field effect was examined by stopping positive pions in a target.
5. The M20 beam line was set for negative muons.
6. At the beginning of the negative muon lifetime measurements, the negative muon lifetime in carbon was measured and this was repeated once a day as a calibration during the lifetime measurements.

7. Targets were changed after enough events and the muon gate was adjusted so that a long (short) lifetime measurement had a 32(16) microsecond gate. For the long lifetime measurements of light elements, the carbon background runs were made for each target.
8. At the end of the first one week run, all data were transfered from a disk file to a magnetic tape for an offline analysis.

After the one week break, the experiment followed the procedure as stated above except step 3. Normally one run took two hours. Numbers of stopped muons, good muons and accepted electrons in histograms are listed in Table II-4.

Table II-4(1) Run Records (Total Events)

Z	Element	Inc Mu	Stop Mu	Tot E	Accepted E
		x10^6	x10^6	x10^3	x10^3
3	Li-6	14.4	12.1	5,630	4,580
	Li-7	17.7	14.7	6,800	5,900
4	Be	4.6	4.1	2,024	1,531
5	B-10	8.1	4.1	1,312	1,100
	B-11	8.8	4.0	1,210	1,023
6	C-12	3.6	2.9	1,320	1,100
	C-13	5.5	2.5	820	570
7	N	5.7	5.6	1,640	1,230
8	O-16	9.0	8.7	2,780	2,236
	O-16(Agar)	10.0	3.9	1,170	956
	O-18(Agar)	8.3	3.2	1,060	885
9	F-LiF	7.3	4.9	1,940	1,550
	-C2F4	3.6	2.9	1,019	842
	-CaF2	3.1	2.5	500	410
	-PbF	5.8	5.0	470	370
11	Na	4.7	4.2	1,290	1,050
12	Mg	8.9	8.7	2,090	1,640
13	Al	5.9	5.1	860	740
14	Si	3.2	2.7	506	420
15	P	5.7	4.7	815	620
16	S	5.6	4.9	710	550
17	Cl-CCl4	3.9	3.7	614	505
19	K	4.3	3.6	510	425
20	Ca	4.7	4.2	550	454
22	Ti	5.5	4.1	365	310
23	V	6.8	2.9	300	250
24	Cr	4.5	3.8	299	254
25	Mn-MnO2	4.2	1.8	490	430
26	Fe	3.8	3.6	103	74
27	Co	6.6	4.7	261	210
28	Ni	3.2	2.9	105	84
29	Cu	3.2	2.7	175	121
30	Zn	4.2	3.9	165	112
32	Ge-GeO2	4.4	2.6	662	490
35	Br-NH4Br	3.2	2.9	503	392
40	Zr	---	---	---	573
41	Nb	4.5	3.4	176	150
42	Mo	4.1	3.4	180	152
47	Ag	3.5	1.7	97	79
48	Cd	4.5	2.5	142	113
49	In	4.4	2.0	160	130

Table II-4(1) Run Records (Total Events)

Z	Element	Inc Mu	Stop Mu	Tot E	Accepted E
		x10^6	x10^6	x10^3	x10^3
50	Sn	2.4	1.6	110	88
53	I	5.5	4.9	217	179
56	Ba-BaO	4.3	3.7	402	323
60	Nd-NdO	5.8	2.2	591	447
64	Gd	3.9	2.5	132	106
66	Dy	4.5	3.5	230	195
68	Er	4.8	3.9	158	134
74	W	3.8	2.9	199	169
80	Hg-HgO	6.0	5.2	427	333
82	Pb	4.1	3.4	118	95
83	Bi	3.1	2.0	137	109
* Other oxide targets for muon atomic capture experiment					
6	CO_2	4.0	3.4	1,487	1,182
11	Na_2O_2				
12	MgO	3.2	2.9	913	718
13	Al_2O_3	4.6	4.2	1,421	1,113
14	SiO_2	2.2	1.0	343	278
15	P_2O_5	4.7	3.4	1,232	989
20	$Ca(OH)_2$	4.3	3.8	1,129	891
22	TiO_2	3.4	2.2	589	451
24	Cr_2O_3	3.9	3.5	696	548
	CrO_3	5.5	5.1	1,195	935
29	CuO	1.6	1.3	141	111
30	ZnO	3.5	2.7	463	362
32	GeO	6.1	3.7	993	735
48	CdO	11.6	9.7	1,553	1,214
50	SnO_2	5.6	5.0	1,015	776
82	PbO_2	4.6	3.8	439	342
	Pb_3O_4	3.5	3.0	238	188

CHAPTER III

Data Analysis

III.A Data Analysis Procedure

All data analysis was performed on the UBC Amdahl 470 V/6 computer. A computer program called MINUIT (JAM71), which was developed at CERN, was used for a chi-squared minimization.

Two fitting procedures were employed. In the case of the chi-squared minimization fitting of a positive muon histogram, three parameters: lifetime, amplitude, and background were searched for the entire spectrum, since the fitting was done very quickly for three parameters. In the case of a negative muon histogram, there were more than four parameters to fit and more events appeared at earlier times due to the nuclear capture. Therefore, the background was fitted first by MINUIT for the tail of each histogram. Then, the background was fixed and other parameters for several elements were found for the front part of the spectrum.

Figure III-1 shows a typical positive muon decay curve. After 26 microseconds, there are only background events. A ratio of the background to the amplitude at T=0 (B/N(0)) is roughly equal to 3×10^{-4}. These background events came mainly from random coincidences with charged

particles scattered around in the M20 counting area. There were also some backgrcund events from cosmic rays. The experiment made at Saclay (DUC73) was affected only by the cosmic ray background events. This was because there was no incoming beam for 500 microseconds after every beam bunch due to the special beam structure of Saclay's Electron Linac. The B/N(0) ratio of Saclay's experiment was equal to $3x10^{-5}$, which is smaller than our ratio by a factor of 10. There was also an experiment by Balandin (BAL75), who built a Cerenkov detector with a 4 π solid angle. Their B/N(0) ratio was equal to $1x10^{-4}$. Since the solid angle of our detector was about 2 π radians and the beam repetition rate was 23 MHz, the B/N(0) ratio of figure III-1 seems satisfactory when ccmpared to the other good measurements mentioned abcve.

Figure III-2 shows the negative muon experiment in Cr_2O_3. After 16 microseconds, there are only background events. As mentioned above, in the fitting cf this spectrum, the background was found from the flat section between 20 and 30 microseconds. Then the spectrum between 0 and 12 microseconds was fitted for the chromium lifetime, and the chromium, oxygen, and carbon amplitude, keeping fixed the amplitude cf the backgrcund as well as the lifetimes of oxygen and carbon.

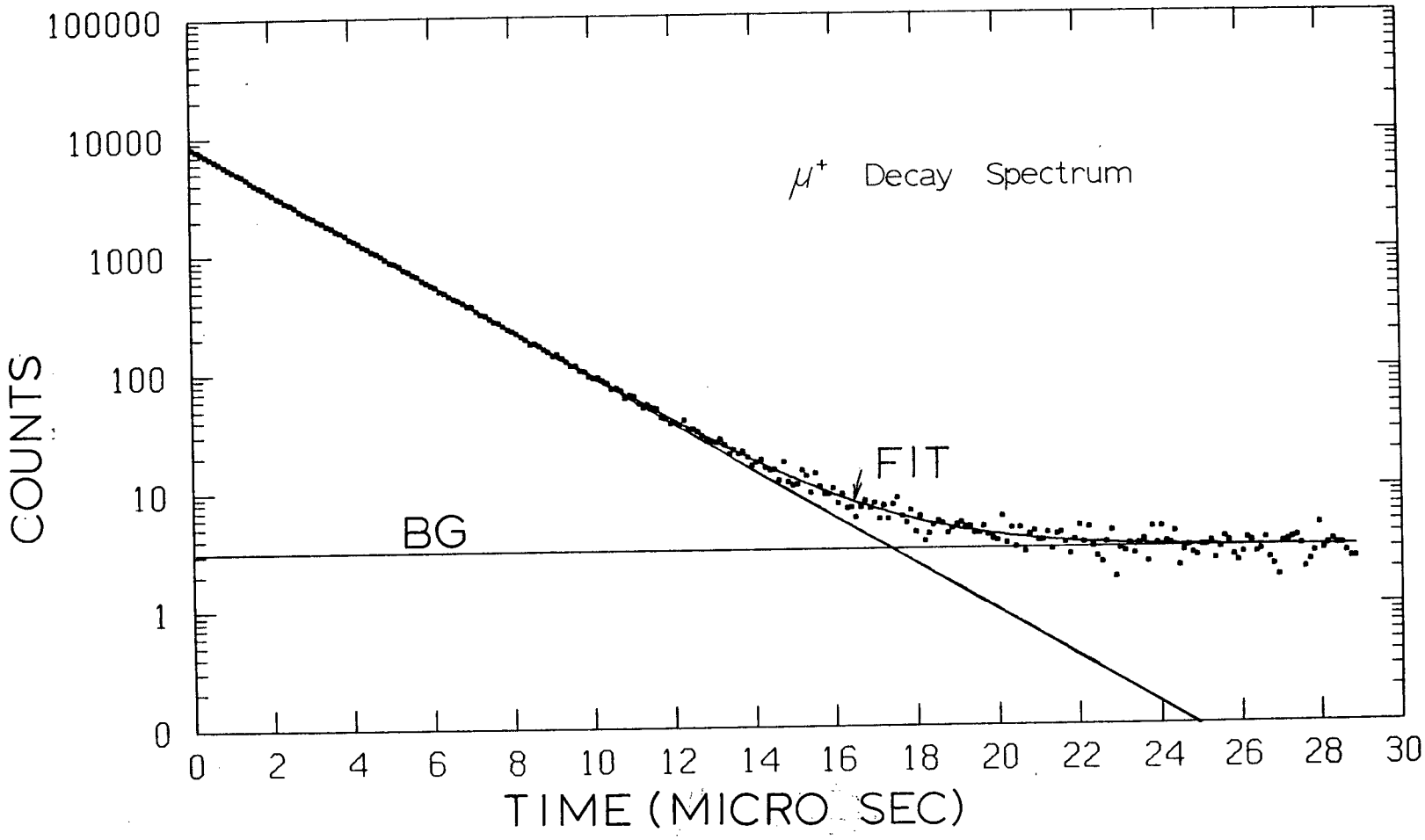

Figure III-1, Positive muon decay curve.

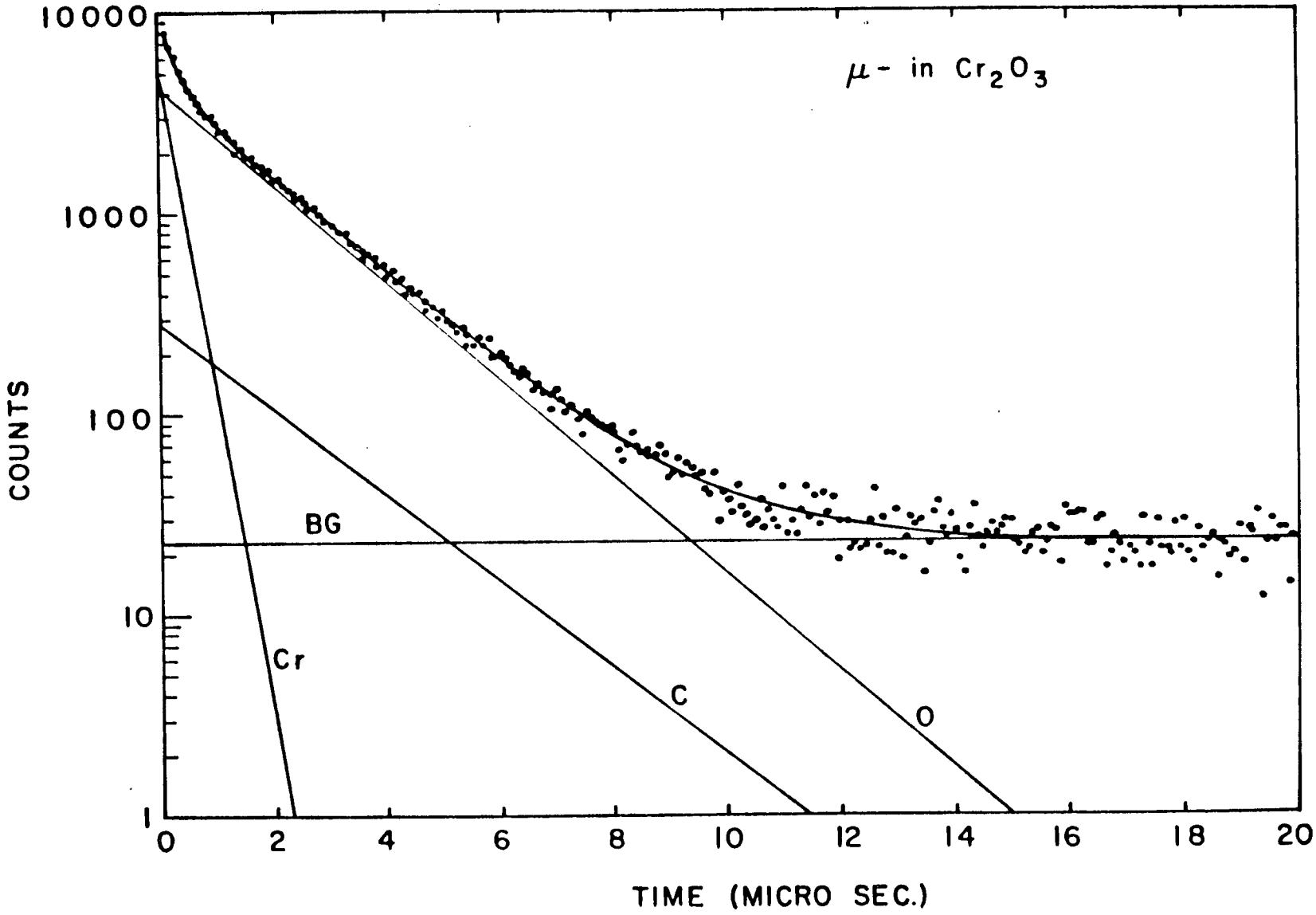

Figure III-2, Negative muon decay curve in Cr_2O_3.

III.B Magnetic Field Effect

The time intervals between the start signals from the muon stops in the target and stop signals from decay electrons were recorded as a histogram. In the case of positive muons, the histogram shows a lifetime of 2.2 microseconds. Without a magnetic field effect, the histogram shows a decay curve which is simply expressed as

$$N(t)=N(0)\cdot\exp(-t/Tm) + Bg \qquad (3.1)$$

where Tm is the lifetime of positive muons, Bg the time independent background and N(0) the amplitude at t=0.

If there is not a strong depolarization of muons and if the target is under the influence of a magnetic field, equation (3.1) must be modified due to the muon precession. The new equation is given by

$$N(t)=N(0)\cdot\{1 + A\cdot\cos(wt+p)\}\cdot\exp(-t/Tm) + Bg \qquad (3.2)$$

where A,w and p are an asymmetry, an angular frequency and a phase, respectively. In our positive muon lifetime measurement, carbon, which does not show any muon depolarization (SWA58), was used as a target. If a highly polarized muon does not show any depolarization in a target, the asymmetry A is close to 0.33. In the target region of

our experimental set-up, the magnetic field was quite small because of Mu metal shielding, as discussed in section II.C. Under a small magnetic field, like 0.05 G, positive muons with a 100% polarization precess by 0.09 radians (5 degrees) within 10 muon lifetimes. This precession affects the apparent muon lifetime and the following approximation can be made

$$Tm = Tm(0) \cdot \{1 \pm A \cdot w \cdot Tm(0) + 0.5 \cdot (A \cdot w \cdot Tm(0))^2\} \qquad (3.3)$$

where + (-) sign can be applied to the left(right) detector or vice versa. With A=0.33, w=85,500•0.05/sec for 0.05G and Tm(0)=2.2 microseconds, the first order distortion has a 0.3% effect, which changes the lifetime by 7 ns. Since four electron telescopes were arranged symmetrically, as discussed in section II.B, the average of the four lifetimes cancels the first order distortion and the average lifetime has a negligible second order effect.

In order to check the magnetic field effect, pions were stopped in a target as if they were positive muons. Since pions stopped in the target are ideal unpolarized muon sources, no difference in lifetimes among the electron telescopes is expected. In this case, the distribution of decay electrons is given by

$$N(t) = Np(0) \cdot \frac{\{\exp(-t/Tp) - \exp(-t/Tm)\}}{(Tp - Tm)} + Bg \qquad (3.4)$$

where Tm(Tp) is the muon(pion) lifetime. After 10 pion lifetimes (=260 ns), the contribution from the pion decay becomes negligible and, then, equation (3.4) shows the same decay curve as equation (3.1).

In Table III-1, the lifetimes of four electron telescopes for 10 runs are listed. The summary of the table is as follows.

Beam	Error	Counters L and R	T and B
Muon Beam	Standard deviation of each electron telescope from the average lifetime	6.4 ns	5.0 ns
	Statistical error	4.4 ns	4.4 ns
	Magnetic field effect by a quadratic relation	4.6 ns	2.4 ns
Pion beam	Standard deviation	1.4 ns	3.0ns
	Statistical error	4.4 ns	4.4 ns
	Magnetic field effect	0.0 ns	0.0 ns

Consequently, the distortion of the muon lifetime due to the magnetic field is roughly 4.6(2.4) ns for the left-right (top-bottom) electron telescopes and the distortion corresponds to 0.03(0.02) G. Since the magnetic field measurement with a flux meter (Hewlett Packard Model 428 BR) showed the field to be between 0.02 and 0.05 G near the center of the target, the average field from the lifetime distortion seems to be in good agreement with the field measurement.

Table III-1 Positive Muon Lifetimes of Four Electron Telescopes

(in nanosec)

	Left	Right	Top	Bottom	Average
	2202.7 (4.4)	2193.4 (4.4)	2204.3 (4.4)	2192.1 (4.4)	2198.1 (2.2)
	(+4.6)	(-4.7)	(+6.2)	(-6.0)	
	2211.3	2188.8	2195.7	2187.2	2195.8
	(+5.5)	(-7.0)	(-0.1)	(-8.6)	
	2193.3	2194.3	2202.7	2195.4	2196.4
	(-3.1)	(-2.1)	(+6.3)	(-1.0)	
	2191.8	2203.6	2199.4	2197.7	2198.1
	(-6.3)	(+5.5)	(+1.3)	(-0.4)	
	2188.3	2200.0	2197.4	2195.1	2195.2
	(-6.9)	(+4.8)	(+2.2)	(-0.1)	
	2202.4	2191.2	2201.6	2198.5	2198.4
	(+4.0)	(-7.8)	(+3.2)	(+0.1)	
	2202.9	2191.7	2203.7	2190.1	2197.1
	(+5.8)	(-5.4)	(+6.6)	(-7.0)	
	2201.7	2193.4	2202.9	2188.4	2196.6
	(+5.1)	(-3.2)	(+6.3)	(-8.2)	
*	2197.8	2197.2	2195.8	2202.6	2198.4
	(-0.6)	(-1.2)	(-2.6)	(+4.2)	
*	2197.3	2196.8	2192.0	2195.4	2195.4
	(+1.9)	(+1.4)	(-3.4)	(0.0)	
					2197.0 (0.7)

1) All positive muon lifetimes were measured in the carbon target.

*) These data were taken by stopping pions in the target.

( ) shows the deviation from the average.

We wish to emphasize that the negative muon loses its polarization while it cascades down in the muonic atom. As discussed in section I.D, the residual polarization is always less than 20% of the initial. Thus for the lifetime measurements of negative muons the error in the lifetime due to this effect would be about 1 ns even if we had used a single telescopes whereas in fact the results are always an average of all four telescopes. (On a few occasions one or two of the histograms were lost due to faulty data transfer etc; in these cases the measurement was repeated and none of the partial data were used.)

III.C Muon Stopping Rate Effect

If the bad event rejection discussed in section II.E is not working properly, the muon lifetime determined tends to be shorter for a higher stopping rate. In figure III-3, the rate effect on the positive muon lifetime is shown for the two following experiments:

(a) with a good rejection scheme which is the final electronics logic,

(b) without rejection of bad events which come later than a stop signal into the target by about 8 microseconds or longer.

Before the final electronics logic was completed,

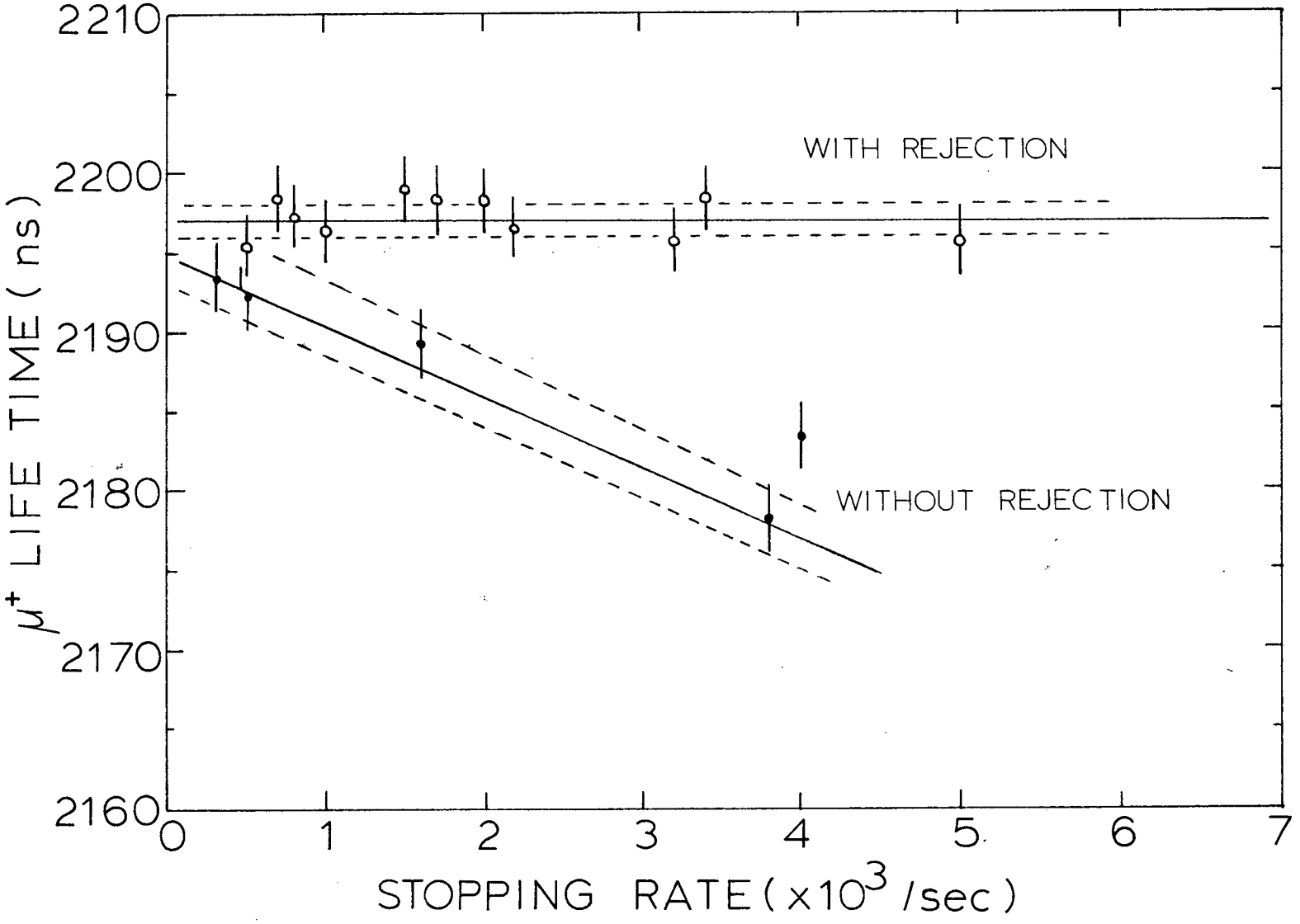

Figure III-3, Stopping rate dependence with and without rejections.

the LAM signal was produced by a TDC-100 clock 4 microseconds after an electron stop event. It took another 4 microseconds for the pattern unit to be read by the MBD (the electronics logic has been given in section II-E). Actually, in order to check 2nd muons or 2nd electrons within a muon gate, the LAM signal had to be generated at the end of the gate 32 microseconds after a good muon start. Since, in the case of (b), the LAM signal came earlier than the signal produced at the end of the gate, there was no proper rejection between the two signals. Figure III-3 shows the strong rate dependence of the muon lifetime without the good rejection scheme. On the other hand, there is no systematic rate dependence up to 5000/sec with the good logic.

The Russian group (BAL75) measured accurately the positive muon lifetime with a 7000/sec stopping rate and they obtained the same result as the Saclay group (DUC73) whose stopping rate was about 1500/sec. In this experiment, the muon rate was varied only in the positive muon life time measurements so as to investigate the rate dependence. In the case of negative muon lifetime measurements, the rate was kept below 1000/sec which was the safe rate to avoid the muon stopping rate effect. This was also the maximum negative muon beam rate with a 2.5 cm diameter collimator and a 20 micro-ampere proton current on a beryllium production target.

III.D 2nd Muon Rejection

Without proper rejections of bad events, there is a distortion in the histogram as discussed in the last section. In order to examine the distortion, the chi-squared minimization analyses were made for several different initial times (T1) of the histogram. The end of the analyses was fixed at 30 microseconds. Thus, the analyses were taken between T1 and 30 microseconds. Figure III-4 shows the lifetime dependence on the initial time T1 for the following three cases:

(a) with the good rejection scheme, same as III-B (a),

(b) without rejection of bad events, same as III-B (b),

(c) with the good rejection scheme in which 2nd muon rejections are generated by the incoming beam.

According to the summary of the ultimate logic described in section II.E, in the final logic, there are four rejections: the 2nd muon, the 2nd electron, the pulse height and the pre-muon rejections (see figure II-6 for the definitions). In this logic, the 2nd muon signal is generated by the stopping muon events (1,2,3,4,5). Alternatively the 2nd muon signal can be produced by the incoming beam (1,2,3) instead of the stopping muon events. Let us discuss in some detail this choice of rejection logic which may seem bizarre. In a typical run with the 2nd muon rejection by the incoming beam, there were 8.6×10^6 incoming muons through

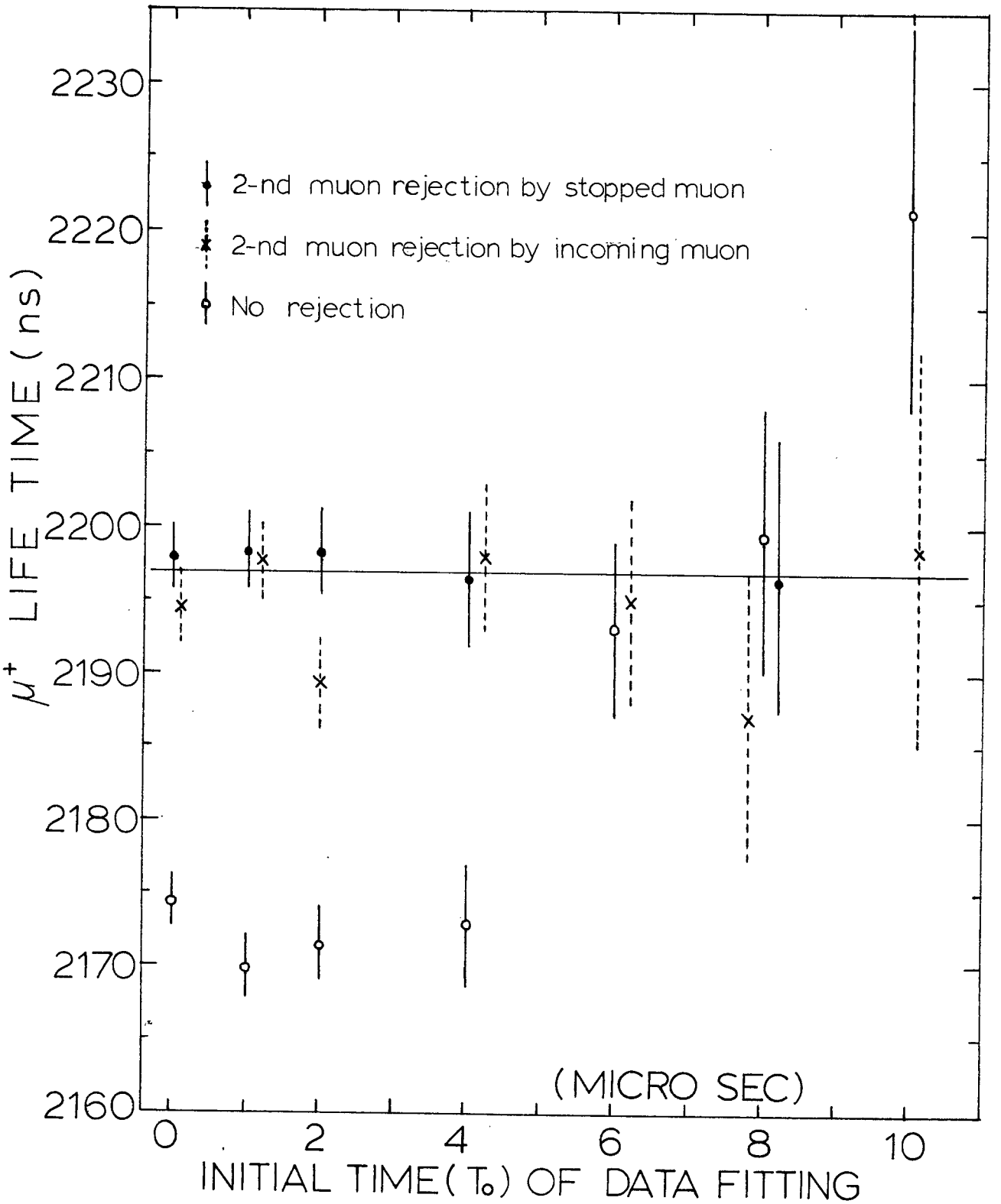

Figure III-4, Lifetime distortion in positive muon decay curve.

the lead collimatcr, 0.4×10^6 2nd muon signals were generated, and 6.4×10^6 (74%) muons stopped in the target. If the 2nd muon signal had been produced from the stopped muons, 0.25×10^6 2nd mucn signals would have been generated. Producing the 2nd muon rejection signals from the incoming beam, there was an extra 0.15×10^6 rejections. This was about 6% cf 2.4×10^6 electron events accepted in the histogram.

In principle, 2nd muon rejection by the incoming muons seems better than the rejection by the stopped muons in a target, because the former rejection does not allow any two mucns ccming into the target area within the muon gate. Since a large number of particles in the incoming beam (26% in the typical case shown above) go through the target and are detected by veto counters (S4 and S5), most of these muons may not affect the spectrum as 2nd muons. Thus, if the incoming beam is used for the 2nd muon rejection, many good events are unnecessarily rejected. This caused a lifetime distortion by 3 ns (=0.015% distortion).

If there is no proper rejection of bad events (figure III-4 b), there is a large distortion. The lifetime is shorter in front of the spectrum and longer in the tail.

III.E Distortion from Counter Efficiency and Dead Time of Electronics

The efficiencies of counters are listed in Table II-1. Since the (1,2,3) coincidence which monitors the incoming beam has 99.4% efficiency, 0.6% of incoming muons would not be detected even if they stopped in the target. These muons can be considered as undetected 2nd muons and so cause a distortion problem. In order to find the degree of the distortion, an empirical approach can be applied.

Figure III-4 shows the stopping rate dependence of lifetime with and without rejections. Since undetected and detected muons follow a Poisson distribution, the distortion due to undetected muons can be estimated by

$$Tdis = DT \cdot \frac{\text{Poisson distribution of undetected muons within twice the time of the muon gate}}{\text{Poisson distribution of stopping muons within twice the time of the muon gate}}$$

$$= DT \cdot \frac{(1-E)\cdot N\cdot 2\cdot Tm\cdot \exp\{-(1-E)\cdot N\cdot 2\cdot Tm\}}{N\cdot 2\cdot Tm\cdot \exp(-N\cdot 2\cdot Tm)} \qquad (3.5)$$

where DT= empirical lifetime distortion,

E = counter efficiency,

N = stopping muon rate,

Tm= muon gate (32 microseconds).

At 5000/sec stopping rate, the lifetime distortion with no rejection is about 25 ns, from figure III-4, and from equation (3.5), the distortion due to undetected muons is 0.2 ns for a 99.4% counter efficiency. However only 25% of undetected muons contribute to the distortion because of the 2nd electron rejection by the electron telescopes with the 2 π radian solid angle. Considering that the counter efficiency of 99.4% was measured with a ruthenium 4 MeV electron source and the efficiency for muons was better than that for electrons, the distortion due to undetected muons was less than 0.05 ns. So it was negligible at or below the 5000/sec stopping rate used.

If two muons came into the target region within 10 ns, the pulse height rejection could eliminate the event from a histogram. However, if the second muon came after more than 10 ns but less than the electronics dead-time (about 60 ns for a counter output), the pulse height and the 2nd muon rejection could not reject the event. Incident muons were monitored by counters S1, S2 and S3, and the 2nd muon signal was generated by a pile-up gate generator (PUG). Thus, the dead times of a LRS-621BL leading edge type discriminator (S1 and S2), an ORTEC-934 constant fraction discriminator (S3) and an EGG-100 (PUG) must be considered. From the dead time measurements, the LRS-621BL showed a dead time of 60 ns, the ORTEC-934 40 ns and the EGG-100 18 ns. Consequently, the dead time in the determination of the 2nd muon rejection was 60 ns. Even with this system, more than

50% of two muons within 30 ns can be rejected. In order to find the probability of two muons within 60 ns, the Poisson distribution can be applied and, for 5000/sec stopping rate, the probability is 2.5×10^{-4}. Also, this effect can be estimated by equation (3.5). It changes the lifetime by one part in 10^5 and the effect on the lifetime distortion is negligibly small.

III.F Analysis of Negative Muon Lifetime

The procedure for the analysis of the negative muon lifetime has been discussed in section III.A for Cr_2O_3. In the negative muon lifetime measurements, the muon stopping rate was kept below 1000/sec and the systematic distortion caused by the rate was negligible as shown in the former section. Since the negative muons lose their polarization quickly in the mesonic atom stage, the magnetic field effect discussed in section III.B is small. For example, from the bound muon decay experiment discussed in section I-C, the residual polarizations of negative muons in carbon and titanium were 15% and 5%, respectively.

The main cause of the systematic error in the negative muon lifetime measurement of light elements (Li, Be, B, N, O) is the carbon background. The main carbon backgroumd source is the defining counter S3. Also, the

light guide of cylindrical counter S5, and wrapping tapes of counters S4 and S5 can be carbon background sources. The carbon background depends on the target size and its thickness. Therefore, carbon background runs were made after every muon lifetime determination in a light element by using a duplicated target made of brass. In the lifetime fitting of the light element, the carbon background was subtracted using the result of the background run. In Table III-2, the fitting results are listed. The carbon corrections have changed the lifetimes by a few ns for the case of small correction. The uncertainty of the carbon background determination is also taken into account as shown in Table III-2.

As mentioned in section II-D, powder targets were enclosed in containers. There were chemical compound targets as listed in Table II-2. In the lifetime fitting of the decay electron spectrum from the powder or the chemical compound target, the contribution from the elements of container materials and chemical compounds must be included in the fitting equation. Thus, figure III-2 is fitted to the following equation

$$Ne(t) = A(Cr) \cdot \exp\{-t/T(Cr)\} + A(O) \cdot \exp\{-t/T(O)\} + A(C) \cdot \exp\{-t/T(C)\} + Bg \qquad (3.6)$$

where A and T are the amplitude and the lifetime of each element (Cr, O, C). In this fitting, T(C) and T(O) are

Table III-2 Carbon Background Effect in Light Elements

	Lifetime without C Background	% of C Background	Lifetime with C Background
Li-6	2175.9 ± 1.5 nsec	1.0 (±0.5) %	2177.0 ± 2.0 nsec
Li-7	2186.9 ± 1.5	1.0 (±0.5)	2188.3 ± 2.0
Be	2160.8 ± 1.3	1.5 (±0.5)	2162.0 ± 2.0
B-10	2067.0 ± 2.0	7.5 (±1.0)	2070.7 ± 3.0
B-11	2089.6 ± 2.0	7.5 (±1.0)	2096.1 ± 3.0
C-13	2028.1 ± 3.0	6.8 (±1.0)	2029.1 ± 3.0
N	1909.1 ± 2.0	1.6 (±0.5)	1906.8 ± 3.0
O (H2O)	1799.6 ± 1.3	1.6 (±0.5)	1795.4 ± 2.0
O-18	1865.4 ± 3.0	13.0 (±2.0)	1844.0 ± 4.5

1) The numbers in parentheses are the estimates of the uncertainty in the carbon background.

fixed. Although there is also hydrogen in the plastic counter and container, the hydrogen component in the decay curve is negligible. This is because of the high transfer rate of negative muons from hydrogen to heavy elements. A recent discussion of this phenomenon is that of Vitale (VIT80). As confirmation we note that Zinov et al. (ZIN64) studied the absolute intensity of muonic K series X-rays from a hydro-carbon (CH_2) and pure carbon, and obtained $A(CH2)/A(C) = 0.996 \pm 0.007$. Their result has indicated the almost complete transfer of the negative muon from hydrogen to carbon in CH_2. Due to this fast transfer, the hydrogen amplitude is also negligible in a decay curve of H_2O target.

In order to determine the negative muon lifetimes, the weighted average of four lifetimes, obtained by the fitting of decay electron spectra from four electron telescopes, is taken , using the weights supplied from the MINUIT program.

III.G Hyperfine (hf) Effect in a Decay Curve

In section I.D the hf effect in nuclei has been discussed. This section explains how the effect is obtained by detecting decay electrons. Muons in the K orbit of the muonic atom have their own spin coupled to the nuclear spin resulting in two hf states. At t=0, the time of their arrival in the K orbit, the muons populate the two states

statistically and then undergo the hf transition from the higher level to the lower level. The conversion rates have been calculated by Winston (WIN63) for various nuclei. His results are listed in Table IV-6 along with past experimental results. In a histogram of decay electrons, there is an effect from this conversion and this is not negligible for flucrine in particular. This will be discussed in section IV.D.

Figure III-5 shows the hf doublet and the definitions of Rh, R^+, R^- and D. At t=0, muons populate the F^+ and F^- states statistically as follows

$$n^+ = (I+1)/(2I+1)$$
$$n^- = I/(2I+1) \qquad (3.7)$$

The muon populations $N^+(t)$ and $N^-(t)$ of F^+ and F^- states are determined by

$$\frac{d}{dt} N^+(t) = -(Rh + R^+) \cdot N^+(t) \qquad (3.8\text{-}1)$$

$$\frac{d}{dt} N^-(t) = Rh \cdot N^+(t) - R^- \cdot N^-(t) \qquad (3.8\text{-}2)$$

The time spectrum of decay electrons, Ne(t), is given by

$$Ne(t) = Rd \cdot \{N^+(t) + N^-(t)\} \qquad (3.9)$$

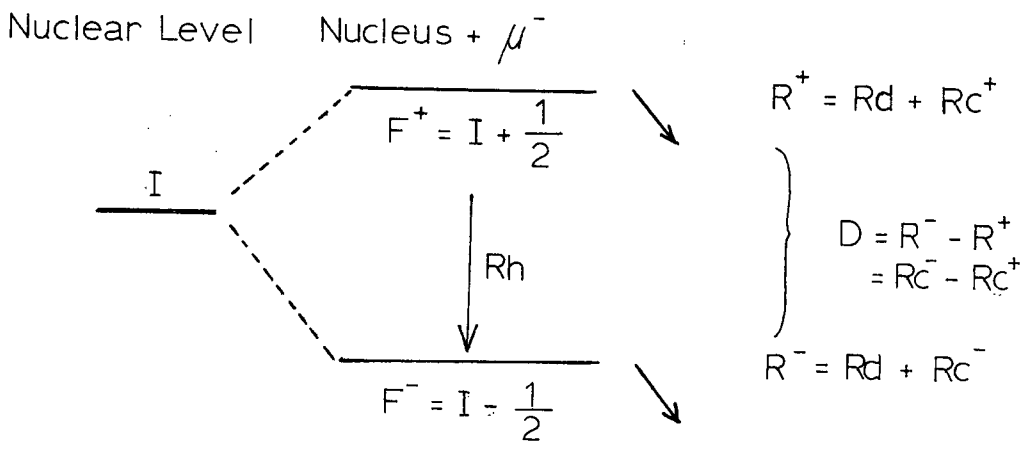

Figure III-5, Hyperfine doublet of muonic atom. Rh is conversion rate, Rc capture rate, Rd decay rate, and R total disappearance rate. The +ve(-ve) sign shows the rate from F=I+1/2 (F=I-1/2) state.

Since Rh>>D for most nuclei (WIN63), from equations (3.8) and (3.9), we have the simple form

$$Ne(t)=const\cdot\{1 - Ae\cdot\exp(-Rh\cdot t)\}\cdot\exp(-R^{-}\cdot t) \qquad (3.10)$$

$$Ae=n^{+}\cdot D/Rh. \qquad (3.11)$$

Since I=1/2 and D/Rh=0.02 for ^{19}F (WIN63), the hf effect Ae is equal to 0.015, which is quite a small effect.

In the case of a nucleus which has the hf effect, equations (3.6) and (3.10) are combined to yield the following equation

$$Ne(t)=Bg + A(1)\cdot\exp(-t/T(1)) + A(2)\cdot\exp(-t/T(2)) + A(3)\cdot\exp(-t/T(3))\cdot\{1 - A(4)\cdot\exp(-Rh\cdot t)\} \qquad (3.12)$$

This is used for the chi-squared minimization. The average capture, (Rc)av, and total disappearance rates of the hf doublet, (Rt)av, are defined by

$$(Rc)av=n^{+}\cdot Rc^{+} + n^{-}\cdot Rc^{-} \qquad (3.13)$$

$$(Rt)av=n^{+}\cdot R^{+} + n^{-}\cdot R^{-} \qquad (3.14)$$

$$T = 1/(Rt)av \qquad (3.15)$$

where T is the mean life. These equations will be applied in section IV.D.

The measurements of capture events (neutrons or gamma rays) is suitable for experiments on the hf effect in

muon capture (WIN61). In the capture process, Ae in equation (3.10) is replaced by An which is given by

$$An=n^{+}\bullet D/Rc^{-} \qquad (3.16)$$

From equations (3.11) and (3.16),

$$An=Ae\bullet(Rh/Rc^{-}) \qquad (3.17)$$

For most nuclei, $Rh>>Rc^{-}$, thus, the capture event measurements show a large hf effect. In the case of ^{19}F,

$$An=25\bullet Ae$$

and the large enhancement of the hf effect has been observed in the neutron and gamma ray measurement (WIN63).

CHAPTER IV

Experimental Results and Discussions of Lifetime Measurements

Our results for lifetimes and capture rates of negative muons in complex nuclei are listed in Table IV-1. In Table IV-2 past measurements are shown along with our results listed in Table IV-1. In our calculation of capture rates, our result of the positive muon lifetime, 2197.0 ± 0.7 ns, and the Huff correction factor of the bound muon decay are employed. In this experiment, the accuracy of the lifetime measurement has been improved for many light elements (Be, B, N, O, F, Na, Cl, K) and new measurements have been made for ^{13}C, ^{18}O, Dy and Er. Many past measurements had systematic errors, especially for the positive muon lifetime which was many standard deviations away from the currently accepted value. The systematic error of our system has been studied carefully, as discussed in Chapter III, and the correct positive muon lifetime has been obtained as shown in the following section IV.A.

Table IV-1(1) Results of Lifetime Measurements in This Experiment

Z	Element	Mean Life (ns)	Capture Rate ($\times 10^6$ /sec)	Huff Fac. (Q)	(A-Z)/2A
3	Li-6	2177.0±2.0	4.18±0.45 $\times 10^{-3}$	1.0	0.25
	Li-7	2188.3±2.0	1.81±0.45 $\times 10^{-3}$	1.0	0.2857
4	Be	2162.1±2.0	7.35±0.45 $\times 10^{-3}$	1.0	0.2778
5	B-10	2070.7±3.0	2.81±0.07 $\times 10^{-2}$	1.0	0.25
	B-11	2096.1±3.0	2.22±0.07 $\times 10^{-2}$	1.0	0.2727
6	C	2026.3±1.5	3.88±0.05 $\times 10^{-2}$	1.0	0.25
	C-13	2029.1±3.0	3.77±0.07 $\times 10^{-2}$	1.0	0.2692
7	N	1906.8±3.0	6.93±0.08 $\times 10^{-2}$	1.0	0.25
8	O	1795.4±2.0	10.36±0.04 $\times 10^{-2}$	0.998	0.25
	O-18	1844.0±4.5	8.80±0.15 $\times 10^{-2}$	0.998	0.2778
9	F-LiF	1464.7±4.0	0.228±0.002	0.998	0.2632
	F-C2F4	1458.8±4.0	0.231±0.002	0.998	0.2632
	F-CaF2	1463.2±5.0	0.229±0.003	0.998	0.2632
	F-PbF2	1462.2±6.0	0.230±0.003	0.998	0.2632
11	Na	1204.0±2.0	0.377±0.001	0.996	0.26
12	Mg	1067.2±2.0	0.484±0.002	0.995	0.2533
13	Al	864.0±1.0	0.705±0.001	0.993	0.2593
14	Si	756.0±1.0	0.871±0.002	0.992	0.2510
15	P	611.2±1.0	1.185±0.003	0.991	0.2581
16	S	554.7±1.0	1.352±0.003	0.990	0.2507
17	Cl	560.8±2.0	1.333±0.006	0.989	0.2605
19	K	437.0±1.0	1.839±0.005	0.987	0.2570
20	Ca	332.7±1.5	2.557±0.014	0.985	0.2505
22	Ti	329.3±1.3	2.590±0.012	0.981	0.2705
23	V	284.5±2.0	3.069±0.025	0.980	0.2745
24	Cr	255.3±2.0	3.472±0.031	0.978	0.2695
25	Mn	232.5±2.0	3.857±0.037	0.976	0.2727
26	Fe	206.0±1.0	4.410±0.024	0.975	0.2675
27	Co	185.8±1.0	4.940±0.029	0.971	0.2712
28	Ni	156.9±1.0	5.932±0.041	0.969	0.2618
29	Cu	163.5±1.0	5.676±0.037	0.967	0.2721
30	Zn	159.4±1.0	5.834±0.039	0.965	0.2709
32	Ge	180.0±2.0	5.118±0.062	0.960	0.28
35	Br	133.3±1.0	7.069±0.056	0.952	0.2810

Table IV-1(2) Results of Lifetime Measurements in This Experiment

Z	Element	Mean Life (ns)	Capture Rate ($\times 10^6$ /sec)	Huff Fac. (Q)	(A-Z)/2A
40	Zr	110.0±1.0	8.663±0.083	0.940	0.2810
41	Nb	92.7±1.5	1.036±0.018 X10	0.939	0.2796
42	Mo	99.6±1.5	0.961±0.015 X10	0.936	0.2810
47	Ag	87.0±1.5	1.107±0.020 X10	0.925	0.2823
48	Cd	90.7±1.5	1.060±0.018 X10	0.921	0.2869
49	In	84.6±1.5	1.140±0.021 X10	0.920	0.2868
50	Sn	92.1±1.5	1.044±0.018 X10	0.918	0.2867
53	I	83.4±1.5	1.158±0.021 X10	0.910	0.2913
56	Ba	96.6±1.5	0.994±0.016 X10	0.902	0.2959
60	Nd	77.5±2.0	1.250±0.033 X10	0.895	0.2919
64	Gd	81.8±1.5	1.182±0.022 X10	0.885	0.2964
66	Dy	78.8±1.1	1.229±0.018 X10	0.880	0.2969
68	Er	74.4±1.5	1.304±0.027 X10	0.875	0.2968
74	W	78.4±1.5	1.237±0.024 X10	0.860	0.2984
80	Hg	76.2±1.5	1.274±0.026 X10	0.848	0.3
82	Pb	72.3±1.1	1.345±0.021 X10	0.844	0.3022
83	Bi	74.2±1.0	1.310±0.018 X10	0.840	0.3014

Table IV-2(1) Muon Lifetimes and Capture Rates

Z (Zeff)	Element	Mean Life (ns)	Capture Rate (10^6 /sec)	(A-Z)/2A	Refs.
1 (1.0)	H	2195.6±0.3	651±57 x10^{-6}	0.	-19-
		2194.97±0.15	467±43 x10^{-6}		-28-
		2198±2			-14-
2 (1.98)	He-3		2170+170(-430) x10^{-6}	0.1667	-17-
			1410±140 x10^{-6}	0.1667	- 7-
	He-4		336±75 x10^{-6}	0.25	-15-
			375+30(-300) x10^{-6}		-17-
3 (2.94)	Li-6	2173 ±5	6100±1400 x10^{-6}	0.25	-10-
		2175.3±0.4	4678±104 x10^{-6}		-26-
		2177.0±2.0	4180±450 x10^{-6}		*
3	Li-7	2194 ±4	1800±1100 x10^{-6}	0.2857	-10-
		2186.8±0.4	2260±104 x10^{-6}		-26-
		2188.3±2.0	1810±440 x10^{-6}		*
4 (3.89)	Be	2140 ±20	0.018 ±0.01	0.2778	- 1-
		2156 ±10	0.010 ±0.002		-10-
		2169.0±1.0	0.0059±0.0002		-29-
		2162.1±2.0	0.0074±0.0005		*
5 (4.81)	B-10	2082 ±6	0.0265±0.0015	0.25	-10-
		2070.7±3.0	0.0278±0.0007		*
	B-11	2102 ±6	0.0218±0.0016	0.2727	-10-
		2096.1±3.0	0.0219±0.0007		*
6 (5.72)	C	2020 ±20	0.044 ±0.010	0.25	- 1-
		2043 ±3	0.0373±0.0011		- 3-
		2041 ±5	0.0361±0.0013		- 4-
		2040 ±30	0.037 ±0.007		- 5-
		2025 ±4	0.0397±0.0013		-10-
		2035 ±8	0.0365±0.0020		-13-
		2060 ±30	0.0303±0.007		-16-
		2030.0±1.6	0.0376±0.0004		-29-
		2026.3±1.5	0.0388±0.0005		*
	C-13	2029.1±3.0	0.0376±0.0007	0.2692	*
7 (6.61)	N	1860 ±20	0.086 ±0.011	0.25	- 1-
		1927 ±13	0.065 ±0.004		-10-
		1940.5±2.8	0.0602±0.0008		-29-
		1906.8±3.0	0.0693±0.0008		*
8 (7.49)	O	1640 ±30	0.159 ±0.014	0.25	- 1-
		1812 ±12	0.098 ±0.003		-10-
		1810 ±20	0.098 ±0.005		-16-
		1795.4±2.0	0.1026±0.0006		*
	O-18	1844.0±4.5	0.0880±0.0015	0.2778	*
9 (8.32)	F	1420 ±40	0.254 ±0.022	0.2632	- 1-
		1450 ±20	0.235 ±0.010		- 8-
		1458 ±13	0.231 ±0.006		-13-
		1462.7±5.0	0.229 ±0.001		*

(These F data show lifetimes for lower hf states. See section IV.D (g))

Table IV-2(2) Muon Lifetimes and Capture Rates

Z (Zeff)	Element	Mean Life (ns)	Capture Rate (10^6 /sec)	(A-Z)/2A	Refs.
10 (9.14)	Ne	1520 ±23	0.204 ±0.010	0.2522	-11-
			0.167 ±0.030		-12-
			0.30 ±0.02		-22-
		1450 ±10	0.235 ±0.005		-29-
11(9.95)	Na	1190 ±20	0.387 ±0.015	0.2609	- 1-
		1204.0±2.0	0.3772±0.0014		*
12(10.69)	Mg	1040 ±20	0.507 ±0.020	0.2533	- 1-
		1071 ±2	0.480 ±0.002		- 4-
		1021 ±25	0.52 ±0.02		-18-
		1067.2±2.0	0.4841±0.0018		*
13(11.48)	Al	880 ±10	0.691 ±0.020	0.2593	- 1-
		864 ±2	0.662 ±0.003		- 4-
		905 ±12	0.650±0.015		- 8-
		864.0±1.0	0.7054±0.0013		*
14(12.22)	Si	810 ±10	0.777 ±0.025	0.2510	- 1-
		767 ±2	0.850 ±0.003		- 4-
		758 ±20	0.86 ±0.04		-18-
		756.0±1.0	0.8712±0.0018		*
15(12.90)	P	660 ±20	1.054 ±0.05	0.2581	- 1-
		635 ±2	1.121 ±0.005		- 4-
		611.2±1.0	1.185 ±0.003		*
16(13.64)	S	540 ±20	1.39 ±0.09	0.2507	- 1-
		567.4±8.4	1.31 ±0.03		-18-
		554.7±1.0	1.352 ±0.003		*
17(14.24)	Cl	540 ±20	1.39 ±0.09	0.2605	- 1-
		560.8±2.0	1.333 ±0.006		*
18(14.89)	Ar		1.20 ±0.08		-22-
19(15.53)	K	410 ±20	1.99 ±0.12	0.2573	- 1-
		437.0±1.0	1.839 ±0.005		*
20(16.15)	Ca-40	333 ±7	2.55 ±0.05	0.25	- 1-
		333 ±7	2.549 ±0.063		- 6-
		335.9±0.9	2.977 ±0.008		-21-
		365 ±8	2.286 ±0.050		-25-
		332.7±1.5	2.557 ±0.014		*
	Ca-44	445 ±8	1.793 ±0.040	0.2727	- 6-
22(17.38)	Ti	330 ±7	2.63 ±0.06	0.2705	- 1-
		327.3±4.5	2.60 ±0.04		-18-
		329.3±1.3	2.590 ±0.012		*
23(18.04)	V	264 ±4	3.37 ±0.06	0.2745	- 1-
		271 ±5	3.24 ±0.07		- 5-
		282.6±3.2	3.09 ±0.05		-18-
		284.5±2.0	3.069 ±0.025		*
24(18.49)	Cr	276 ±6	3.24 ±0.08	0.2695	- 1-
		264.5±3.2	3.33 ±0.06		-18-
		255.3±2.0	3.472 ±0.031		*
25(19.06)	Mn	239 ±4	3.67 ±0.08	0.2727	- 1-
		225.5±2.3	3.98 ±0.05		-18-
		232.5±2.0	3.857 ±0.037		*

Table IV-2(3) Muon Lifetimes and Capture Rates

Z (Zeff)	Element	Mean Life (ns)	Capture Rate (10^6 /sec)	$\frac{(A-Z)}{2A}$	Refs.
26(19.59)	Fe	201 ±4	4.53 ±0.01	0.2675	- 1-
		196 ±8			- 2-
		207 ±3	4.38 ±0.07		- 5-
		206.7±2.4	4.40 ±0.05		-18-
		206.0±1.0	4.411 ±0.024		*
27(20.13)	Co	188 ±3	4.89 ±0.09	0.2712	- 5-
		184.0±1.7	4.96 ±0.05		-18-
		185.8±1.0	4.940 ±0.029		*
28(20.66)	Ni	154 ±3	6.03 ±0.14	0.2618	- 1-
		158 ±3	5.9 ±0.1		- 5-
		159.4±3.1	5.83 ±0.11		-18-
		156.9±1.0	5.932 ±0.041		*
29(21.12)	Cu	160 ±4	5.79 ±0.16	0.2721	- 1-
		169±6	5.47 ±0.20		- 8-
		164.0±2.3	5.66 ±0.09		- 9-
		163.5±2.4	5.67 ±0.09		-18-
		163.5±1.0	5.676 ±0.037		*
	Cu-63	162.1±1.4	5.72 ±0.05	0.2698	-18-
30(21.61)	Zn	161 ±4	5.76 ±0.17	0.2709	- 1-
		169 ±4	5.5 ±0.1		- 5-
		161.2±1.1	5.76 ±0.05		-18-
		159.4±1.0	5.834 ±0.039		*
31(22.02)	Ga	163.0±1.6	5.70 ±0.06	0.2779	-18-
32(22.43)	Ge	167.4±1.8	5.54 ±0.06	0.28	-18-
		180.0±2.0	5.119 ±0.061		*
33(22.84)	As	153.8±1.7	6.07 ±0.07	0.28	-18-
34(23.24)	Se	163.0±1.2	5.70 ±0.05	0.2850	-18-
35(23.65)	Br-79	133.7±6.5	7.03 ±0.34	0.2785	-20-
	Er-81	125.3±7.9	7.53 ±0.48	0.2840	-20-
	Er	133.3±1.0	7.069 ±0.056	0.2810	*
37(24.47)	Rb	136.5±2.7	6.89 ±0.13	0.2838	-18-
38(24.85)	Sr	130.1±2.3	7.25 ±0.14	0.2834	-18-
	Sr-88	142.0±5.5	6.61 ±0.27	0.2841	-18-
39(25.23)	Y	120.2±1.4	7.89 ±0.11	0.2809	- 9-
40(25.61)	Zr	110.8±0.8	8.59 ±0.07	0.2810	-18-
		110.0±1.0	8.663 ±0.083		*
41(25.99)	Nb	92.3±1.1	10.40 ±0.14	0.2796	- 9-
		92.7±1.5	10.36 ±0.17		*
42(26.37)	Mo	105 ±2	9.09 ±0.18	0.2810	- 1-
		103.5±0.7	9.23 ±0.07		-18-
		99.6±1.5	9.614 ±0.15		*
45(27.32)	Rh	95.8±0.6	10.01 ±0.07	0.2816	-18-
46(27.63)	Pd	96.0±0.6	10.00 ±0.07	0.2841	-18-
47(27.95)	Ag	85 ±3	11.25 ±0.5	0.2823	- 1-
		88.7±0.9	10.86 ±0.13		- 9-
		88.6±1.1	10.88 ±0.14		-18-
		87.0±1.5	11.07 ±0.20		*

Table IV-2(4) Muon Lifetimes and Capture Rates

Z (Zeff)	Element	Mean Life (ns)	Capture Rate (10^6 /sec)	$\frac{(A-Z)}{2A}$	Refs.
48(28.20)	Cd	95 ±5	10.05 ±0.5	0.2869	- 1-
		90.5±0.8	10.63 ±0.11		- 9-
		90.7±1.5	10.61 ±0.18		*
49(28.42)	In	84.8±0.8	11.37 ±0.13	0.2868	- 9-
		84.6±1.5	11.40 ±0.21		*
50(28.64)	Sn	92 ±3	10.5 ±0.4	0.2867	- 5-
		89.9±1.0	10.70 ±0.14		- 9-
		92.1±1.5	10.44 ±0.18		*
51(28.79)	Sb	91.7±1.1	10.49 ±0.14	0.2907	- 9-
52(29.03)	Te	105.5±1.2	9.06 ±0.11	0.2964	-18-
53(29.27)	I	86.1±0.7	11.20 ±0.11	0.2913	- 9-
		83.4±1.5	11.58 ±0.22		*
55(29.75)	Cs	87.8±1.9	10.98 ±0.25	0.2932	- 9-
56(29.99)	Ba	94.5±0.7	10.18 ±0.10	0.2959	- 9-
		96.6±1.5	9.941±0.16		*
57(30.22)	La	89.9±0.7	10.71 ±0.10	0.2950	- 9-
58(30.36)	Ce	84.4±0.7	11.44 ±0.11	0.2928	- 9-
59(30.53)	Pr	72.1±0.6	13.45 ±0.13	0.2908	- 9-
60(30.69)	Nd	78.5±0.8	12.32 ±0.14	0.2919	- 9-
		77.5±2.0	12.50 ±0.33		*
62(31.01)	Sm	79.2±1.0	12.22 ±0.17	0.2937	- 9-
64(31.34)	Gd	80.1±1.0	12.09 ±0.16	0.2964	- 9-
		81.8±1.5	11.82 ±0.22		*
65(31.48)	Tb	76.2±0.7	12.73 ±0.13	0.2956	- 9-
66(31.62)	Dy	78.8±1.1	12.29 ±0.18	0.2969	*
67(31.76)	Ho	74.9±0.6	12.95 ±0.13	0.2970	- 9-
68(31.90)	Er	74.4±1.5	13.04 ±0.27	0.2968	*
72(32.47)	Hf	74.5±1.3	13.03 ±0.21	0.2982	-18-
73(32.61)	Ta	75.5±0.6	12.86 ±0.13	0.2983	- 9-
74(32.76)	W	81 ±2	11.9 ±0.3	0.2984	- 1-
		72 ±3	13.5 ±0.6		- 5-
		74.3±1.2	13.07 ±0.21		-18-
		78.4±1.5	12.36 ±0.24		*
79(33.64)	Au	75.6±0.5	13.39 ±0.11	0.2995	- 9-
80(33.81)	Hg	76.2±1.5	12.74 ±0.26	0.3	-18-
		76.2±1.5	12.74 ±0.26		*
81(34.21)	Tl	75 ±4	12.90 ±0.75	0.3019	- 1-
		70.3±0.9	13.83 ±0.20		- 9-
82(34.18)	Pb	82 ±5	11.70 ±0.75	0.3022	- 1-
		67 ±3	14.50 ±0.7		- 5-
		74.9±0.4	12.98 ±0.10		- 9-
		73.2±1.2	13.27 ±0.22		-18-
		72.3±1.1	13.45 ±0.21		*
	RPb[1]	71.5±0.4	13.61 ±0.10		- 9-

Table IV-2(5) Muon Lifetimes and Capture Rates

Z (Zeff)	Element	Mean Life (ns)	Capture Rate (10^6 /sec)	$\frac{(A-Z)}{2A}$	Refs.
83(34.0)	Bi	79 ±5	12.20 ±0.75	0.3014	- 1-
		73.3±0.4	13.26 ±0.10		- 9-
		74.2±1.0	13.10 ±0.18		*
90(34.73)	Th-232	80.4±2.0	12.1 ±0.3	0.3061	-23-
		79.2±2.0	12.2 ±0.3		-24-
92(34.94)	U -235	78 ±4	(12.4 ±0.6)	0.3043	-23-
		75.4±1.9	12.9 ±0.3	0.3043	-24-
	U -238	88 ±4	10.9 ±0.5	0.3068	- 1-
		81.5±2.0	(11.9 ±0.3)		-23-
		73.5±2.0	13.2 ±0.4		-24-
93(35.05)	Np	71.3±0.9	(13.6 ±0.2)	0.3038	-27-
94(35.16)	Pu-239	77.5±2.0	(12.5 ±0.3)	0.3033	-23-
		73.4±2.8	13.3 ±0.4		-24-
		70.1±0.7	(13.9 ±0.2)		-27-
	Pu-242	75.4±0.9	(12.9 ±0.2)	0.3058	-27-

References:

- 1- (SEN59), - 2- (BAR59), - 3- (REI60), - 4- (LAT61),

- 5- (BLA62), - 6- (CRA62), - 7- (FAL62), - 8- (ECK62),

- 9- (FIL63), -10- (ECK63), -11- (ROS63), -12- (CON63),

-13- (WIN63), -14- (MEY63), -15- (BIZ64), -16- (BAR64),

-17- (AUE65), -18- (ECK66), -19- (ALB69), -20- (POV70),

-21- (DIL71), -22- (EER73-2), -23- (HAS76), -24- (JOH77),

-25- (HAR77), -26- (BAR78), -27- (SCH79), -28- (BAR79),

-29- (MAR80)

Note:

*: Denotes the results of this experiment.
(Zeff) with underlines are estimated values.
( ) : Numbers are not given in references and estimated from capture rates or lifetimes.

1) RPb = radiogenic lead (88%Pb-206,9%Pb-207,3%Pb-208)

IV.A Positive Muon Lifetime in Carbon

In this experiment the positive muon lifetime ($T(+)$) was used to calibrate the experimental set-up and the data taking system, since the lifetime has been measured precisely at several laboratories as shown in Table IV-3. The accepted value of the lifetime is 2197.120±0.077 ns in the Review of Particle Properties (KEL80). Before 1960, there was difficulty in the detection of microsecond time intervals, because a delayed coincidence or a time to pulse height converter (TAC) was employed to determine time distributions. Swanson (SWA60) pointed out that there was a non-linearity of 1 to 2 % and a calibration instability of 0.6% in the TAC. After 1960, a digital technique with a high frequency oscillator became common and was able to reduce the systematic error in the timing of the intervals. However, it was pointed out by Lundy (LUN62) that there was still a systematic error due to the time dependent background caused by 2nd muons. As shown in Table IV-3, an accurate measurement was done by Baladin et al. (BAL74) by using a positron detector with a 4π radian solid angle.

In this experiment, as discussed in Chapter III, the systematic errors have been studied carefully by checking the event rejection effects, the stopping muon rate effect, and the magnetic field effect. It has been concluded that the systematic error in the positive muon

Table IV-3 Past Positive Muon Lifetimes

Auther and Refs.		Year	Result (ns)
W.E.Bell et. al.	(BEL51)	1951	2220 ± 20
R.W.Swanson et al.	(SWA59)	1959	2261 ± 7
J.Fisher et al.	(FIS59)	1959	2200 ± 15
J.C.Sens et al.	(SEN59)	1959	2210 ± 20
R.A.Reiter et al.	(REI60)	1960	2211 ± 3
J.L.Lathrop et al.	(LAT61)	1961	2203 ± 2
R.A.Lundy et al.	(LUN62)	1962	2203 ± 4
S.L.Meyer et al.	(MEY63)	1963	2198 ± 2
M.Eckhause et al.	(ECK63)	1963	2202 ± 4
J.Barlow et al.	(BAR64)	1964	2197 ± 2
R.W.Williams et al.	(WIL72)	1972	2200.26 ± 0.81
J.Duclos et al.	(DUC73)	1973	2197.3 ± 0.4
M.P.Balandin et al.	(BAL74)	1974	2197.11 ± 0.08
G.Bardin et al.	(BAR78)	1978	2196.8 ± 0.4
	(BAR79)	1979	2197.09 ± 0.14
TRIUMF	(SUZ80)	1979	2197.0 ± 0.7
Particle DATA Group	(KEL80)	1980	2197.120± 0.077
Decay rate			0.455141 ± 0.000016 x10^6 s^{-1}

lifetime is negligible. The lifetimes of 10 runs are listed in Table III-1 and the average positive muon lifetime is

$$T(+) = 2197.0 \pm 0.7 \qquad (4.1)$$

which is in good agreement with the accepted value.

This result can be applied in calculating the coupling constant, Gm, for a muon decay. Assuming V-A interaction, Roos and Sirlin (ROO71) derived the following relation

$$(Gm)^2 = \frac{192\cdot(\pi)^3}{T(+)}\cdot\frac{(Me\cdot\hbar)^5}{(Mm\cdot Me\cdot c)^5}\cdot\frac{\hbar^2\cdot c\cdot(1+d)}{(1-8\cdot(Me/Mm)^2)} \qquad (4.2)$$

$$Gm = 1.4356(7) \times 10^{-49} \text{ erg}\cdot\text{cm}^3$$

where $Mm/Me = 206.7682(5)$ (CRO72)

$\hbar/(Me\cdot c) = 3.8614\times10^{-11}$ cm

$\hbar = 1.0545\times10^{-27}$ erg·sec

$d = 0.00422$ (radiative correction, ROO71)

$T(+) = 2197.0(1.0)$ ns

Shrock and Wang (SHR78) have determined Gm with the precise lifetime obtained by Balandin et al. (BAL74) and their new formula for Gm. Their number for Gm is

$$Gm = 1.43582(4) \times 10^{-49} \text{ erg}\cdot\text{cm}^3$$

For the muon lifetime given by (4.1), the muon decay rate defined by equation (4.2) is

$$Rd(+) = (4.551 \pm 0.002)\times10^5 \text{ /sec} \qquad (4.3)$$

IV.B Muon Capture Rate and its Accuracy

As discussed in section I.C, The bound muon decay rate is nct the same as the free positive mucn decay rate and the relation between the two rates is written as

$$Rd(-) = Q(Z) \cdot Rd(+)$$
$$= Q(Z)/T(+) \qquad (4.4)$$

where Q(Z) is called a Huff factor (Huf60). Huff's theory for the bound muon decay in the mesonic atoms predicts that a bound muon in heavy elements has a reduced decay rate. The theory is in gcod agreement with subsequent measurements (BLA62-2, YAM74). Also, Uberall (UBE60) calculated the muon bound effect in the nucleus. He obtained a simple form

$$Q(Z) = 1-0.5(Z/137)^2 \qquad (4.5)$$

This result has been obtained for a point nucleus. For heavy elements, the K crbit of the mesonic atom is formed inside the nucleus, thus the effective charge, which is responsible fcr the mucn capture, becomes much smaller than the nuclear charge. Hence Uberall's formula (4.6) overestimates the bound effect in the heavy nuclei. Calculations by Huff and Uberall are shown in figure IV-1. In this work Huff's values were employed and listed in Table

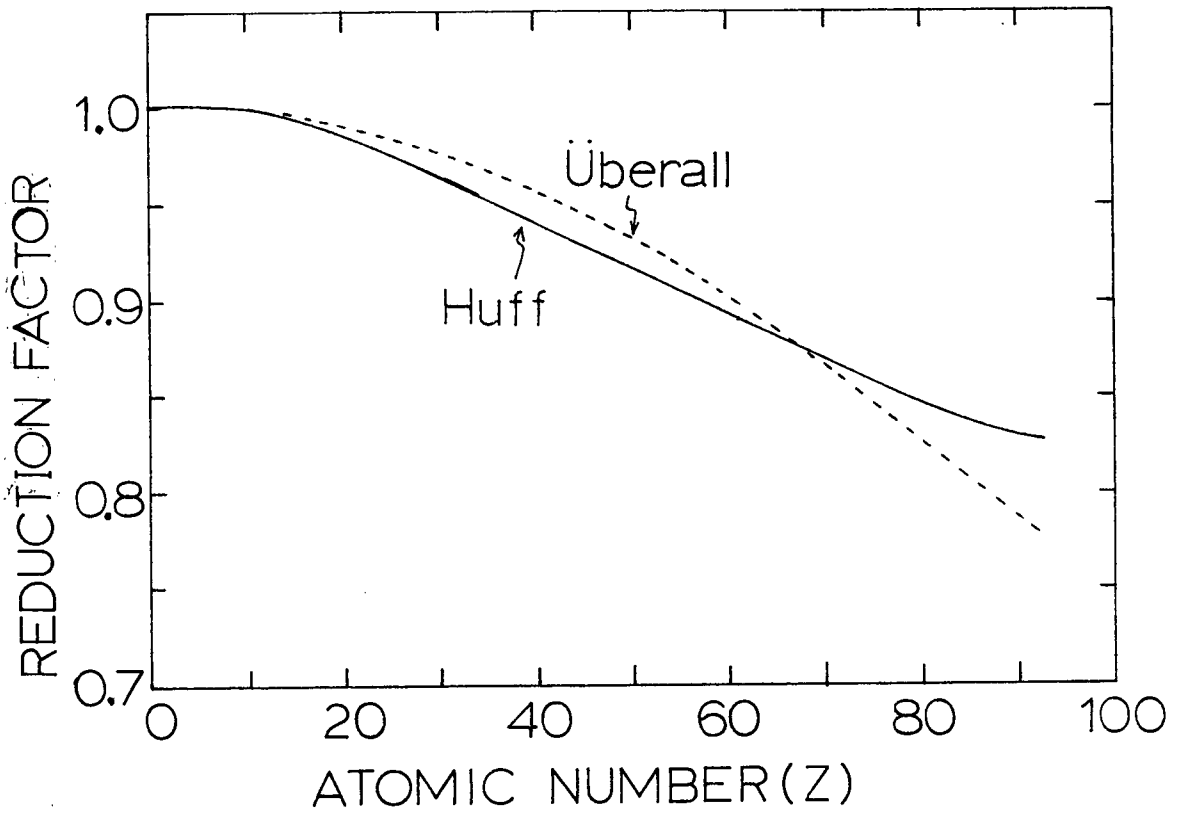

Figure IV-1, Ratio of bound decay rate to free decay rate.

IV-1.

In muon capture experiment, the total disappearance rate, the nuclear capture rate, and the decay rate are frequently used. For reasons of convenience, those relations are summarized in the following.

Decay rate of free muons; $Rd(+)=1/T(+)$,

$T(+)$: positive or negative free muon lifetime (2197.0 ns)

Total disappearance rate; $Rt=1/T(-)$

$T(-)$: negative muon lifetime in nucleus

$$Rt=Rc + Q(Z)\cdot Rd(+)$$
$$=Rc + Rd(-)$$

Nuclear capture rate ; $Rc=Rt - Rd(-)$

$$=1/T(-) - Q(Z)/T(+) \qquad (4.6)$$

When the nuclear capture rate is obtained from lifetime measurements, equation (4.6) is used.

$T(-)$; listed in Tables IV-1 and IV-2

$T(+)$; 2197.0±0.7 ns (our measurement)

$Q(Z)$; figure IV-1, Huff factor

The accuracy of the total disappearance rate is defined by

$$dRt/Rt = 1/\sqrt{(Ne)} \qquad (4.7)$$

where Ne is the total number of electron events. From

equation (4.6), the capture rate Rc is equal to R-Rd with the approximation of Q(Z)=1. The accuracy of Rc is expressed as

$$\frac{dRc}{Rc}=\frac{1}{Rc}\sqrt{\frac{Rt^2}{Ne^-}+\frac{Rd^2}{Ne^+}} \qquad (4.8)$$

For example, in the case of ^{6}Li, we have the following approximate numbers and equations for a 0.1% accuracy of lifetime measurement

$$T(-)=2175.0\pm2.0 \quad (0.1\%)$$

$$Rt=Rd=4.5\times10^5 \text{ /sec}$$

$$Rc=5000 \text{ /sec}$$

$$Ne^-=Ne^+=4\times10^6 \text{ events}$$

$$dRc/Rc=Rd/Rc\cdot\sqrt{(2/Ne)} \qquad (4.9)$$

Thus the accuracy of Rc in ^{6}Li is about 6 %. In the case of heavy elements (Z>20), Rc is greater than Rd and Ne^- is much less than Ne^+. Therefore, the accuracy of the capture rate Rc is approximated by

$$dRc/Rc=1/\sqrt{(Ne^-)} \qquad (4.10)$$

Equation (4.10) gives a 1 % accuracy of Rc for $Ne^-=10^4$ total events, which is equivalent to a 1% accuracy in a lifetime measurement in a lead target.

IV.C Negative Muon Lifetime Measurements in Carbon and System Calibration

The lifetime in carbon was measured several times throughout this experiment, since the lifetime was used as the calibration of the system. The results of seven measurements are listed in Table IV-4, along with a result from the spring of 1979. The weighted average of the separate runs is recorded in Table IV-1. The error is determined from the statistics and the deviations of each of the different runs from the mean. The changes in the lifetime, as shown in the table, are quite small and it assures that the system was working properly throughout this experiment.

As listed in Table IV-2, around 1960, there are three precise measurements for ^{12}C by Eckhause et al., Lathrop et al., and Reiter et al.. Their measurements for the lifetime of the positive muon, as shown in Table IV-3, are 2202±4 ns, 2203±2 ns and 2211±3 ns, respectively, which all disagree with the presently accepted value of 2197.13 ± 0.08 ns. It seems their systems were not well calibrated and, from the point of view of system calibration, our negative muon lifetime in carbon would appear therefore to be more reliable. The Saclay group has a well calibrated system with which they determined the positive muon lifetime to be 2197.18 ±0.12 ns (DUC80, BAR79). Their value for the

Table IV-4 Negative Muon Lifetimes in Carbon

	Run #	Events (x10^6)	Lifetime (ns)
1979 SPRING		1.6	2026.5 ± 1.6
1979 FALL	1178	1.0	2026.0 ± 2.1
	1197	0.9	2025.2 ± 2.2
	1259	0.6	2026.1 ± 2.7
	1264	0.5	2025.3 ± 2.9
	1272	0.8	2023.5 ± 2.3
	1275	0.5	2026.3 ± 2.9
	1291	0.6	2030.3 ± 2.7
	Total	6.5	2026.3 ± 1.5

negative muon lifetime in carbon is 2030.0 ±1.6 ns (MAR80).

Our result of 2026.3±1.5 ns is in adequate agreement with Eckhause's result of 2025±4 ns and the finding of the Saclay group, but disagrees with the two results of 2043±3 ns by Reiter and 2041±5 ns by Lathrop. Although if one subtracts off 14 ns and 6 ns (their positive muon lifetime deviation from the accepted value), respectively, the agreement is better, but this simple minded procedure is not necessarily valid because almost certainly there would have been different systematic errors. Within error, our capture rate barely overlaps with past measurements as shown in Table IV-2.

The calculation by Walecka (WAL75) gave a capture rate of 0.35×10^5 /sec which is lower than our result $(0.388 \pm 0.005) \times 10^5$ by 6%.

IV.D Negative Muon Lifetime Measurements in 48 Elements

(a) Lithium (^{6}Li and ^{7}Li)

The first measurement was made by Eckhause et al. (ECK63) but their results had large errors. Furthermore, their result for ^{6}Li was inconsistent with the theoretical estimate by Lodder and Jonker (LOD67), which indicated that further experiments would be useful. Recently, considerably greater precision was achieved in a measurement by the Saclay group (BAR78). A comparison of the theoretical and

experimental capture rates is given in Table IV-5(1). As shown in Table III-2, our data depend on the carbon background. According to the carbon background run, a 1.0 % carbon background is allowed in the results of Table IV-5. Our results, without the carbon background, agree well with Saclay's results, which are free from the carbon background.

The capture rate, shown in Table IV-5, is an average capture rate. At first negative muons populate the hyperfine states according to a statistical distribution. Then there is a change in the population due to the transition between the hyperfine states. For lithium, Favart et al.(FAV70) showed, by a muon precession experiment, that the conversion rate was less than 2×10^4 /sec of which the conversion time was longer than 50 microseconds. In order to explain the partial capture rate experiment of ^{6}Li-^{6}He(g.s.) (=1600 /sec) (DEU68), Primakoff (PRI77) and Hwan (HWA78) added a 16 % effect from the hyperfine conversion to the statistically averaged rate. Since the conversion rate is very small and the transition occurs within milli seconds, our experiment, in which all events appear within 25 microseconds, is not adequate to find the hyperfine transitions.

The simple formula of Primakoff, which will be shown in the next Chapter, has a neutron excess term. This originates from the Pauli principle and is claimed to be valid for Z>6. The difference of the total capture rate between ^{6}Li and ^{7}Li is mainly due to the allowed transition

Table IV-5(1) Capture Rates in Li-6 and Li-7

	Li-6 (/sec)	Li-7 (/sec)	Rc(7)/Rc(6)
Theory (LOD67)	3480	2080	0.60
Experiments			
Eckhause (ECK63)	6100±1400	1800±1100	0.30±0.19
Saclay (BAR78)	4680±120	2260±120	0.48±0.03
TRIUMF	4180±450	1810±440	0.43±0.11

Table IV-5(2) The Different Contribution to the Total Muon Capture Rate by Lodder and Jonker(LOD67)

(unit in /sec)

Isotope	Allowed	Dipole	Other Multipole	Relativistic Term	Rc(Total)
Li-6	1248	1263 (1044)	621	348	3480 (3261)
Li-7	----	1182	620	281	2083(±12%)

in ^{6}Li according to Lodder's calculation (LOD67) as shown in Table IV-5(2). The neutron excess term in Primakoff's formula predicts the isotope effect, Rc(7)/Rc(6) =0.48, which is clcse to our measurement, Rc(7)/Rc(6) =0.43±0.02.

(b) Beryllium

There have been three measurements of the negative muon lifetime in Be by Sens (SEN58), Eckhause et al. (ECK63), and Martino et al. (MAR80), who obtained lifetimes of 2140±20 ns, 2156±10 ns, and 2169.0±1.0 ns, respectively. Our result of 2162.1±1.8 ns is in good agreement with the earlier measurements of Sens and Eckhause et al., but the result from Martino and Duclos is longer than ours by 7 ns. This disagreement can not be explained with the hyperfine effect. Since Be has a negative magnetic moment as shown in Table IV-6, the hyperfine state with $F^{+}=I+1/2$ is lower in energy than the hyperfine state with $F^{-}=I-1/2$. In the lifetime measurements at Saclay, the detection of the decay electrons started a few microseconds after the muons stopped, so their experiment may have detected decay electrons from the lower hyperfine level (F^{+}). From Table IV-6, it is evident that T^{+} (lifetime in F^{+} state) is longer than T^{-} (lifetime in F^{-} state). Since our experiment started taking data directly after muons stcpped in a target, we were measuring the mean lifetime, Tmean. However, the hyperfine transition time has been determined experimentally tc be longer than 20 microseconds by Favart et al. (FAV70), so that, within a few

microseconds, the hyperfine effect would not be large. Assuming that the transition time is 20 microseconds and the data taking starts at 4 microseconds after the muon stop, the hyperfine effect would be less than 20%, and the lifetime measured by the Saclay group should be about 2 nsec longer than the mean lifetime. This correction is in the right direction but insufficient to explain the 7 nsec discrepancy. No theoretical calculation has been made for the muon capture in Be.

(c) Boron (^{10}B and ^{11}B)

Eckhause et al. (ECK63) have measured the negative muon lifetimes in ^{10}B and ^{11}B. Our result in ^{11}B agrees with their result within error; in the case of ^{10}B our result is shorter than their result by two standard deviations. The capture rates and isotope effects are in good agreement as shown below.

		^{10}B	^{11}B	Rc(11)/Rc(10)
Eckhause	life	2082±6 ns	2102±6 ns	
	cap	25,800±1500 /sec	21,200±1500 /sec	0.82±0.08
TRIUMF	life	2070.7±2.0 ns	2096.1±2.0 ns	
	cap	27,760±490 /sec	21,910±480 /sec	0.79±0.02

There is no theoretical calculation which can be compared

with the total muon capture rates in ^{10}B and ^{11}B.

(d) Carbon (^{12}C and ^{13}C)

The lifetime of ^{12}C has been discussed in section IV.C. Our measurement of the lifetime in ^{13}C is the first such measurement. As listed in Table IV-1, there is no difference in lifetimes between ^{12}C and ^{13}C and the isotope effect Rc(13)/Rc(12) is equal to 0.97±0.03. From the Primakoff thecry which implemented the Pauli principle, the expected isotope ratio is equal to 0.71 which is not compatible with our experimental result. The total muon capture rates for limited numbers of transitions between states with the same parity have been reported by Desgrolard et al. (DES78), using the shell model and impulse approximation. Their calculations indicate that there is no difference in the capture rate between ^{12}C and ^{13}C, and this agrees with our experiments. Although the shell model approach by several authors (LUY63, GOU71, JOS72, DUP75) has not succeeded in reproducing the actual experimental values, the results can be utilized qualitatively in discussing capture rates.

Strong isotope effects have been observed for Li, B, and O in our experiment. The difference between these nuclei and C, except for level structures, is the Q value. The isotopes of Li, B, and O have different Q values, but the Q values of ^{12}C and ^{13}C are the same. These same Q values may be one of reasons for the same muon capture rate

in ^{12}C and ^{13}C (FUJ79).

(e) Nitrogen

The muon lifetime in nitrogen has been measured with great precisicn in our experiment. Our lifetime result does not agree with previous results, as shown in Table IV-2, but our capture rate just overlaps with the value of Eckhause. The value of the Saclay group is 1.8% (nearly 1σ) higher than our result. Since their data taking started a few microseconds after the muons stopped in the target, it is possible that their result is affected by the hyperfine transition. If so, their result should be shorter than ours, because nitrogen has a positive magnetic moment and the muon lifetime in the lower hyperfine state is shorter than in the higher hyperfine state. If their target (NH_4I) had water contamination, the lifetime would be shorter than ours also. Using chemical compounds (NH_4Cl), we had difficulty determining muon lifetimes in nitrogen, which varied from 1905ns to 1925ns. Consequently, we decided to use liquid nitrogen as a target. We believe that our result is significantly more reliable because of the generally consistent and reasonable behavior of the electronic equipment. A theoretical calculation has been made to find the muon capture in N (KIS73), using shell model wave functicns. The calculated total capture rate, 1.09×10^5 /sec, exceeds the experimental results by 70 %. There is no other theoretical value.

(f) Oxygen (^{16}O and ^{18}O)

As shown in Table IV-2, three measurements of the muon lifetime in ^{16}O have been made previously. Our result has a considerably improved accuracy. Although our result for ^{16}O (water target) is lower than two recent measurements, it does fall within the large error limits of the previous measurements. A theoretical attempt was made by Walecka (WAL75) using the Foldy-Walecka resonance model. His result of muon capture rate in ^{16}O is 1.07×10^5 /sec, which is quite close to our result of $1.018 \pm 0.005 \times 10^5$ /sec.

Ours is the first measurement of the muon lifetime in ^{18}O. Since this target was formed in Agar, the carbon background was determined by the lifetime measurement of the ^{16}O target in the same form using the fixed ^{16}O lifetime obtained above from the water target. There is no theoretical calculation. The isotope effect Rc(18)/Rc(16) is equal to 0.80 ± 0.01. This is quite different from the ratio of 0.60, which is calculated by Primakoff's formula. It seems that in light elements the details of the nuclear structure are more important, since this formula fails for both ^{12}C-^{13}C and ^{16}O-^{18}O.

(g) Fluorine

The hf effect of muon capture can be expected in this nucleus, as demonstrated by Winston (WIN63); hence the histogram of decay electrons has been fitted to equation (3.12). The data analyses of the histograms of four

chemical compcunds give the mean lives (T^-) and the disappearance rates (R^-) of the lower hf states. The results are listed in the following

Ccmpound	T^- (ns)	R^- ($\times 10^6$ /sec)	$Rc^-=R^--Rd$ ($\times 10^5$ /sec)
LiF	1464.7±4.0	0.683±0.002	0.228±0.002
C2F4	1458.8±4.0	0.686±0.002	0.230±0.002
CaF2	1463.2±5.0	0.683±0.002	0.228±0.003
PbF2	1464.2±6.0	0.683±0.003	0.228±0.003
Average	1462.7±5.0	0.684±0.002	0.229±0.003

As discussed in section III.G, the amplitude of the hf transition effect (Ae) is about 0.015. In order to see this effect clearly in a decay electron histogram, the data points within the time of the transition (=200 ns) must have better than a 1 % statistics. In our F data listed above, only the LiF data, which has 8000 electron events from the mucn decay in F at t=0, can be used for the hf effect study. The fitting results are

$$Rh=(8.8\pm4.0)\times10^6\ /sec, \quad Ae=0.017\pm0.010 \qquad (4.11)$$

Winston (WIN63) whose histogram had five times more events than ours cbtained

$$Rh=(6.3\pm1.8)\times10^6\ /sec, \quad Ae=0.026\pm0.007 \qquad (4.12)$$

(from electron data)

$$Rh=(5.8\pm0.8)\times10^6\ /sec, \quad An=0.30\pm0.02$$

(from neutral data)

Although cur results (4.11) are in agreement with Winston's results (4.12), our data does not have enough statistics to determine the hf effect terms, Rh and Ae.

The capture rates of the hf doublet are estimated from the following relations (BER58, PRI59)

$$\frac{R^-(I-1/2) - R^+(I+1/2)}{Rav} = 0.945 \cdot \frac{1}{Z} \begin{cases} (2I+1)/I & : I=L+1/2 \\ -(2I+1)/(I+1) & : I=L-1/2 \end{cases} \qquad (4.13)$$

where the definitions of R^+, R^- and Rav have been given in section III.G. Since equation (4.13) was derived by Bernstein, Lee, Yang, and Primakoff, this is often named the BLYP estimate. In the case of F, I=1/2 and Z=9, so that

$$(Rc^- - Rc^+)/(Rc)av = 0.42 \qquad (4.14)$$

This value was determined experimentally by Winston to be 0.77±0.13. Using these two values and equations (3.13), (3.14) and (3.15), our results and Winston's results are summarized as follows

	Rc^- (lower) ($\times 10^5$ /sec)	Rc^+ (upper) ($\times 10^5$ /sec)	Tmean (ns)
Winston (neutral)	2.31±0.06	1.57±0.04[1]	1584±11
		1.18±0.09[2]	1663±20
TRIUMF (electron)	2.29±0.02	1.56±0.02[1]	1590±5
		1.17±0.09[2]	1667±20

1, 0.42 from equation (4.13) (BLYP estimate)
2, 0.77±0.13, Winston's experimental value

Our results agree with Winston's neutron and gamma data. In Table IV-2, the past measurements of lifetimes of the lower hf state are listed. Our result shows agreement with the

other measurements.

(h) Search for the hf transitions in Be, ^{10}B, ^{11}B, ^{13}C, N, Na, and Cl.

In Table IV-6, the information of hf states for nuclei with a spin is listed. According to the theoretical estimates of the conversion rates (WIN63) or experimental determinations (FAV70), it is possible that the hf transitions of nuclei listed above could be observed in our experiment. Thus our data were fitted tc equation (3.12). The results obtained do not show any indication of the hyperfine effect and are listed below.

Element	Ae	Rh (10^6 s^{-})	Ref.	Amp[1] at t=0
Be	0.006±0.002	0.05 fixed	(FAV70)	5000
^{10}B	0.001±0.002	0.2 fixed	(FAV70)	3500
^{11}B	0.001±0.003	0.33 fixed	(FAV70)	3500
^{13}C	0.01 ±0.01	(0.2±0.2)	fit	2000
N	0.008±0.01	(1.2±1.5)	fit	4000
Na	0.01 ±0.02	14 fixed	(WIN63)	3000
Cl	0.01 ±0.02	8 fixed	(WIN63)	2000

1) Amplitude at t=0 in equation (3.6)

As discussed in section III.G, the hf transition coefficient (Ae) is expected to be around 0.01 or less. From Table IV-6 in which Ae is estimated for various nuclei, it is evident that Ae is very small for most of the nuclei. Thus, in order to see the effect clearly in the decay electron spectrum, the spectrum has to have more than 10^4 events at t=0 even for the nuclei which seem to be good candidates for

Table IV-6(1) The hyperfine effects in various nuclei

Element	Spin	Mcment	D/Rav	An[1]	Ae[1]	Rh(10^6 /sec)
Li(3,6)	1+	0.82				<0.02[2]
Li(3,7)	3/2-	3.26	0.84[3]			<0.02[2]
Be(4,9)	3/2-	-1.18	0.63[3]			<0.05[2]
B(5,10)	3+	1.80				0.21±0.05[2]
B(5,11)	3/2-	2.69	0.51[3]	0.24	0.009	0.25[1]
			1.2[4]	0.43	0.017	0.33±0.05[2]
C(6,13)	1/2-	0.70	-0.21[3]			
N(7,14)	1+	0.40				
F(9,19)	1/2+	2.63	0.42[3]	0.24	0.01	0.58±0.08[5]
			0.76[4]	0.36	0.015	0.63±0.18[6]
			0.77±0.13[1]	0.30±0.02	0.026±0.007	
Na(11,23)	3/2+	2.22	-0.14[3]	0.08	0.002	14[1]
Al(13,27)	5/2+	3.64	0.18[3]	0.09	0.001	41[1]
			0.28[4]	0.14	0.002	
P(15,31)	1/2+	1.13	0.25[3]	0.16	0.003	58[1]
			0.37[4]	0.22	0.004	
Cl(17,35)	3/2+	0.82	-0.09[3]	-0.06	-0.01	8[1]
			-0.14[4]	-0.06	-0.01	
K(19,39)	3/2+	0.39	-0.08[3]	-0.05	-0.005	22[1]
			-0.11[4]	-0.07	-0.001	

Note:
1, Winston' data or estimate (WIN63)
2, Favart et al. (FAV70)
3, BLYP equation (text equation (4.11), Berstein (BER58)
4, Primakoff's estimate quoted in WIN63
5, Winston's neutral data(WIN63)
6, Winston's electron data(WIN63)

Table IV-6(2) Hyperfine Effect in Lifetime and Capture Rate

Elem	D/Rav	Rc^- (/sec) (T^- ns)	Rc^+ (/sec) (T^+ ns)	(Rc)av (/sec) (Tmean ns)
^{6}Li				4678±104 (2175.3±0.4)[7]
^{7}Li		7260±130 (2162.3±0.7)	3260±80 (2181.2±0.5)	4680±120 (2186.8±0.4)[7]
Be	0.63[3]	10500±560 (2147.5±2.7)	5730±300 (2169.7±2.0)	7500±400 (2162.1±2.0)

Table IV-6(3) Hyperfine Effect in Lifetime and Capture Rate

Elem	D/Rav	Rc^- (10^6/sec) (T^- ns)	Rc^+ (10^6/sec) (T^+ ns)	(Rc)av (10^6/sec) (Tmean ns)
^{10}B				0.0281±0.0005 (2070.7±3.0)
^{11}B	0.51[3]	0.0293±0.005 (2064. ±3)	0.01794±0.0004 (2114. ±2)	0.0222±0.0005 (2096.1±3.0)
	1.2[4]	0.0389±0.0007 (2024±4)	0.0122±0.0003 (2140±2)	0.0222±400
^{13}C	-0.21[3]	0.0318±0.0008 (2054±3)	0.0397±0.0008 (2021±3)	0.0383±0.0007 (2029.1±3.0)
N				0.0699±0.0004 (1906.8±3.0)
F	0.42[3]	0.229±0.003 (1463±5)	0.156±0.002 (1635±6)	0.175±0.003 (1590±6)
	0.76[4]		0.118±0.002 (1746±6)	0.145±0.003 (1666±5)
	0.77±0.13[1]		0.117±0.009 (1749±30)	0.145±0.008 (1667±20)
Na	-0.14[3]	0.377±0.001 (1204±2)	0.435±0.001 (1123±2)	0.413±0.001 (1151±2)
Al	0.18[3]	0.705±0.001 (864±1)	0.590±0.001 (957±1)	0.638±0.001 (915±1)
	0.28[4]		0.536±0.001 (1009±1)	0.606±0.001 (942±1)
P	0.25[3]	1.185±0.003 (611±1)	0.935±0.003 (719±1)	0.997±0.003 (688±1)
	0.37[4]		0.841±0.003 (771±1)	0.972±0.003 (723±1)
Cl	-0.09[3]	1.333±0.003 (561±1)	1.460±0.004 (522±1)	1.413±0.003 (536±1)
	-0.14[4]		1.538±0.004 (502±1)	1.456±0.003 (522±1)
K	-0.08[3]	1.839±0.005 (437±1)	1.994±0.006 (408±1)	1.936±0.005 (418±1)
	-0.11[4]		2.056±0.006 (398±1)	1.974±0.005 (412±1)

Note:
1, Winston' data or estimate (WIN63)
2, Favart et al.(FAV70)
3, BLYP equation (text equation (4.11), Berstein (BER58)
4, Primakoff's estimate quoted in WIN63
5, Winston's neutral data(WIN63)
6, Winston's electron data(WIN63)
7, Saclay group data(BAR78)
-- Lifetimes underlined are our experimental results except Li and all other lifetimes are estimated values.

the hf effect (eg F, Cl). In the case of Na, by using equation (3.1), Ae is calculated to be 0.003. This is too small to be determined by the electron decay spectrum. As summarized above, the total number of events in our experiments is not large enough to obtain Ae. It is also difficult tc measure the effect for light nuclei by the lifetime method if the conversion is slow (for instance Li, Be, B), because most events appear within 4 microseconds. In Table IV-6, past experimental results and estimates of the hf effect are summarized. From the table the most suitable targets are F and Cl for the lifetime method. With sufficient experimental running time, the hf effects in these nuclei could be detected. There have been no estimates of the hf effects in N and ^{13}C. Although these are alsc pcssible candidates, the short lifetimes in the container materials (Fe for N and Cu for ^{13}C) give large distortion for times near zero and this makes it difficult to separate the small hf effect.

(i) From Z=11(Na) to Z=83(Bi)

The follcwing remarks may be made from Z=11(Na) to Z=83(Bi) on the basis of the results obtained in our experiment.

(1) As listed in Table IV-2, our measurements are in fairly good agreement with past measurements for most of the nuclei between Z=11 and 83.

(2) Our lifetime measurements in Na, K, and Cl have been

made with great precision. The lifetimes in Na and Cl are in agreement with earlier measurements (SEN59) within error, but our result in K is substantially longer than the earlier measurement. Our value for the lifetime in Ge is larger than the previous result. Our targets were GeO_2 and GeO, and the muon lifetimes obtained from both oxides were the same. If the constituents of a chemical compound have quite different atomic numbers, then there should be no difference in the lifetime measurement for the element when it is in a chemical compound target and when it is an element target itself. However our result should be checked with germanium metal.

(3) These are the first measurements of lifetimes in Dy, and Er. The lifetimes in Dy and Er seem to be reasonable when they are compared with other rare earth nuclei. Adding our two measurements of Dy and Er to past results, all nuclei between Z=64 and Z=68 have now been studied and this makes it possible to discuss the even-odd Z effect in rare earth nuclei (see section IV.F).

(4) From Table IV-2, it is evident that the odd Z nuclei for $Z \geq 40$ show systematically larger capture rates than the even Z nuclei. Past measurements (FIL63) and our experiment support the fact that the capture rate in Nb(Z=41,A=93) is anomalously higher ($10.35 \pm 0.17 \times 10^6$) than the estimated value from the Primakoff formula

(9.35×10^6) (WAT75). Watson (WAT75) has suggested that the large capture rate in Nb could be due to the vanishing of the Cabibbo angle Qc. In section IV.F, this will be discussed in more detail by comparing experimental total capture rates with the Goulard-Primakoff formula.

IV.E Primakoff Formula in Muon Nuclear Capture

Primakoff derived a formula for the total muon capture rata Rc(A,Z) in a complex nucleus with the mass number A and atomic number Z (PRI59). In his derivation, he started with the effective Hamiltcnian, Heff, deduced by Fujii and Primakoff (FUJ59). In their work, the lepton-bare nucleon ccupling is V and A (Axial vector), and the muon-bare nucleon and electron-bare nucleon coupling constants follow electron-muon universality. Also, assuming the conserved vector current, the nucleon coupling constants are well defined. The Hamiltonian is as follows (FUJ59, PRI59)

$$H_{eff}^{\mu} = \frac{1}{\sqrt{2}} \tau^{+} \frac{1-\bar{\sigma}\cdot\bar{\nu}}{\sqrt{2}} \sum_{i=1}^{A} \tau_i^{-} \{ G_V^{\mu}\, \bar{1}\cdot\bar{1}_i + G_A^{\mu}\, \bar{\sigma}\cdot\bar{\sigma}_i - G_P^{\mu}\, \bar{\sigma}\cdot\bar{\nu}\bar{\sigma}_i\cdot\bar{\nu} \} \delta(\bar{r}-\bar{r}_i) \qquad (4.14)$$

with

$$\begin{aligned} G_V^{\mu} &\equiv g_V^{\mu} \left(1 + \frac{\nu}{2m_p} \right) \\ G_A^{\mu} &\equiv g_A^{\mu} - g_V^{\mu} \left(1 + \mu_p - \mu_n \right) \frac{\nu}{2m_p} \\ G_P^{\mu} &\equiv \{ g_p^{\mu} - g_A^{\mu} - g_V^{\mu} \left(1 + \mu_p - \mu_n \right) \} \frac{\nu}{2m_p} \end{aligned} \qquad (4.15)$$

In equation (4.14), $\bar{\nu}$ is the momentum of the neutrino; $\bar{1}$, $\bar{1}_i$ and $\bar{\sigma}$, $\bar{\sigma}_i$ are 2x2 matrix unit operators and spin angular momentum operators for the lepton and the i-th nucleon; $\bar{r}$ and $\bar{r}_i$ are space co-ordinates for the lepton and the i-th nucleon; τ^+ , τ_i^- are isobaric spin operators which transform a lepton muon state into a lepton neutrino state and an i-th nucleon proton state into an i-th nucleon neutron state (FUJ59).

With equations (4.14) and (4.15), the square of the muon capture transition matrix element between the states of initial and final nuclei was calculated by the closure approximation. In the approximation all energeticaly accessible states of the final daughter nucleus are excited by the muon capture and the sum over all the excited states is performed. Using this approximation, Primakoff obtained

$$Rc(A,Z) = (Zeff)^4 Rc(1,1) K\{1 - g(A-Z)/(2A)\} \qquad (4.16)$$

where Rc(1,1) is the muon capture rate in hydrogen, K represents the reduction of phase space for the neutrino and g is the nucleon-nucleon correlation parameter. The second term, $\{(A-Z)/2A\}g$, embodies the Pauli exclusion principle and is proportional to the fraction of neutrons. The estimated value for g is equal to 3 (PRI59). Hence for a nucleus with A=2Z, the bracket reduces the capture rate by a factor of 4. Therefore, the Pauli exclusion term is a large

effect for heavy nuclei.

In order to compare our experimental results with the Primakoff formula, equation (4.16) is parameterized as follows

$$Rc(A,Z) = (Zeff)^4 X(1) \{1 - X(2)(A-Z)/(2A)\} \qquad (4.17)$$

The effective charges have been calculated for most of the nuclei by Ford et al. (FOR62). Their results are listed in Table IV-2. The effective charges, which are not provided in the reference, are obtained by the linear interpolation method and shown in Table IV-2 underlined. For the best fit of equation (4.17) to our data and past measurments (ECK66), a chi-squared minimization program MINUIT was used. The results are listed in Table IV-7. In these fittings, elements lighter than Z=7 and odd proton nuclei between Z=8 and Z=22 are not included. The result of fitting X(2) agrees well with the estimated value for g by Primakoff. The calculation by Primakoff has shown X(1)=161 /sec and this is reproduced by the experiment as shown in Table IV-7. Without the conserved vector current (CVC) hypothesis, his calculation gave X(1)=137 /sec, so the experiment and theory agree well with the assumption of CVC (PRI59).

If the neutron excess term satisfies (A-Z)g/(2A) =1, equation (4.16) breaks down. The condition implies Z/A= 1-2/X(2)= 0.36. For ^{238}U, Z/A is about 0.39, thus Z/A becomes close to this condition for heavy nuclei. Hence

higher order Pauli corrections become necessary for heavy nuclei. Goulard and Primakoff (GOU74) obtained

$$Rc(A,Z)=X(1)\,(Zeff)^{4}\{1+\frac{A}{2Z}X(2)-\frac{(A-Z)}{2A}X(3)$$

$$-(\frac{A-Z}{2A}+\frac{A-2Z}{8ZA})X(4)\} \qquad (4.18)$$

where X(i) (i=1 to 4) are constants. In X(1), kinematic factors are included. The best fits to all existing data are listed in Table IV-8. From Tables IV-7 and IV-8, it is clear that the Goulard-Primakoff formula gives a little better chi-square fit than the Primakoff formula. Figures IV-2 and IV-3 show the fitting curves for the best chi-square fits listed in Table IV-7 and IV-8. From the two figures, it is evident that the two formulae show almost the same behavicr.

IV.F The Even-Odd Z Effect in Heavy Nuclei

As stated in section IV.D, the odd-Z nuclei for Z>40 show larger capture rates than the even-Z nuclei. In light elements with odd Z, most of the large capture rates can be attributed to the hf effect. For heavy nuclei the hf effect is small, since the effect is proportional to 1/Z, as shown in equation (4.13), and the capture rates from the two hf states are nearly the same. This 1/Z dependence is illustrated by figures IV-4 and IV-5. Figure IV-4 shows

Table IV-7, Fitting Results for Primakoff Formula (4.16)

	TRIUMF Data[1]	Past Results[2]
Number cf data	30	58
X(1)	170	170
X(2)	3.125	3.125
(exp-fit)/exp	4.6%	5.8%

1) Our experimental results listed in Table IV-1.

2) Past results summarized by Eckhause et al. (ECK66).

Table IV-8, Fitting Results for Goulard-Primakoff Formula (4.18)

	TRIUMF Data[1]	Past Results[2]
Number cf Data	30	58
X(1)	261	252
X(2)	-0.040	-0.038
X(3)	-0.26	-0.24
X(4)	3.24	3.23
(Exp-Fit)/Exp	4.1%	5.6%

1), 2) see Table IV-7 above.

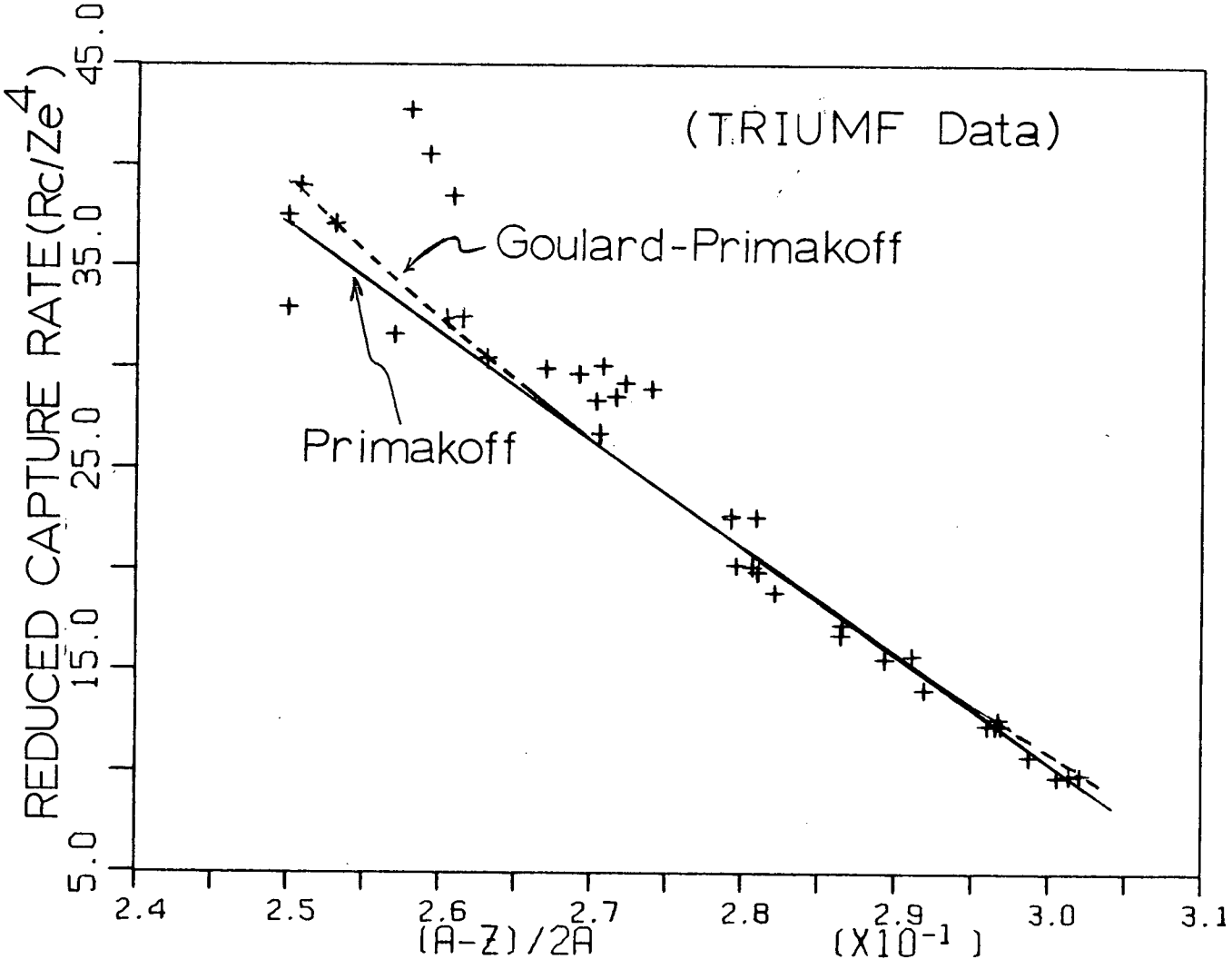

Figure IV-2, The TRIUMF data are fitted to the Primakoff and the Goulard- Primakoff formula.

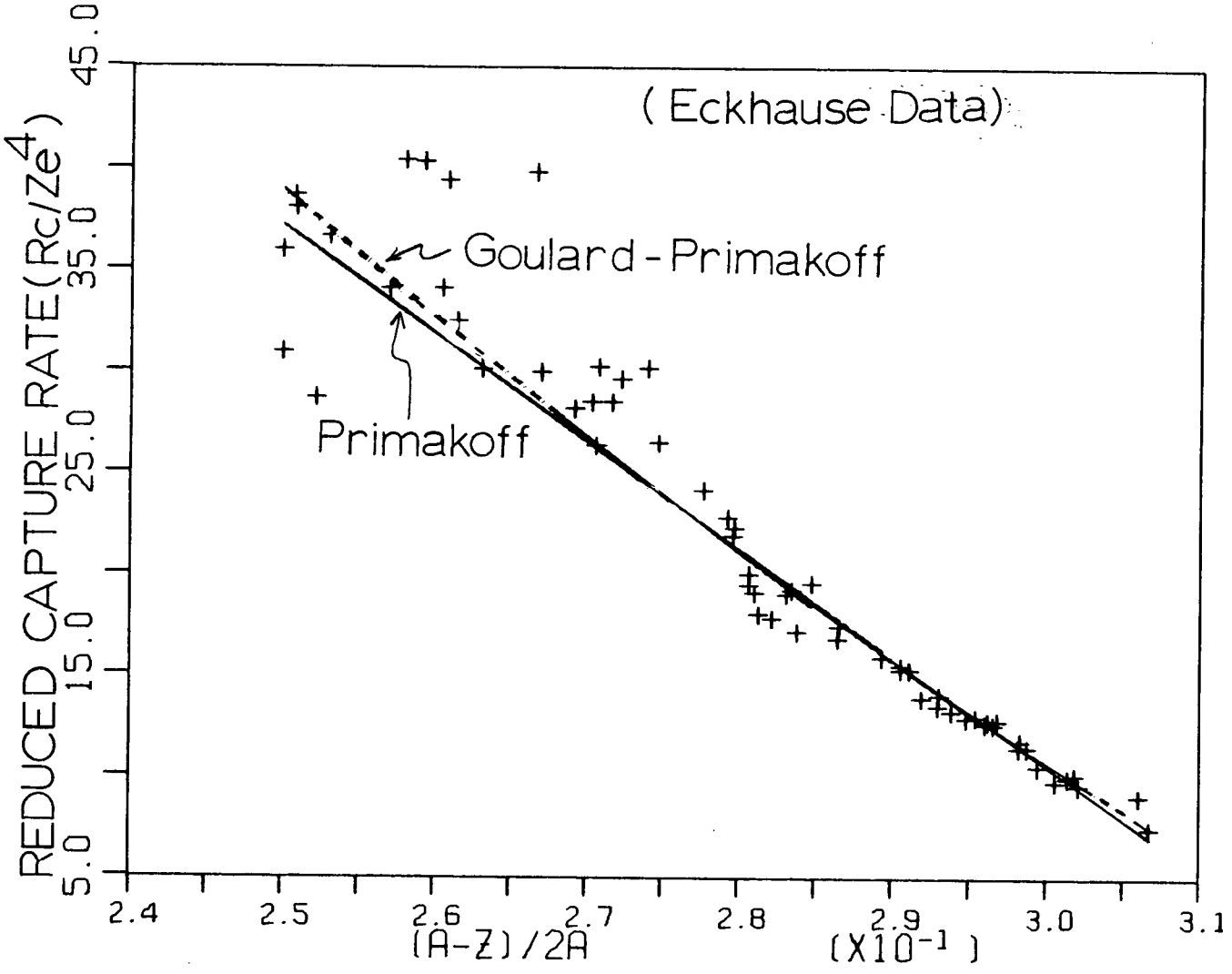

Figure IV-3, Past findings summarized by Eckhause et al.(ECK66) are fitted to the Primakoff and the Goulard-Primakoff formula.

deviations of experimental capture rates from the Goulard-Primakoff (G-P) formula. Note that we are now plotting against the atomic number Z in order to illustrate that the pattern of deviation is connected with shell effects. In this section, all TRIUMF data are used for a comparison between the experimental results and the G-P formula. In the comparison, data lacking in the TRIUMF set are taken from the reference of Eckhause et al. (ECK66). The experimental results of nuclei with atomic numbers smaller than Z=10 are excluded from the discussion below, because the formula seems to be valid only for nuclei heavier than Z=8 as claimed by the authors (PRI59, GOU74). In figure IV-5, the absolute deviations of figure IV-4 have been shown. From figure IV-5, it is clear that most of the odd-Z data between Z=10 and Z=40 deviates from the G-P formula. Since the deviations decrease as the atomic number increases, this tendency agrees with the 1/Z dependence of the hf interactions (see BLYP equation (4.13)). This is understood clearly from Table IV-6. In the table, the average capture rates, $(Rc)_{av}$, and the capture rates from the lower level, Rc^-, are listed for light nuclei. Due to fast conversions from the higher hf level to the lower hf level, all muons decay from the lower hf levels in nuclei heavier than fluorine. The large deviations of estimates by the G-P formula from experiments are caused by differences between $(Rc)_{av}$ and Rc^- (eg 20% in P), because the theory deals with the average capture rates $(Rc)_{av}$.

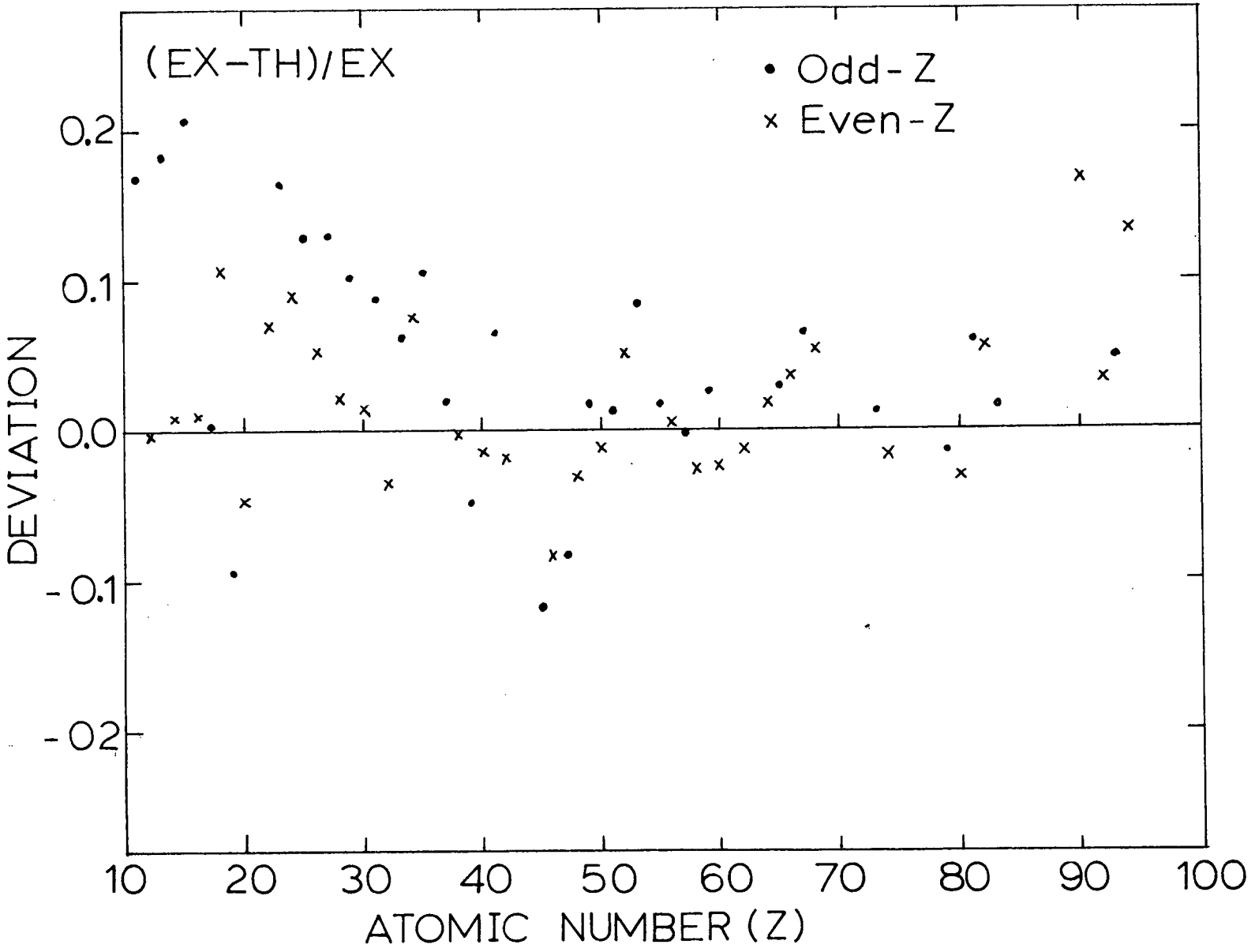

Figure IV-4, Deviations of experimental capture rates from the Goulard-Primakoff formula.

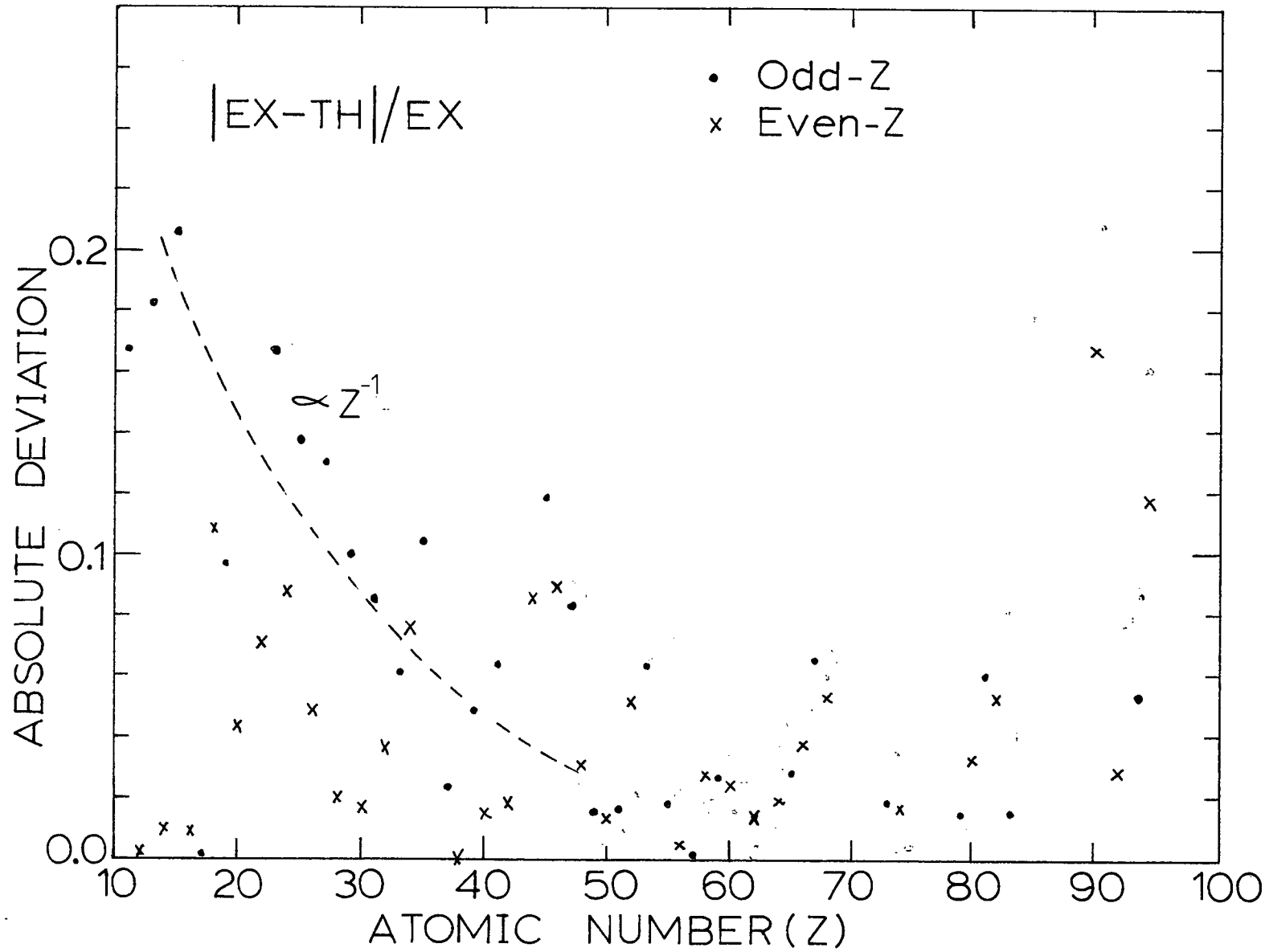

Figure IV-5, Absolute deviations of experimental capture rates from the Goulard-Primakoff formula. Figure IV-4 is redrawned.

Figure IV-6 shows data points for odd-Z nuclei only. In this figure, the odd data points are normalized as follows

Odd Z data - {Even (Z-1) data + Even (Z+1) data}/2

In the discussion of the even-odd effect, the difference of capture rates between odd-Z and its neighboring even-Z nuclei is important. After this manipulation, the large deviations of odd-Z nuclei from the G-P formula in figure IV-4 and IV-5 turn out to be small for some nuclei. For example, Tb(Z=65) and Ho(Z=67) have 3% and 6.5% deviations, respectively, as shown in figure IV-5. In figure IV-6, these deviations are only 0.5% and 2%, respectively. In this figure, the odd-Z nuclei between Z=10 and Z=30 have large deviations due to the hf effect as expected. Between Z=35 and Z=70, Nb seems to have an anomalously large deviation. The hf effects are estimated by equation (4.13) to be about 3% and these effects are not large enough to explain the anomalous deviation (=large capture rate).

Watson (WAT75) has suggested that the large capture rate in Nb could be due to the vanishing of the Cabibbo angle (θ_C). This concept was proposed by Salam et al. (SAL74) who showed that a strong external magnetic field ($\geq 10^{16}$ gauss) causes the Cabibbo angle θ_C to vanish. Such high fields can be easily achieved in the interior of the odd nuclei (SUR75).

The total muon capture rate is proportional to

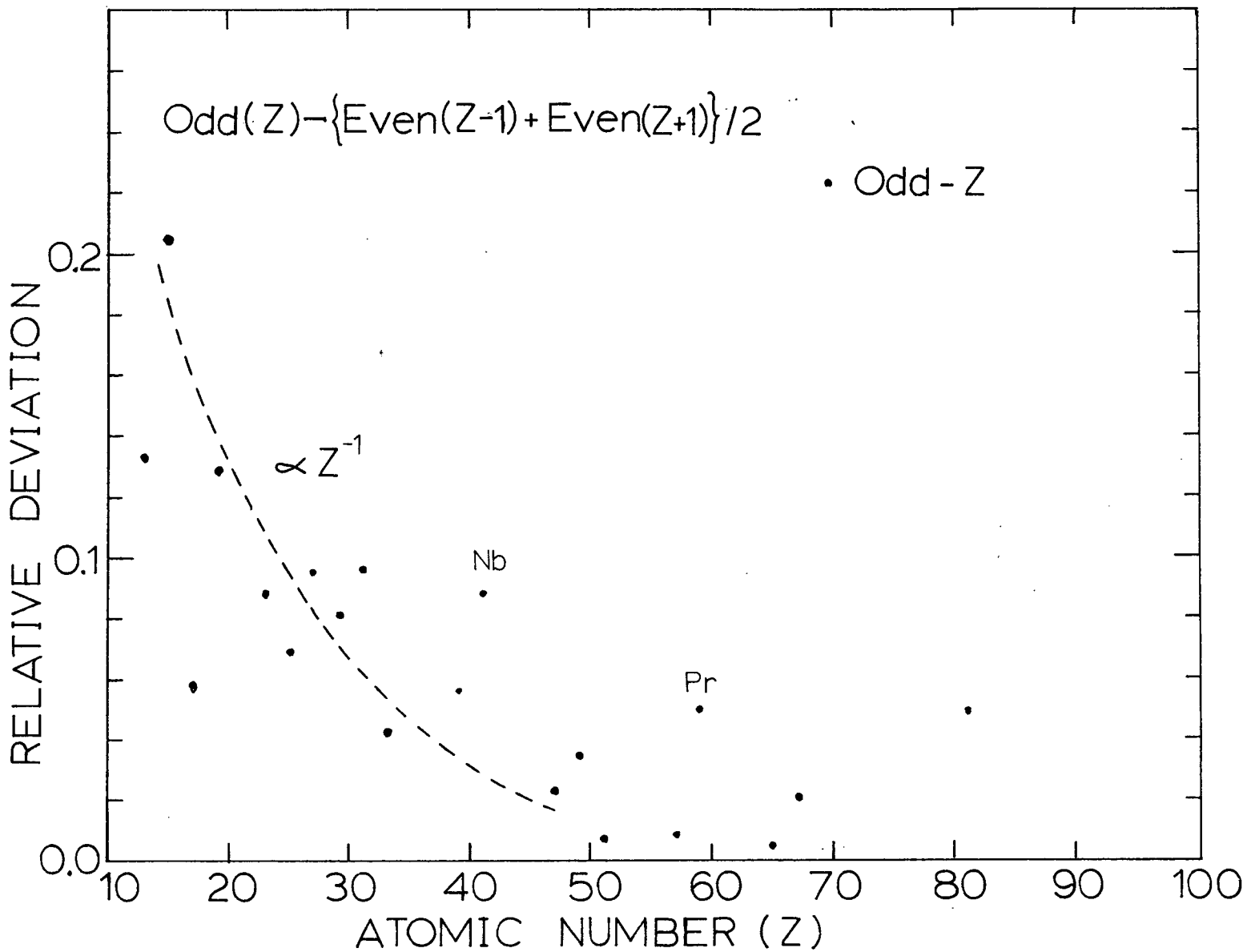

Figure IV-6, The normalized deviations of odd-Z nuclei.

$\{Gm \cdot \cos(Qc)\}^2$ (BLI73). The coupling constant, Gm, obtained from equation (4.2), is related to the vector coupling constant Gv in a beta decay by

$$Gv = Gm \cdot \cos(Qc)$$

We expect the effect of the vanishing of Qc to be given by

$$Rc(\text{odd } A)/Rc(\text{even } A) = 1/\cos^2(Qc) \qquad (4.19)$$

The Cabibbo angle, determined from eight hyperon beta-decays (ROO74), is equal to 0.234 ± 0.003 radians. Using this angle, equation (4.19) predicts about a 6% increase in the theoretical capture rate. In the case of Nb our capture rate is 9% higher than the theoretical rate. If the Cabibbo angle is quenched, it could explain larger experimental values.

If this is a universal rule, the large capture rates (>5%) have to be observed for most of the odd nuclei heavier than Z=40. But it is evident from figure IV-6 that this does not hold true for many odd-Z heavy nuclei. As discussed in the following section IV.G, there is a correlation between nuclear muon capture and nuclear structure. Thus in order to discuss the even-odd Z effect, we have to choose nuclei which are not strongly affected by nuclear structure. Figure IV-8 shows that nuclei between Z=45 and Z=55 or Z=63 and Z=75 satisfy this condition. As seen in figure IV-6, these nuclei deviate from the G-P formula by 2%. This is not such a large deviation as expected from the vanishing of Cabibbo angle.

Also the vanishing of the Cabibbo angle has been

investigated in actinide nuclei by Parthasarathy et al.(PAR78). According to their calculation, the large total muon capture rates in ^{235}U and ^{239}Pu measured by Johnson et al.(JOH77) are reproduced by adding the increase due to the vanishing of the Cabibbo angle. But the recent paper by Wilcke et al.(WIL80-2) has shown that the large capture rates in actinide nuclei are well described by the alternate model of Kozlowski and Zglinski (KOZ78). In their model, the total muon capture rate is the sum of the rates for each multipolarity of giant resonance excitations. According to their results, in the case of Ca, the giant dipole resonance is dominant,whereas in the case of Pb both the dipole and octupole resonances are important. As discussed in section I.D, the giant resonance model works very well for total muon capture rates in light nuclei. It seems that in actinide nuclei the capture rates are better explained by the resonance model which includes higher multipole excitations (WIL80-2).

The hypothesis of the vanishing of the Cabibbo angle is based on the assumption of an ultra high magnetic field (10^{16} gauss) in odd-A nuclei. According to the recent elaborate calculation by Lee and Khanna (LEE78), the internal magnetic field in odd heavy nuclei is less than 5×10^{14} gauss. Hence the actual magnetic field may not be high enough for the vanishing of the Cabibbo angle.

Finally, in conclusion, the concept of the vanishing of the Cabibbo angle in muon capture has not been

proved and in fact the weight of the evidence is slightly against it. Since there is a strong correlation between total mucn capture rate and nuclear structure, when considering the even-odd Z effect in muon capture, the nuclear structure has to be taken into account.

IV.G Nuclear Structure Effect in Muon Capture

In this section, the correlation between capture rates and nuclear structure will be examined.

Figure IV-7 is different from the Primakoff plot (figures IV-2 and IV-3). This plot has been presented by Kohyama and Fujii (KOH79), and is based on the following general formula for total capture rates

$$\Lambda c = K \frac{(Zeff)^4}{Z} \sum_{b\leq} \left| \frac{\bar{\nu}ba}{m_\mu} \right|^2 \int \frac{d\bar{\nu}}{4\pi} \left| \langle b | J^- \left(|\bar{\nu}ba| \right) | a \rangle \right|^2$$

The y axis of figure IV-7 is equal to the total 'strength' of the nuclear transition as follows

$$\frac{\Lambda c^{exp}}{(Zeff)^4} Z = K \sum_{b\leq} \left| \frac{\bar{\nu}ba}{m_\mu} \right|^2 \int \frac{d\bar{\nu}}{4\pi} \left| \langle b | J^- \left(|\bar{\nu}ba| \right) | a \rangle \right|^2 \qquad (4.20)$$

In figure IV-7, the experimental results are used for the capture rates in equation (4.20). In the figure, the experimental capture rates reduced by $(Zeff)^4$ increase

linearly until Z=30, and then become constant. The nuclear transition matrix for muon capture has a contribution from Z protons and A-Z neutrons. In the case of small Z, the Z protons in the nucleus contribute linearly to the muon capture and, for heavy nuclei, only a fraction of the Z protons in the nucleus takes part in the muon capture. This reduction is implemented by the effective charge, Zeff, in the nucleus.

In figure IV-7, there is a clear oscillation and, surprisingly, the minima correspond to the atomic closed shells (Ar, Kr, Xe). But this does not mean that the structure of the atomic closed shells affect nuclear capture rates. By chance this is one of the characteristics of the nuclear structure. This can be explained by figure IV-8. In figure IV-8, the amount of the neutron excess in nuclei versus atomic number is plotted. This amount is called the Pauli exclusion strength in the Primakoff formula. In this figure, the maxima accidentally correspond to the atomic closed shell and, in muon capture of the nucleus near the maxima, the large Pauli exclusion inhibition can be expected. This effect causes oscillations in figure IV-7 and the experimental results clearly reflect the nuclear shell effect. In the figure, the reduced capture rate of Ar is anomalously small. Although there have been no measurements of total muon caputure rates in Kr and Xe, their reduced capture rates are expected to be very small. On the other hand, the minima in figure IV-8 are located

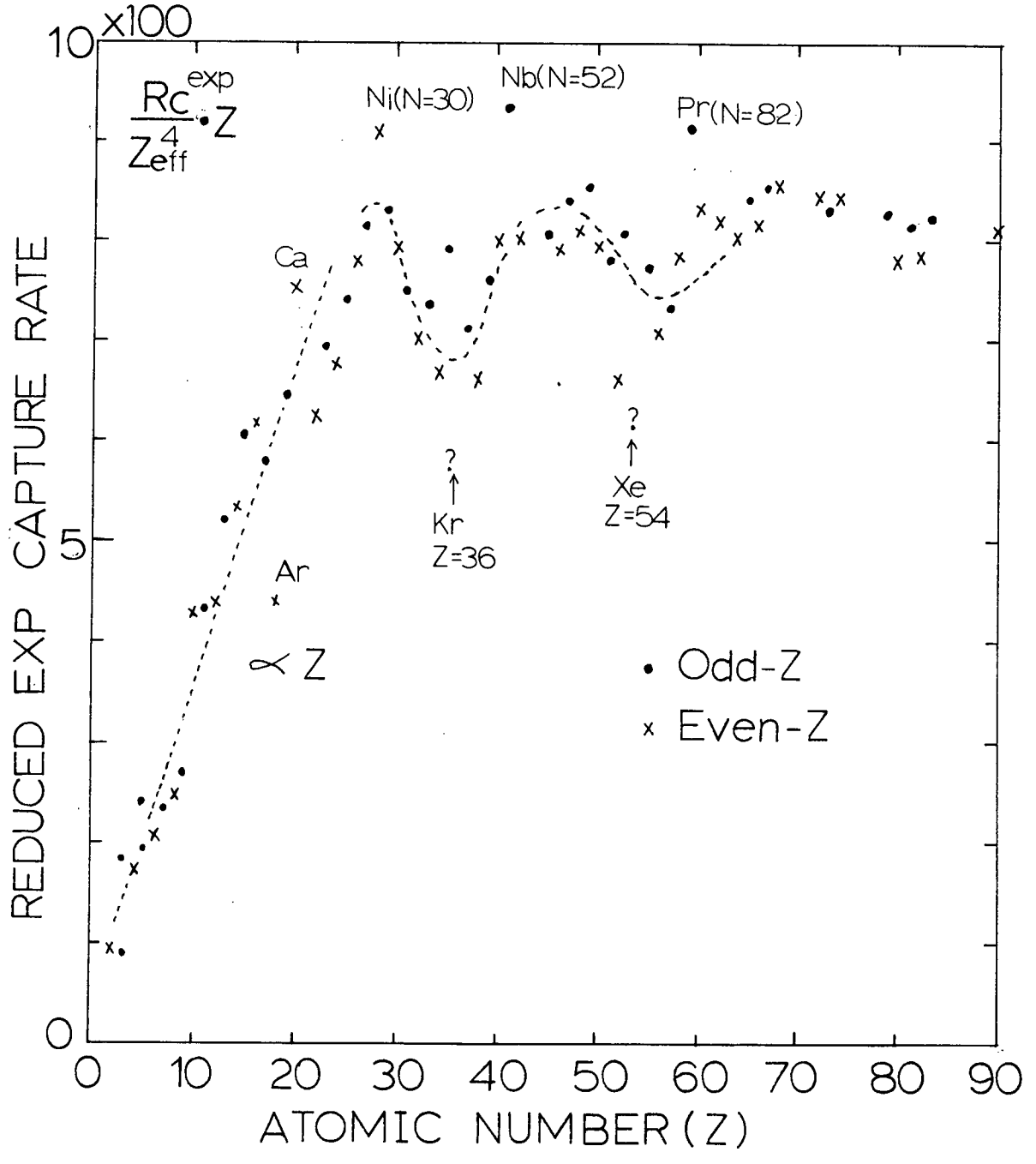

Figure IV-7, Reduced capture rates versus atomic number. This graph is adapted from Kohyama and Fujii(KOH79).

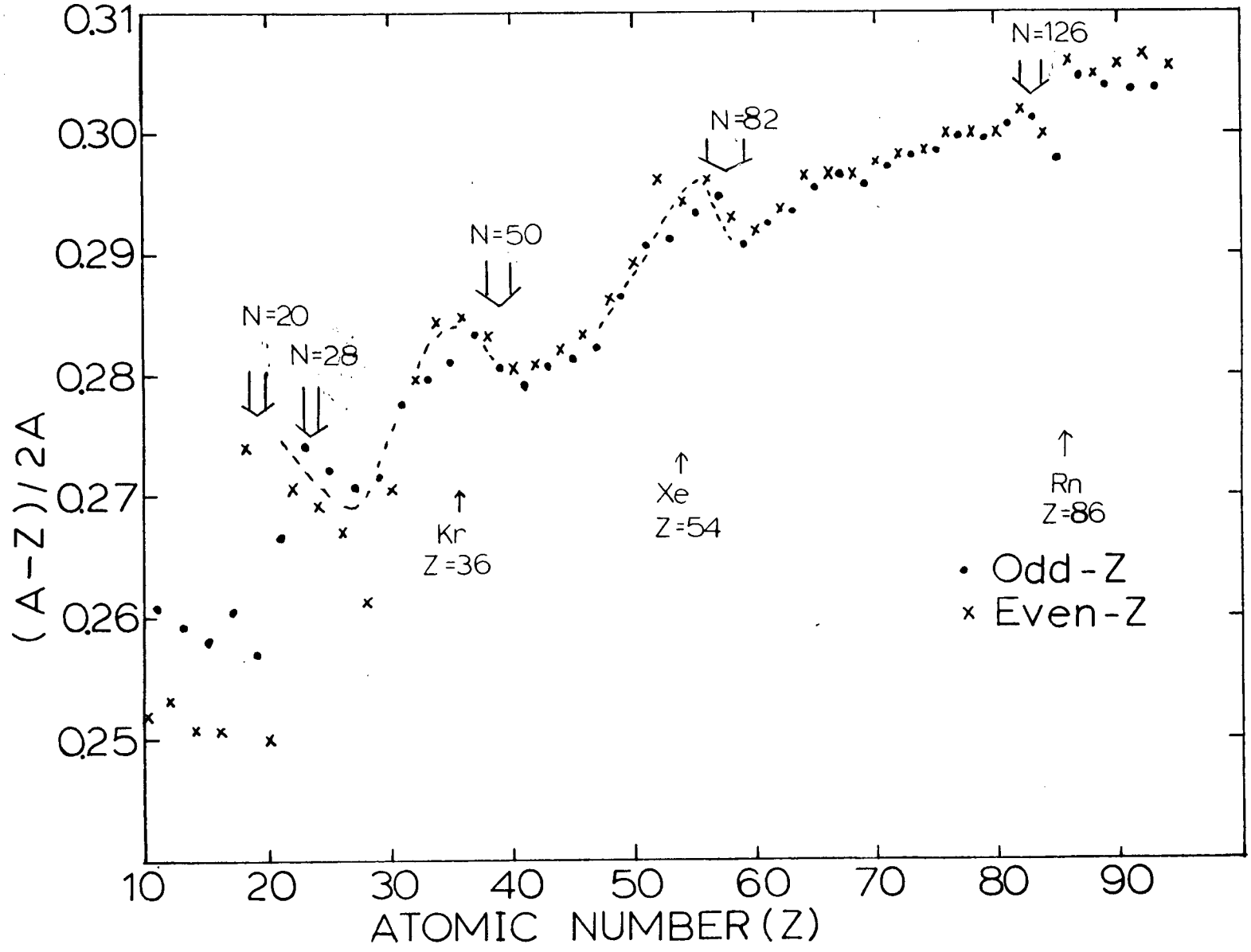

Figure IV-8, The neutron excess versus atomic number. This excess term is named Pauli exclusion term by Primakoff.

near the nuclei with nuclear magic numbers listed below. At the minima, the Pauli inhibition is small and the experimental capture rates seem tc be large.

From figure IV-7, Ca(20,40), Ni(28,51), Nb(41,93) and Pr(59,141) appear to have larger capture rates than other nuclei. Ca and Pr have neutron magic numbers, and Ni and Nb have neutron numbers near magic numbers. The magic numbers ccrrespond tc neutron or proton number N or Z equal to 2, 8, 20, (28), (40), 50, 82, (114), 126. The numbers in parentheses are rather weak magic numbers. Nuclei having Z or N equal to a magic number have characteristics which are different frcm other nuclei. In muon capture, the basic process is expressed by (1.9) and for complex nuclei the process is (1.10). Thus the exclusion inhibition against neutrcns produced by the muon capture seems to affect the capture rates. Frcm figure IV-8 this inhibition is apparently small for nuclei having N equal to a magic number. This explains the relatively large capture rates for Ca(N=20) and Pr(N=82). Although, in the case of Ni(N=30) and Nb(N=52), the neutron numbers exceed the magic numbers (28,50) by twc, from figure IV-8 the Pauli inhibition is still small for Ni and Nb. In these nuclei the closed shell effect still remains and affects the muon capture rates. There are some nuclei which have magic numbers of neutron (eg Y(39,89)) but they do not show anomalously large capture rates and do not deviate extremely from the G-P formula. Although Y(39,89) is similar to Nb(41,93), the muon capture rates of Y are not anomalous

like Nb. This seems to be due to the difference in their nuclear magnetic moments. Y has a small negative magnetic moment (=-0.137), whereas Nb has a large positive magnetic moment (=6.167). In the case of the negative magnetic moment, the $F^+=I+1/2$ hf state is lower than the $F^-=I-1/2$ hf state. Since there is a rapid conversion from F^- to F^+ in Y, the capture rate from F^+ seems to be suppressed. The hf effects for the nuclei with negative magnetic moments appear to be one of the reasons for the different behavior of Y from Nb, although there has been no estimate of its magnitude.

The nuclear charge radii of molybdenum and strontium isotopes have been measured by Fricke et al. (FRI79). Their experiment has suggested that the nuclear charge radius of Mo(Z=42,N=52) is 1% larger than that of Mo(Z=42,N=50) which has the neutron magic number 50. From their result, protons in a nucleus with a neutron magic number seem to be more tightly bound but, when the number of neutrons moves away from a magic number, the binding force becomes weaker and the radius of the protons tends to increase. This seems to be the case for Nb(Z=41,N=52). Since the radius of the muonic S orbit in Nb is 6.4 fermi (10^{-13} cm) and the nuclear radius is about 6 fermi, the muonic wave function is comparable in size to the nucleus and so the muon capture rate will be very sensitive to the exact distribution of the protons in the nucleus. This has been pointed out by Eckhause et al. (ECK66).

CHAPTER V

Muon Capture in Chemical Compounds

V.A Introduction

Fermi and Teller (FER47) proposed a model in which the relative capture probability was proportional to the atomic number Z of each atom in a chemical compound. This so called Fermi-Teller Z law implies that the ratio of atomic capture rates of negative muons in a compound $(Z1)_m(Z2)_n$ is given by

$$W(Z1/Z2) = (m \cdot Z1)/(n \cdot Z2) \qquad (5.1)$$

It soon became clear that the Z-law did not explain the experimental observations (BRI63) and the capture process was much more complicated. Zinov et al. (ZIN66) demonstrated that the relative atomic capture rates in the metallic oxides have a pericdic characteristic. The positions of the minima correspond to the alkali metals. The experimental results clearly indicated that the electronic structure of chemical compounds affects the atomic capture rate of muons.

So far, there have been a significant amount of data collected by many groups but they were often inconsistent. Most studies of the atomic capture rates have been made by detecting the muonic K X-rays (the Lyman

series). In this method, the sum of the intensity of the X-ray has been assumed to be equal to the numbers of muons captured. In some earlier experiments (SEN58, ECK62, BAI63), the atomic capture rate was obtained by detecting decay electrons from muons which spent most of their life in the K orbit. These earlier experiments had poor statistics and very few targets were measured. In the present experiment, their method has been applied to study the atomic capture rate of muons in metallic oxides. Since the lifetime of a negative muon in oxygen (1795 ns) is significantly longer than the lifetime in elements heavier than sodium (1204 ns), it is easy to decompose the decay electron spectrum into the oxygen and metal constituents by using their lifetimes.

As discussed in Chapter I, it is a good approximation that all muons trapped in an atom reach the K orbit without their disappearance by decay, or nuclear capture during the cascade. Within this approximation, the number of muons deduced from the decay electron spectrum should be equal to that obtained from the intensity of the muonic X-ray.

V.B Muon Atomic Capture Ratio by the Lifetime Method

In order to obtain the number of muons from a decay electron spectrum, we must correct for the fact that in heavy elements most of the muons are absorbed by the nucleus. Thus, the total number of decay electrons, $Ne^-(Z)$, from the nucleus with the atomic number Z is given by

$$Ne^-(Z) = \frac{Q(Z) \cdot Rd}{Rc(Z) + Q(Z) \cdot Rd} \cdot Nm^-(Z) \cdot E1 \cdot E2(Z) \qquad (5.2)$$

where the definitions of Q,Rd and Rc are given by equations (4.4) and (4.5), E1 is the counter efficiency including the effect of limited solid angle, E2(Z) is the correction for the loss cf low energy decay electrons in the target, and $Nm^-(Z)$ is the number of negative muons trapped in the nucleus with Z. Figure I-3 showed the energy spectrum of decay electrons in the targets C, Ti, Cu, and Pb (SUZ79). It is clearly seen that the peaks of the energy spectra in heavy elements are shifted to lower energy due to the binding cf the negative muon. Hence, the rate of the loss of low energy electrons in the target is larger in the case of heavy elements than in the case of light elements. This correction is acccunted for by E2(Z). In order to determine E2(Z), we have tc know the energy loss for decay electrons

in the target, plastic walls of the target container, and the counter telescope. The different path lengths that electrons can experience are estimated and averaged. Thus we can calculate the cut off energy in the energy spectrum of decay electrons. In our analysis, the calculated energy spectrum by Huff (HUF61) is employed. For example, in Pb_3O_4, the cut off energy is 18 MeV and the losses of decay electrons in Pb and O are 26% and 11%, respectively. Also, in Cr_2O_3, the cut off energy is 11 MeV and the loss is 4% in Cr and 2.4% in O. The corrections are small for oxides with Z smaller than Z=30, while they are severe in oxides with heavy constituents. Since the total corrections in the atomic capture rate always appear as the difference between two values of E2(Z) and E2(O), the corrections tend to be smaller.

Negative muons in metallic oxides Z_mO_n are trapped either in the metal(Z) or in the oxide(O). By the analysis of the decay electron spectrum, the spectrum can be decomposed into the metal and the oxygen components. From this manipulation, $Ne^-(Z)$ and $Ne^-(O)$ are obtained. Thus, $Nm^-(Z)$ and $Nm^-(O)$ are found from equation (5.2). The ratio of atomic capture rates per atom in Z_mO_n is defined by

$$W(Z/O) = \{n \cdot Nm^-(Z)\} / \{m \cdot Nm^-(O)\} \qquad (5.3)$$

In the fitting of the spectrum, equation (3.6) has been used and, from equations (5.2) and (5.3), we get

$$W\left(\frac{Z}{O}\right) = \frac{n}{m} \cdot \frac{Q(O)}{Q(Z)} \cdot \frac{E2(O)}{E2(Z)} \cdot \frac{A(Z)}{A(O)} \qquad (5.4)$$

where A(Z) and A(O) are the amplitudes of the metal and the oxygen component at t=0, respectively. In the case of Z<30, Q(Z) and E2(Z) are almost equal to the values for oxygen (Q(O), E2(O)), because of the small bound muon effect.

One of the shortcomings of the lifetime method is the difficulty in separating the different lifetime components for elements with similar atomic numbers. In order to study this problem, a Monte Carlo programme was written to simulate a run with dry ice (CO_2) as a target material. Assuming A(C)/A(O) =0.25, 4×10^5 muons out of 5×10^5 trials were captured in oxygen and the numbers of muons was estimated at 3.99×10^5 by fitting the artificially created spectrum. Since the difference between the Monte Carlo and the fitting is only 0.3%, it seems that if we have enough statistics, we can separate events even for compounds having components with nearly the same Z, such as CO_2. We have measured a muon atomic capture ratio in dry ice. The result seems quite reasonable, when it is compared with the atomic capture ratio of oxides with B or Be (SCH78-2) near C.

Our results are listed in Table V-1 along with past results of X-ray measurements done by previous workers.

Table V-1, Per Atom Capture Ratios A(Z/O) of Muons in Metallic Oxides

Z	ZmOn	TRIUMF	Past Result	Ref.
6	CO2	0.43 ± 0.02		
11	Na2O2	0.87 ± 0.02		
12	MgO	0.80 ± 0.02	0.83 ± 0.07	(1)
13	Al2O2	0.84 ± 0.03	0.85 ± 0.06	(1)
			0.65 ± 0.06	(2)
14	SiO2	0.96 ± 0.04	0.79 ± 0.07	(1)
			0.57 ± 0.05	(2)
			0.86 ± 0.07	(3)
15	P2O5	0.87 ± 0.03	0.93 ± 0.11	(2)
20	Ca(OH)2	1.49 ± 0.06		
	CaO		1.36 ± 0.10	(1)
	CaO		1.45 ± 0.09	(4)
22	TiO2	2.17 ± 0.11	2.70 ± 0.20	(1)
			1.90 ± 0.10	(4)
24	Cr2O3	2.63 ± 0.13	3.00 ± 0.17	(1)
			2.04 ± 0.11	(4)
	CrO3	2.96 ± 0.20		
25	MnO2	3.00 ± 0.17		
29	CuO	4.06 ± 0.23	3.60 ± 0.40	(1)
			6.14 ± 0.85	(6)
30	ZnO	2.39 ± 0.10	2.66 ± 0.32	(1)
32	GeO	2.20 ± 0.12		
	GeO2	2.40 ± 0.13		
48	CdO	1.93 ± 0.07	6.70 ± 1.50	(1)
			2.47 ± 0.22	(4)
			2.50 ± 0.28	(5)
50	SnO2	2.15 ± 0.11	3.17 ± 0.24	(1)
56	BaO	2.27 ± 0.09	2.27 ± 0.22	(1)
			1.45 ± 0.18	(5)
60	NdO2	4.13 ± 0.29		
80	HgO	3.75 ± 0.29		
82	PbO2	3.21 ± 0.23	4.17 ± 0.30	(1)
			4.10 ± 0.42	(5)
	Pb3O4	3.87 ± 0.29		

References:

(1) ZIN66
(2) SEN58
(3) MAU77
(4) KNI75
(5) DAN77
(6) BAI63

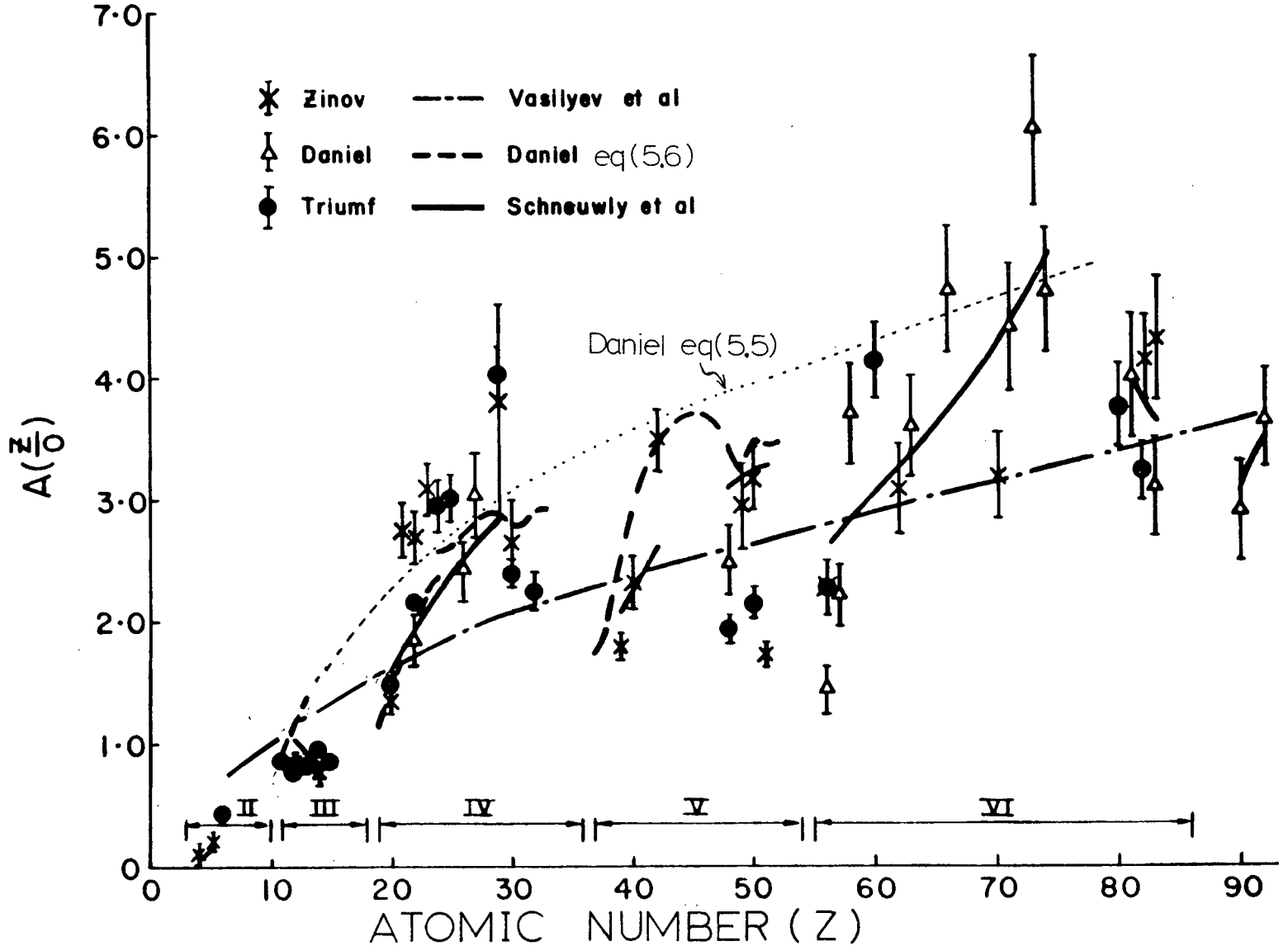

Figure V-1, Atomic capture ratio in metallic oxides.

In figure V-1, our results, past measurements and various theoretical curves are shown together. It is evident that our results are in adequate agreement with the X-ray measurements (ZIN66, DAN77).

The Fermi-Teller Z-law explains the experiments qualitatively below Z<30, but in heavy elements the Z-law predicts twice the values of the experimental capture rates. Daniel (DAN75) performed a calculation of the atomic capture ratio for negative muons in condensed matter. His calculation is based on the treatment of Fermi and Teller in which the electrons are treated as a Fermi gas. He obtained the atomic capture ratio per atom in the case of a binary compound with elements Z1 and Z2

$$W\left(\frac{Z1}{Z2}\right) = \frac{(Z1)^{1/3}\cdot\ln(0.57\cdot Z1)}{(Z2)^{1/3}\cdot\ln(0.57\cdot Z2)} \qquad (5.5)$$

This formula gives better agreement than the Z-law as shown in figure V-1.

The chemical bond also affects the structure of the cascade intensities. Zinov el al.(ZIN66) and Kessler et al.(KES67) have shown that the muonic X-ray K-series spectra in pure metal Ti have more transitions from high orbits than the spectra in titanium oxides. Schneuwly et al.(SCH78-1) performed the systematic measurements of capture ratios in

selected compounds of nitrogen, sulfur and selenium, and confirmed that the chemical structure plays an important role in the muonic atomic capture process. The first successful theory to take into account the effect of core and valence electrons was proposed by Schneuwly et al. (SCH78-2) and, as shown in figure V-1, their theoretical curve reproduces the periodicity observed in the experiments.

Recently, it has been shown that there is a strong correlation between atomic capture and atomic radii with the atomic capture rate being high for atoms with small radii (DAN78). Daniel (DAN79) proposed a model which takes the actual atomic radii into account and modified his formula (5.5) to give

$$W\left(\frac{Z1}{Z2}\right) = \frac{(Z1)^{1/3} \cdot \ln(0.57 \cdot Z1) \cdot R(Z2)}{(Z2)^{1/3} \cdot \ln(0.57 \cdot Z2) \cdot R(Z1)} \qquad (5.6)$$

where R(Z) is the atomic radius for an atom of atomic number Z. As shown in figure V-1, equation (5.6) clearly gives the periodicity of the atomic capture rate and gives better agreement than equation (5.5).

Even though, as discussed above, the theories of Schneuwly and Daniel have revealed the important features of the atomic capture rate, there is still difficulty in interpreting the experiments. In our experimental results,

it is evident that the capture ratios in different oxides of the same element are different. Daniel's model can reproduce this difference only weakly via the different atomic radii for different valency states. Schneuwly's model, which takes the chemical bond effect into account, also gives slightly different capture ratios for the different oxides of the same element. However the differences predicted by these models are not large enough to explain the differences observed in the experiments. Thus, the thecretical development will have to be pursued further to solve the chemical effects in the atomic capture rate.

CHAPTER VI

Summary

Our lifetime measurements for negative muons bound in various nuclei have produced many successful results. Forty eight elements were studied altogether, which is a somewhat larger survey than has been attempted before.[1] This large number of measurements by one group removes the differences due to systematic errors among various experimental groups. For the lifetime measurment, systematic errors due to 2nd muons and 2nd electrons are important, and in previous experiments very few groups have succeeded in the determination of the positive muon lifetime. Hence, the past results of negative muon lifetimes in nuclei were affected by systematic errors which shifted the positive muon lifetime. The positive muon lifetime determined by our system was 2197.0 ±0.7 ns which agrees well with the accepted value of 2197.120±0.077 ns (KEL80).

We have improved the accuracy of negative muon lifetimes in many light elements (Be, B, N, O, F, Na, Cl, K) and new determinations were made for ^{13}C, ^{18}O, Dy, and Er. Most of our measurements are in adequate agreement with past findings. In the case of ^{6}Li and ^{7}Li, there was a

---

[1] Sens et al. (SEN59) had 30 elements in 1959.

disagreement between the Lodder-Jonker calculation (LOD67) and the experiment cf Eckhause et al.(ECK63). The two recent experiments, ours and Bardin's (BAR78), are in agreement with each other and also with the theoretical calculation. A large isotope effect was observed in Li, B, and O, however, there was no isotope effect observed in C. Calculations of partial capture rates in ^{12}C and ^{13}C have been performed by Desgrolard et al.(DES78) using a shell model, and their results indicated no difference in the capture rates for these isotopes. This prediction for the partial muon capture rate seems to hold even for the total capture rate as demonstrated by our experiment.

Recently, it was pointed out that odd-Z heavy nuclei might be showing larger total muon capture rates than even-Z heavy nuclei due to the presence of an ultra high magnetic field (10^{16} G) (WAT75) which causes the vanishing of the Cabibbo angle (WAT75, SAL74). The discussion was based on the observation of a large nuclear capture rate in Nb which has been confirmed in this work. However as discussed in section IV.F, this effect seems to have a correlation with nuclear structure. In order to avoid any nuclear structure effects, the even-odd effect has been investigated between Z=45 and Z=55 and between Z=64 and Z=68. Although the odd-Z nuclei show slightly larger capture rates than even-Z nuclei, the amount is not as large as expected from the vanishing of the Cabibbo angle. Since there has been no study of the nuclear structure effects on

the total muon capture rate in even and odd nuclei, the effect should be investigated in detail with this in mind.

Our capture rates determined by lifetimes were compared with the Primakoff and Goulard-Primakoff theory. As expected, the latter theory gave a slightly better fit to the experimental data than the former theory. In the case of the Primakoff formula, the parameters obtained by the chi-squared minimization were in good agreement with his estimate.

It was necessary to use a chemical compound to perform the lifetime measurements for some elements. In a decay spectrum of a chemical compound, there is not only the information about lifetimes but also the information on muon atomic capture rates. The relative atomic capture ratio is given by the ratio of the amplitudes in equation (3.6) (see equation (5.4)). We have extended our experiment to include many more compounds than had been anticipated initially. This was the first attempt to apply the lifetime method in investigating systematically the atomic capture rates in metallic oxides of the type Z_mO_n. Our results between Z=6 and Z=30 showed the periodic dependence and were in good agreement with earlier atomic capture rates obtained by X-ray measurements, although our results around Z=50 were lower than the X-ray measurements. The muon atomic capture rate for atoms with Z larger than 30 will be studied by the lifetime method at TRIUMF during the fall of 1980.

In conclusion we note that this thesis has made a

significant contribution to the data base not only in muon capture by atoms but also to muon capture by nuclei; physical effects which have different scientific interests but which can be conveniently studied utilizing the same basic equipment. Both types of experiment are fraught with systematic errors and so great care has been taken to double check wherever possible. This conservatism may be the most important feature of the experimental technique.

References

ALB69 A.Alberigi-Quarata, A.Bertin, G.Matone, F.Palmonari, G.Torelli, P.Dalpiaz, A.Placcio, and E.Zavattini, Phys.Rev. 177,2118(1969)

AND38 C.D.Anderscn and S.H.Neddermeyer, Phys.Rev.50,263(1963), 51,584(1937), 54,88(1938)

AST61 A.Astbury, P.M.Hattersley, M.Hussain, M.A.R.Kemp, H.Muirhead, and T.Woodhead, Proc.Phys.Soc.78,1144(1961)

AUE65 L.B.Auerbach, R.J.Esterling, R.E.Hill, D.A.Jenkins, J.T.Lach, and N.H.Lipman Phys.Rev.138B,127(1965)

BAI63 B.J.S.Baijal, J.A.Diaz, S.N.Kaplan, and R.V.Pyle, Nuovo Cimento 30,711(1963)

BAL75 M.P.Balandin, V.M.Grebenyuk, V.G.Zinov, A.D.Konin, and A.N.Poncmarev, Sov.Phys.JETP 40,811(1975)

BAR59 W.A.Barrett, F.E.Holmstrom, and J.W.Kenffel Phys.Rev.113,661(1959)

BAR64 J.Barlcw, J.C.Sens, P.J.Duke, and M.A.R.Kemp Phys.Lett.9,84(1964)

BAR65 M.Bardcn, P.Norton, J.Peoples, A.M.Sachs,J.L.Franzini Phys.Rev.Lett.14,449(1965)

BAR78 G.Bardin, J.Duclos, J.Joseph, A.Magnon, J.Martino, E.Zavattini, Phys.Lett.79B,52(1978)

BAR79 G.Bardin, et al., High Energy Physics and Nuclear Conference(1979) Contribution 5B16

BAR80 G.Bardin, J.Duclos, A.Magncn, J.Martino, A.Richter, E.Zavattini, A.Bertin, M.Piccinini, A.Vitale, and D.Measday, CERN-EP/80-121 (Submitted to Nuclear Physics A)

BEI68 P.B.Beilin, Nuovo Cimento 54A,871(1968)

BEL51 W.E.Bell and E.H.Hincks, Phys.Rev.84,1243(1951)

BER73-1 J.Bernabeu, Nucl.Phys.A201,41(1973)

BER73-2 A.Bertin, A.Vitale, and A.Placci

Phys.Rev.A7,2214(1973)

BIZ64 R.Bizzari, Nuovo Cimento 33,1497(1964)

BLA62-1 I.M.Blair, H.Muirhead, and T.Woodhead, Proc.Phys.Soc.80,945(1962)

BLA62-2 I.M.Blair, H.Muirhead, and T.Woodhead, Proc.Phys.Soc.80,938(1962)

BLI73 R.J.Blin-Stoyle, Fundamental Interactions and the Nucleus, North-Holland Publishing Comp.(1973)

BRE75 J.H.Brewer, K.M.Crowe, F.N.Gygax, and A.Schenck, Muon Physics vol.3, ed. V.Hughes and C.S.Wu, New York Academic Press(1975)

BRI78 C.Bricman et al.(Particle Data Group), Phys.Lett.75B,1(1978)

CAN74 F.Cannata and N.C.Mukhopadhyay, Phys.Rev.C10,379(1974)

CHR73 P.Christillin, A.Dellafiore, and M.Rosa-Clot, Phys.Rev.Lett.31,1012(1973)

CHR75 P.Christillin, A.Dellafiore, and M.Rosa-Clot, Phys.Rev.C12,691(1975)

CLE48 E.Clementel and G.Puppi, Nuovo Cimento 5,505(1948)

CON47 M.Conversi, E.Pancini, and O.Piccioni, Phys.Rev.68,232(1945), 71,209(1947)

CON63 G.Conforto, C.Rubbia, and E.Zavattini, Phys.Lett.4,239(1963)

CRA62 W.A.Cramer, V.L.Telegdi, R.Winston, and R.A.Lundy, Nuovo Cimento 24,546(1962)

CRO72 K.M.Crowe, J.F.Hague, J.E.Rothberg, A.Schenck, D.L.Williams, R.W.Williams, and K.K.Young, Phys.Rev.D5,2145(1972)

CUL61 G.Culligan, et al., D.Harting, N.H.Lipmann, and G.Tibell, Conf.Int.on Elementary Particles, Aix-de-Provence, V1,143(1961), This is cited in "Muons" by A.O.Weisenberg (North-Holland,Amsterdam,1967)a

DAN75 H.Daniel, Phys.Rev.Lett.24,1649(1975)

DAN77 H.Daniel, W.Denk, F.J.Hartmann, J.J.Reidy and

W.Wilhelm, Phys.Lett. 71B,60(1977)

DAN78 H.Daniel, W.Denk, F.J.Hartmann, W.Wilhelm, and T.von Egidy, Phys.Rev.Lett.41,853(1978)

DAN79 H.Daniel, Z.Physik A291,29(1979)

DES78 P.Desgrclard, P.A.M.Guichcn, and J.Joseph Nucvc Cimento 43A,475(1978)

DEU68 J.P.Deutsch, L.Grenacs, P.Igo-Kemenes, P.Lipnik, and P.C.Macq, Phys.Lett.26B,315(1968)

DIL71 L.diLella, I.Hammerman, and L.M.Rosenstein Phys.Rev.Lett.27,830(1971)

DUC73 J.Duclos, A.Magnon, and J.Picard Phys.Lett.47B,491(1973)

DUC80 J.Duclos, Exotic Atoms '79, Fundamental Interaction and Structure of Matter, ed. K.Crowe, J.Duclos, G.Fiorentini, and G.Torelli, Plenum Publishing Corporation (1980)

DUP75 D.Duplain, B.Goulard, and J.Joseph, Phys.Rev.C12,28(1975)

DZH72 A.A.Dzhuraev, V.S.Evseev, G.G.Myasishcheva, Yu.V.Obukhcv, and V.S.Roganov, Sov.Phys.JETP 35,748(1972)

ECK62 M.Eckhause, T.A.Filippas, R.B.Sutton, R.E.Welsh, and T.A.Romanowski, Nuovo Cimento 24,666(1962)

ECK63 M.Eckhause, T.A.Filippas, R.B.Sutton and R.E.Welsh Phys.Rev.132,422(1963)

ECK66 M.Eckhause, R.T.Siegel, R.E.Welsh, and T.A.Filippas, Nucl.Phys.81,575(1966)

FAL62 I.V.Falcmkin, A.I.Filippov, M.M.Kulyukin, B.Pontecorvo, Yu.A.Scherbakov, R.M.Sulyaev, V.M.Tsupko-Sitnikov, and O.A.Zaimidoroga, Phys.Lett.1,318(1962), 3,229(1962), 6,100(1963)

FAV70 D.Favart et al. Phys.Rev.Lett.25,1348(1970)

FER47 E.Fermi and E.Teller, Phys.Rev.72,399(1947)

FIL63 T.A.Filippas, P.Pabit, and R.T.Siegel, Phys.Lett.6,118(1963)

FIS59 J.Fisher, B.Lecntic, A.Lundby, R.Meunier, and J.P.Stroot, Phys.Rev.Lett.3,349(1959)

FIS71 E.Fischback, M.M.Nieto, H.Primakoff, C.K.Scott, and J.Smith, Phys.Rev.Lett.27,1403(1971)

FOR62 K.W.Ford and J.G.Wills, Nucl.Phys.35,295(1962)

FRI79 G.Fricke, G.Mallot, A.Ruetschi, L.A.Schaller, L.Schellenberg, H.Schneuwly, and E.B.Shera, SIN Annual Report 1979, Page C37

FRY68 D.Fryberger, Phys.Rev.166,1397(1968)

FUJ59 A.Fujii and H.Primakoff, Nuovo Cimento 12,327(1959)

FUJ79 A.Fujii, Private communication

GAR79 D.Garner, Ph.D.thesis(1979), UBC Chemistry Dept.

GIL60 V.Gilinsky and J.Mathews, Phys.Rev.120,1450(1960)

GOU71 B.Goulard, J.Joseph, and F.O.Ledoyen Phys.Rev.Lett.27,1238(1971)

GOU74 B.Goulard and H.Primakoff, Phys.Rev.C10,2034(1974)

GRA80 R.D.Graves, B.A.Lamers, A,Nagl, H.Uberall, V.Devanathan, and P.R.Subramnnian, Can.J.Phys.58,48(1980)

HAF74 P.K.Haff and T.A.Tombrello, Ann.Phys.86,178(1974)

HAS76 O.Hashimoto, S.Nagamiya, K.Nagamine, and T.Yamazaki, Phys.Lett.62B,233(1976)

HAR77 R.D.Hart, C.R.Cox, G.W.Dodson, M.Eckhause, J.R.Kane, M.S.Pandey, A.M.Rushton, R.T.Siegel, and R.E.Welsh Phys.Rev.Lett.39,399(1977)

HUF61 R.W.Huff, Ann.Phys.16,288(1961)

HWA78 W-Y.P.Hwan, Phys.Rev.C17,1799(1978)

JAM71 F.James and M.Roos, MINUIT, CERN Computer 7600 Interim Programme Library (1971)

JOH77 M.W.Johnson, W.U.Schroder, J.R.Huizenga, W.K.Hensley, D.G.Perry and J.C.Browne, Phys.Rev.C15,2169(1977)

JOS72 J.Joseph, F.Ledoyen, and B.Goulard, Phys.Rev.C6,1742(1972)

KAP58 S.N.Kaplan, B.J.Moyer, and R.V.Pyle
Phys.Rev.112,968(1958)

KEL80 R.L.Kelly et al.(Particle Data Group)
Rev.Mod.Phys.52,S1(1980)

KES67 D.Kessler, H.L.Anderson, M.S.Dixit, H.J.Evans, R.J.McKee, C.K.Hargrove, R.D.Earton, E.P.Hincks, and J.D.McAndrew, Phys.Rev.Lett.18,1179(1967)

KIN57 T.Kinoshita and A.Sirlin, Phys.Rev.107,593(1957)

KIS73 H.E.Kissener, A.Aswad, H.U.Jager, and R.A.Eramzhian, Nucl.Phys.A215,424(1973)

KNI76 J.D.Knight, C.J.Orth, M.E.Schillaci, R.A.Naumann, H.Daniel, K.Springer, and H.B.Knowles, Phys.Rev.A13,43(1976)

KOH76 Y.Kohyama and A.Fujii, Supplement of the Prog.Theor.Phys.60,171(1976)

KOH79 Y.Kohyama and A.Fujii, TRIUMF Report TRI-PP-79-41 (submitted to Nuclear Physics)

KOZ78 T.Kozlowski and A.Zglinski, Nucl.Phys.A305,368(1978)

LAT47 C.M.G.Lattes, H.Muirhead, G.P.S.Occhialini, and C.F.Powell, Nature (London) 159,694(1947)

LAT61 J.L.Lathrop, R.A,Lundy, V.L.Telegdi, R.Winston, and D.D.Yovanovitch, Phys.Rev.Lett.7,107(1961)

LEE78 H.C.Lee and F.C.Khanna, Can.J.Phys.56,149(1978)

LEO79 M.Leon, Los Alamos Report LA-UR-79-1235(1979) (Exotic Atoms '79, Fundamental Interaction and Structure of Matter, ed. K.Crowe, J.Duclos, G.Fiorentini, and G.Torelli, Plenum Publishing Corporation, NY

LOD67 A.Lodder and C.C.Jonker, Nucl.Phys.B2,383(1967) Phys.Lett.18,310(1965)

LUN62 R.A.Lundy, Phys.Rev.125,1686(1962)

LUY63 J.R.Luyten, H.P.C.Rood, and H.A.Tolhoek, Nucl.Phys.41,231(1963), 70,641(1965)

MAN61 R.A.Mann and M.E.Rose, Phys.Rev.121,293(1961)

MAR80 J.Martino and J.Duclos, Private communication (1980)

MAT71 G.Matone, Lett.Nuovo Cimento 2,151(1971)

MAU77 L.F.Mausner, R.A.Naumann, J.A.Monard, and S.N.Kaplan, Phys.Rev.A15,479(1977)

MEY63 S.L.Meyer, E.W.Anderson, E.Bleser, L.M.Lederman, J.L.Rosen, J.Rothberg, and I-T.Wang Phys.Rev.132,2693(1963)

MIC57 L.Michel, Rev.Mod.Phys.,29,223(1957)

MUK77 N.C.Mukhopadhyay, Physics Reports 30C,1(1977)

NAL74 O.Nalcicglu, D.J.Rowe, and C.Ngo-Trong Nucl.Phys.A218,495(1974)

PAR78 R.Parthasarathy and V.N.Sridhar, Can.J.Phys.56,1606(1978)

PET63 V.I.Petrukhin and Yu.D.Prokoshkin, Nuovo Cimento 28,99(1963)

POV70 H.P.Povel, H.Koch, W.D.Hamilton, S.Charalambus, and G.Backenstoss, Phys.Lett.33B,620(1970)

PRI59 H.Primakoff, Rev.Mod.Phys.31,802(1959)

PRI77 H.Primakoff, AIP Conference No37, Weak Interaction Physics-1977 p85

REI60 R.A.Reiter, T.A.Romanowski, R.B.Sutton, and E.G.Chidley, Phys.Rev.Lett.5,22(1960)

ROO71 M.Roos and A.Sirlin, Nucl.Phys.B29,296(1971)

ROO74 M.ROOS, Nucl.Phys.B77,420(1974)

ROS63 J.L.Rosen, E.W.Anderson, E.J.Bleser, L.M.Lederman, S.L.Meyer, J.E.Rothberg, and I-T.Wang, Phys.Rev.132,2691(1963)

SAC75 A.M.Sachs and A.Sirlin, Muon Physics vol2, ed.V.W.Hughes and C.S.Wu (Academic Press 1975)

SAL74 A.Salam and J.Strathdee, Nature 252,569(1974)

SCH77 H.Schneuwly, Proceeding of the 1st course of the International School of Physics of Exotic Atoms, ed.G.Fiorentini and G.Torelli,255(1977)

SCH78-1 H.Schneuwly, T.Dubler, K.Kaeser, B.Robert-Tissort,

L.A.Schaller, and L.Schellenberg
Phys.Lett.66A,188(1978)

SCH78-2 H.Schneuwly, V.I.Pokrovsky, and L.I.Ponomarev,
Nucl.Phys.A312,419(1978)

SCH79 W.U.Schroder, W.W.Wilcke, M.W.Johnson, D.Hilscher,
J.R.Huizenga, J.C.Browne, and D.G.Perry
Phys.Rev.Lett.43,672(1979)

SEN57 J.C.Sens, R.A.Swanson, V.L.Telegdi, and
D.D.Yovanovitch, Phys.Rev.107,1464(1957)

SEN58 J.C.Sens, R.A.Swanson, V.L.Telegdi, and
D.D.Yovanovitch, Nuovo Cimento 7,536(1958)

SEN59 J.C.Sens, Phys.Rev.113,679(1959)

SHM59 I.M.Shmushkevich, Nucl.Phys.11,419(1959)

SHR78 R.E.Shrock and L.L.Wang,
Phys.Rev.Lett.41,1692(1978)

SUR75 P.Suranyi and R.A.Hedinger, Phys.Lett.56B,151(1975)

SUZ79 T.Suzuki et al., CAP Congress, paper BC3 Vancouver 1979

SUZ80 T.Suzuki et al., CAP Congress, paper AD4 Hamilton 1980

SWA58 R.A.Swanson, Phys.Rev.112,580(1958)

SWA59 R.A.Swanson, R.A.Lundy, V.L.Telegdi, and
D.D.Yovanovitch, Phys.Rev.Lett.2,430(1959)

SWA60 R.A.Swanson, Rev.Sci.Instrum.31,149(1960)

TEL59 V.L.Telegdi, Phys.Rev.Lett.3,59(1959)

TIM49-1 J.Timno and J.A.Wheeler, Rev.Mod.Phys.21,144(1949)

TIM49-2 J.Timno and J.A.Wheeler, Rev.Mod.Phys.21,153(1949)

TUR63 L.Turner, Bull.Am.Phys.Soc.Ser.II,8,324(1963)

UBE60 H.Uberall, Phys.Rev.119,365(1960)

VIT80 A.Vitale, Exotic Atoms '79, Fundamental Interaction
and Structure of Matter
ed. K.Crowe, J.Duclos, G.Fiorentini, and G.Torelli,
Plenum Publishing Corporation (1980)

WAL75 J.D.Walecka, Muon Physics, ed.V.W.Hughes and C.S.Wu,
Academic Press 1975

WAT75 P.J.S.Watson, Phys.Lett.58B,431(1975)

WHE49 J.A.Wheeler, Rev.Mod.Phys.21,133(1949)

WIL72 R.W.Williams and D.L.Williams, Phys.Rev.D6,737(1972)

WIL80-1 S.E.Willis, V.W.Hughes, P.Nemethy, R.L.Burman, D.R.F.Cochran, J.S.Frank, R.P.Redwine, J.Duclos, H.Kaspar, C.K.Hargrove, and U.Moser Phys.Rev.Lett.44,522(1980)

WIL80-2 W.W.Wilcke, M.W.Johnson, W.U.Schroder, D.Hilscher, J.R.Birkelund, J.R.Huizenga, J.C.Browne, and D.G.Perry, Phys.Rev.C21,2019(1980)

WIN61 R.Winston and V.L.Telegdi Phys.Rev.Lett.7,104(1961)

WIN63 R.Winston, Phys.Rev.129,2766(1963)

WU69 C.S.Wu and L.Wilets, Ann.Rev.Nucl.Sci.19,527(1969)

YAM74 T.Yamazaki, S.Nagamiya, O.Hashimoto, K.Nakai, K.Sugimoto, and K.M.Crowe, Phys.Lett.53B,117(1974)

YUK35 H.Yukawa, Physico-Mathematical Society of Japan (Nippon Sugaku-butsurigakkawai Kizi) 17,48(1935)

ZIN64 V.G.Zinov, A.D.Konin, and A.I.Mukhin, Sov.Phys.JETP 19,1292(1964)

ZIN66 V.G.Zinov, A.D.Konin, and A.I.Mukhin, Sov.J.Nucl.Phys.2,613(1966)